DISTRIBUTED COOLING FOR DATA CENTERS: BENEFITS, PERFORMANCE EVALUATION AND PREDICTION TOOLS

DISTRIBUTED COOLING FOR DATA CENTERS: BENEFITS, PERFORMANCE EVALUATION AND PREDICTION TOOLS

By Hosein Moazamigoodarzi

A Thesis Submitted to the School of Graduate Studies in Partial Fulfillment of the Requirements for the Degree of Doctor of Philosophy

McMaster University © Copyright by Hosein Moazamigoodarzi, October 2019.

TITLE: Distributed Cooling for Data Centers:

Benefits, Performance Evaluation and Prediction Tools

AUTHOR: Hosein Moazamigoodarzi,

M.A.Sc. (Sharif University of Technology, Iran),

B.Sc. (University of Tehran, Iran).

SUPERVISOR:

Prof. Ishwar K. Puri

NUMBER OF PAGES: XXIII, 176

Abstract

Improving the efficiency of conventional air-cooled solutions for Data Centers (DCs) is still a major thermal management challenge. Improvements can be made in two ways, through better (1) architectural design and (2) operation. There are three conventional DC cooling architectures: (a) room-based, (b) row-based, and (c) rack-based. Architectures (b) and (c) allows a modular DC design, where the ITE is within an enclosure containing a cooling unit. Due to scalability and ease of implementation, operational cost, and complexity, these modular systems have gained in popularity for many computing applications. However, the yet poor insight into their thermal management leads to limited strategies to scale the size of a DC facility for applications gaining in importance, e.g., edge and hyperscale. We improve the body of knowledge by comparing three cooling architecture's power consumption.

Energy efficiency during DC operation can be improved in two ways: (1) utilizing energy efficient control systems, (2) optimizing the arrangement of ITE. For both cases, a temperature prediction tool is required which can provide real-time information about the temperature distribution as a function of system parameters and the ITE arrangement. To construct such a prediction tool, we must develop a deeper understanding of the airflow, pressure and temperature distributions around the ITE and how these parameters change dynamically with IT load. As yet primitive tools have been developed, but only for architecture (a) listed above. These tools are not transferrable to other architectures due to significant differences in thermal-fluid transport. We examine the airflow and thermal transport within confined racks with separated cold and hot chambers that employ rack- or row-based cooling units, and then propose a parameter-free transient zonal model to obtain the real-time temperature distributions.

Key words: Data center, distributed cooling methods, row-based, rack-based, temperature prediction, power consumption, rack mountable cooing unit.

Acknowledgements

First of all, I would like to express my special appreciation and thanks to my supervisor Dr. Ishwar Puri for the patient guidance, great support and warm-hearted advice he has provided throughout my time as his student. I have been extremely lucky to have a supervisor who cared so much about my work. The door to Dr. Puri's office was always open whenever I ran into a trouble spot or had a question about my research or writing. It was a real privilege and an honor for me to share of his exceptional scientific knowledge but also of his extraordinary human qualities.

I also like to extend my sincere appreciation to Dr. Marilyn Lightstone, Dr. James Cotton, and Dr. Douglas Down for their constant support, invaluable guidance, and constructive suggestions, which were determinant for the accomplishment of the work presented in this thesis. They constantly encouraged and challenged me to explore beyond my set criteria. At many stages in the course of this research project I benefited from their advice, particularly so when exploring new ideas.

I am also deeply grateful to Dr. Souvik Pal and Dr. Suvojit Ghosh for their friendship, excellent guidance and continual helps in my project. Their advice on both research as well as on my career have been priceless. Many of the experiments would not have been completed as easily without their brilliant comments and suggestions.

I also want to thank all my lab mates, especially Mr. Rohit Gupta, Mr. Suchitra Nayak, and Dr. Peiying Jennifer Tsai, for their continual support, discussions and debates which helped me to promote my knowledge in my field.

Last, but not least, I wish to express my profound gratitude and love to my parents for their endless love, wise counsel and sympathetic ear throughout my life. This accomplishment would not have been possible without them. I would also like to thank my beloved wife, Sahar, for her love and also unfailing support and continuous encouragement through the process of researching and writing this thesis. Thank you.

This research was supported by the Natural Sciences and Engineering Research Council (NSERC) of Canada under a collaborative research and development (CRD) project titled: Adaptive Thermal Management of Data Centers. I also thank our colleagues from CINNOS Mission Critical Incorporated who provided insight and expertise that greatly assisted the research.

Declaration of Academic Achievements

This dissertation was used to fulfill the requirements of Ph.D. degree. All the research projects were conducted from September 2016 to August 2019. During the period of this study, the power consumption of three DC cooling architectures have been compared. Row- and rack-based distributed cooling architectures are more energy efficient as compared to the conventional room-based architecture. Also, the temperature and airflow distribution inside an enclosed rack that is internally integrated with a rack mountable cooling unit (RMCU) have been experimentally investigated. A model is presented to predict the temperature distribution within an IT server enclosure that is integrated with an RMCU. In contrast to other control schemes, no *a priori* training process is required. An efficient model to characterize the real time temperature distribution within an IT server enclosure that contains an integrated in-row cooling unit has been proposed. The flow field is predicted based on mechanical resistances and coupled with zonal energy balance equations, a process that is computationally less expensive than typical methods. The major contribution of this thesis work was from myself.

This thesis has resulted in 4 manuscripts, and I am the first author of all of them. Three of these 4 manuscripts have been published in Elsevier journals and one is under review. I took the primary role in design and conduction of the experiments, simulations, data analyses, and modeling reported in these papers. Dr. Puri and Dr. Pal provided helpful suggestions and guidance to flourish the initial idea. I wrote the first draft of the manuscripts. Dr. Puri and other authors provided editorial and technical input to generate the final draft of the papers. The papers are listed below:

1. **Hosein Moazamigoodarzi**, Peiying Jennifer Tsai, Souvik Pal, Suvojit Ghosh, and Ishwar K. Puri, *"Influence of Cooling Architecture on Data Center Power Consumption"*, **Published** in *Energy,* 2019.
2. **Hosein Moazamigoodarzi**, Souvik Pal, Douglas Down, Mohammad Esmalifalak, and Ishwar K. Puri, *"Performance of A Rack Mountable Cooling Unit in an IT Server Enclosure"*, **Published** in *Thermal Science and Engineering Progress,* 2019.
3. **Hosein Moazamigoodarzi**, Souvik Pal, Suvojit Ghosh, and Ishwar K, Puri, *"Real-Time Temperature Prediction in IT Server Enclosures"*, **Published** in *International Journal of Heat and Mass Transfer*, 2018.
4. **Hosein Moazamigoodarzi**, Rohit Gupta, Souvik Pal, Peiying Jennifer Tsai, Suvojit Ghosh, and Ishwar K. Puri, *"Modeling Temperature Distribution and Power Consumption in IT Server Enclosures with Row-Based Cooling Architectures"*, **Under review** in *Applied Energy*.

Table of Contents

Table of Figures

List of Tables

List of Abbreviations

ASTD	Active Server Temperature Distribution
CFD	Computational Fluid Dynamic
COP	Coefficient of Performance
CRAC	Computer Room Air Conditioner
CRAH	Computer Room Air Handler
DC	Data Center
DCIE	Data Center Infrastructure Efficiency
ICT	Information and Communications Technology
ITE	Information Technology Equipment
POD	Proper Orthogonal Decomposition
PUE	Power Usage Effectiveness
RCI	Rack Cooling Index
RHI	Return Heat Index
RMCU	Rack Mountable Cooling Unit
SHI	Supply Heat Index
VFD	Variable Frequency Drive

1 Introduction

Exponential growth in the use of information and communications technology (ICT) in our daily lives has necessitated establishment of massive hardware infrastructure that support them. This includes data centers (DCs), which house critical IT equipment (ITE). To house the ITE, DCs must contain a plethora of supporting infrastructure, which may be broadly classified into energy management and thermal management systems.

US DCs consumed about 70 billion kilowatt-hours of electricity in 2014, the most recent year examined, representing 2 percent of the country's total energy consumption [1]. The energy density in DCs is at a minimum 10 times that of residential or office buildings. Since all the electrical energy consumed by the ITE is eventually dissipated into heat, the thermal management system must remove this heat from the DC and release it into the ambient air. While doing so, the ITE must be maintained within a designed operating temperature range. Overshooting a maximum specified temperature negatively impacts the operation and health of the ITE [2]. High temperatures, particularly variations in those temperatures, reduce ITE life span [3]. In addition, hot spots can lead to ITE thermal shut down [4]. Thus, cooling systems have a critical role in continuously maintaining the safe, consistent, and reliable operation of DCs [5], [6].

Nearly 40% of the energy consumed in a DC is used for cooling, which significantly contributes towards operating costs [1]. Thus, an improvement in cooling efficiency would have a major impact on the energy efficiency of DCs. Two main methods for DC cooling are air cooling and direct liquid cooling. Because of implementation difficulties, required infrastructure, and higher cost of direct liquid cooling, most of the current DCs employ air cooling method.

1.1 Air Cooling

The majority of DCs employ air cooling systems to maintain desired operating conditions. Air cooling is typically preferred because of its proven high reliability, and lower initial and maintenance costs as compared to other cooling methods [7]. The heat removal process occurs at different levels: (1) at the chip level, heat sink removes the heat from the CPU and transfers it to the air flow passing over it, (2) at the device level, fans provide steady cold air flow to the heat sink, (3) at the room level, computer room air handler or conditioner (CRAH or CRAC) provides the cold air to the IT equipment, and (4) finally at the facility level, chillers extract the heat to the outside. Usually, an air-cooled DC contains thousands of ITEs each having a cold air inlet and a hot air outlet, thereby making the DC airflow distribution complicated. Designing and controlling these air paths affect the cooling efficiency considerably. All air-cooling architectures are fundamentally described by their [8]:

- Heat removal method,
- Air distribution type, and
- Location of the cooling unit that directly supplies cold air to the ITE (servers).

1.1.1 Heat removal method

There are 13 fundamental methods presented in Figure 1-1 by which heat is removed from servers and transferred to the ambient.

1.1.2 Air distribution type

Airflow management in a DC is critical for maintaining high reliability and efficiency. There are three basic approaches to distribute air in a DC: (a) Flooded: with a flooded supply and return air distribution system, the only constraints to the supply and return air flow are the walls, ceiling, and floor of the room. This type of air distribution causes significant mixing of the hot and cold air flows. (b) Targeted: a targeted supply and return air distribution system uses a mechanism like ducts or perforated tile to direct the supply and return airflow within a short distance (less than 10 feet) of the IT equipment intake and exhaust. (c) Contained: using a contained supply and return air distribution system, the IT equipment supply and return air flow is completely enclosed to eliminate air mixing between the supply and the return air streams.

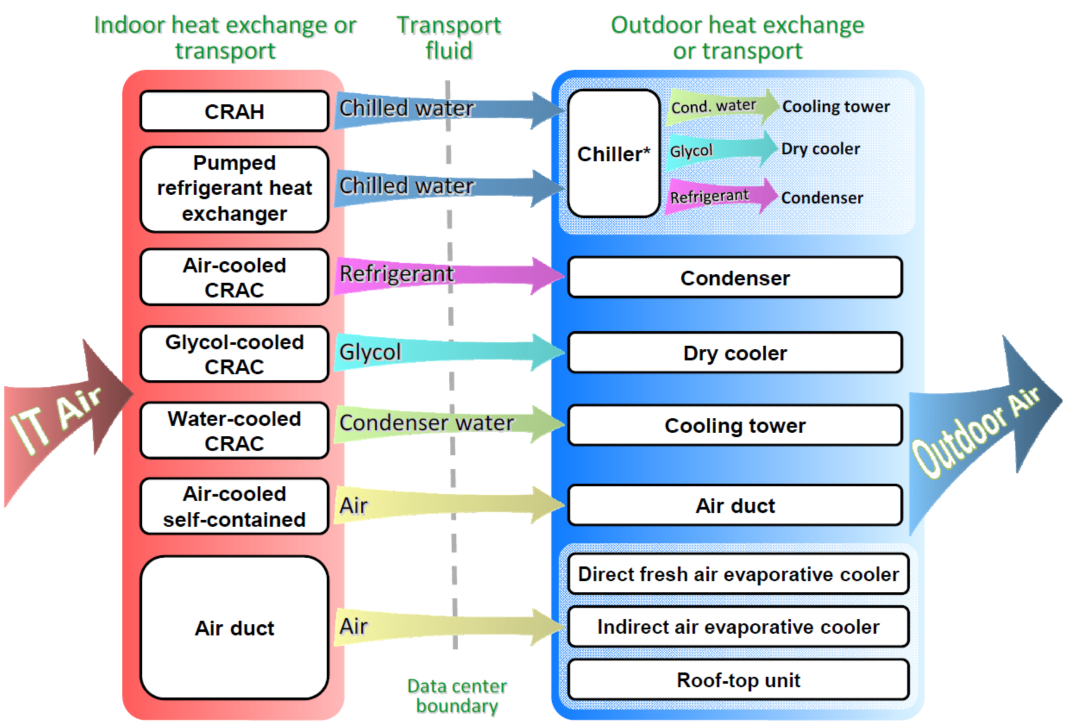

Figure 1-1: Different heat removal methods that employ air cooling to transfer heat from the DC to its ambient [8].

1.1.3 Location of the cooling unit (Architecture)

There are three locations to place a cooling unit that supplies cool air directly to the IT equipment, i.e., in the room, row, or rack [8]: (a) room-based cooling, where cold air is delivered directly to the room through arrangements such as raised floors and hot air return plenums, (b) row-based cooling, where the cooling unit is located between IT racks or mounted above them, thus delivering cold air to a row of racks, and (c) rack-based cooling, where the cooling unit is integrated entirely within a single IT rack [8], [9]. These three architectures are demonstrated in Figure 1-2.

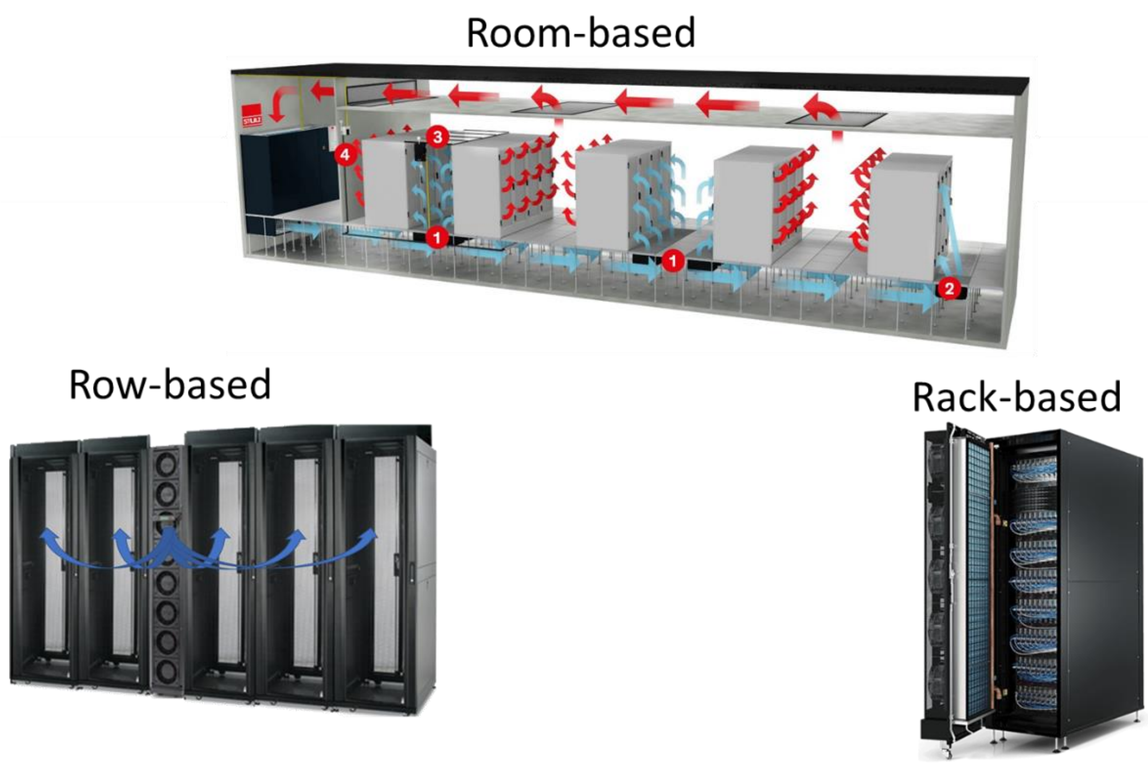

Figure 1-2: Three locations to place a cooling unit (architecture) that supplies cool air directly to the IT equipment.

In order to prevent formation of hot regions, usually the setpoint of the cooling unit is set lower than the IT requirements. Figure 1-3 demonstrates an example of working temperature for an air-cooled DC system from chiller to rack.

Location	Medium	Temperature [°C]	
		Supply	Return
Chiller	Water	10-13	15-18
CRAH	Water	10-13	15-19
CRAH	Air	15-25	30-40
Rack	Air	17-27	35-40

Figure 1-3: Working temperature for different components of air cooled DCs [10].

1.1.4 Recirculation and bypass

Two major air distribution problems identified in DCs are bypass and recirculation [10], [11], as illustrated in Figure 1-4. If the cold air supplied to the ITE is insufficient, the hot air exhausted from servers is recirculated to the ITE inlets by the fans inside the servers, increasing the overall inlet air temperature. Bypass occurs when part of the cold airflow returns to the cooling unit without contributing at all to server cooling [4], [7], [12]. These two problems reduce the cooling efficiency, which leads to localized high temperature regions called “hot spots”. Minimizing these two phenomena immediately translates to more effective cooling and therefore reduced energy consumption. Recirculation and bypass are differently manifested in the three conventional DC cooling architectures. Although reducing the air supply temperature or increasing airflow can solve these problems, both methods require more energy. Usually, the amount of cooling air used in DCs is 2.5 times the required amount [6]. Any solution for efficient cooling must therefore consider thermal conditions and energy cost simultaneously. Servers are typically mounted into the racks such that cold air is provided in front of the rack and hot air is exhausted at the back. This orientation is imposed on all racks in a row. Additional rows are added such that the backs of racks in two rows face each other, creating a ‘Hot Aisle’, and likewise the fronts of the racks in two rows face each other creating a ‘Cold Aisle’. This topology, first introduced in 1992 by Robert Sullivan at IBM, increased cooling efficiency by reducing the recirculation and bypass [13].

1.2 Limitation of traditional (room-based) air cooling

As the power density of ITE increases, resulting in higher heat generation, disadvantages of air-cooling manifest more significantly. Heat generation in a DC is never constant, neither spatially nor temporally. With traditional cooling configuration, it is impossible to selectively cool specific areas and components of the DC with air. Since different components have different high temperature tolerances, certain components are undercooled and may become prone to damage caused by high temperatures even as other components are overcooled leading to energy waste [14], [15]. Second, lack of airflow control results in hot and cold air mixing, which can account for 30% loss in the efficiency of the cooling system [11]. Third, cooling units operate year-round and do not fully utilize cold external conditions during cold seasons and nights [16]. Fourth, since air has a low thermal diffusivity, a lower air temperature is needed for the effective forced convection heat transfer [15], requiring a higher energy expenditure in the refrigeration cycle.

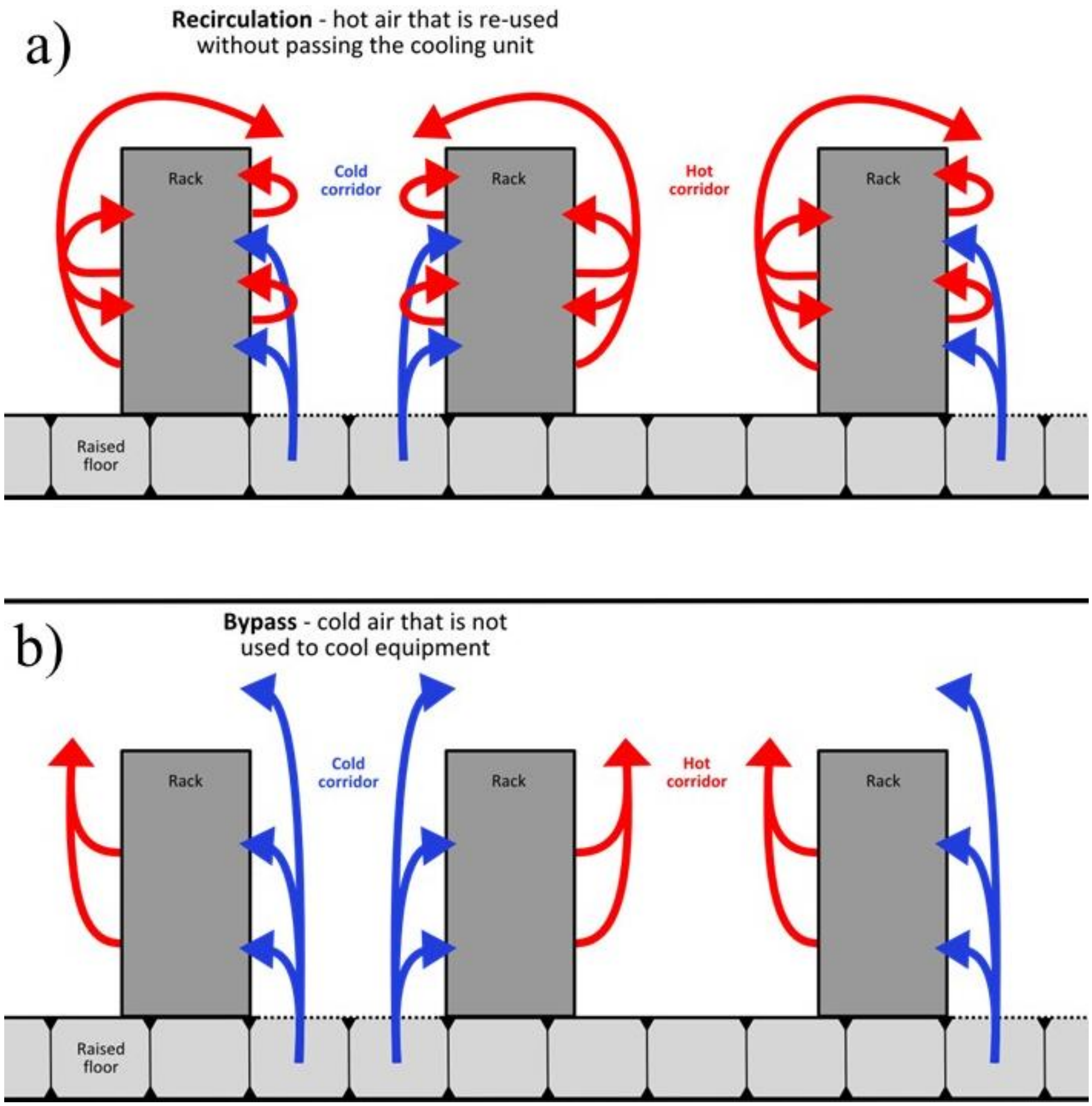

Figure 1-4: : Two major air distribution problems identified in a DC: a) recirculation through which airflow supply to the equipment is insufficient and part of the hot air is recirculated by fans inside the equipment, and b) bypass air which requires a high flow rate or promotes cold air leakage to the hot zone without passing servers.

1.3 Direct liquid and two-phase cooling

With direct liquid cooling, heat sources like microprocessors are maintained in direct contact with cold plates that are themselves in contact with a circulating coolant. By using direct liquid cooling, two of the main thermal resistances between heat source and ambient, i.e., heat sink-to-air and air-to-chilled water, are eliminated. The thermal resistance of liquid cooling systems is lower than 20% of the thermal resistance for air cooling systems. Despite its potential, the adoption of direct liquid cooling is limited due to concerns about (1) potential damage to electronics through water exposure, (2) complex plumbing requirements that make it difficult to withdraw or place a server readily in and out of a rack, (3) complete redesign of existing server hardware to accommodate cold plates, which is an impractical proposition, considering the billions of dollars of sunk-in investment in existing operational servers [2]. The need for an effective cooling solution for devices with higher energy loads is one reason to implement two-phase cooling systems in DCs. Boiling increases the convection heat transfer coefficient and enables an increase in the heat flux. Thus, direct two-phase cooling can provide a higher heat flux with a lower mass flowrate and pumping power as compared to single-phase cooling [17]. Two-phase cooling can also provide a more uniform equipment temperature [2]. However, the adoption of two-phase cooling is also limited because the same problems of direct liquid cooling apply to this method as well.

1.4 Performance metrics

Performance metrics are used to (1) evaluate opportunities to improve the energy efficiency of DCs and design approaches, and (2) compare DCs with each other. Because of complexity of DCs, there is no single comprehensive metric that captures all the relevant aspects. The most used metric for DC energy efficiency is the Power Usage Effectiveness (PUE) defined by The Green Grid Association [18], [19]:

$$PUE = \frac{Total\ facility\ energy\ consumption}{IT\ equipment\ energy\ consumption} \qquad 1.1$$

The inverse of the PUE is DC Infrastructure Efficiency (DCIE):

$$DCIE = \frac{IT\ equipment\ energy\ consumption}{Total\ facility\ energy\ consumption} \qquad 1.2$$

In the two aforementioned metrics, the IT equipment energy consumption is summation of the energy consumption of all the computing equipment. The total facility energy is the IT equipment energy consumption plus the energy consumption of everything that supports the DC operation, e.g., the energy consumption of the electric power delivery and cooling system components. Value of 1.0 for PUE indicates 100% efficiency. The PUE and DCIE are associated with the DC infrastructure and do not reflect the productivity of the IT equipment.

2 Literature review

2.1 Improving thermal performance and cooling energy efficiency

Energy efficiency of a DC is one of the most important factors for evaluating its performance. Since thirty percent of this energy consumption is attributed to cooling, most of the studies focused on increasing the energy efficacy of cooling cycle. Several factors are required to be optimized for reducing the cooling energy consumption. Control system of the cooling systems as one of these factors have been studied in the literature. Bash et al. [20] tried to adjust the air flowrate and supplied cold air temperature by changing the setpoint of cooling units. They developed a cascaded control concept that uses different sensors. Salient findings show that the cooling power consumption can be reduced up to fifty percent. Controlling the cooling units with variable frequency drive (VFD) to improve the cooling energy efficiency has been investigated in multiple studies [21], [22]. New control algorithms have been proposed to control the local temperature distribution by deploying controllable vent tiles, resulting in an improvement in racks inlet air temperature [23]-[25].

Another way to improve the cooling energy efficiency is thermal aware workload management. A concept of distributing the workload between servers in order to maintain a uniform inlet air temperature distribution was proposed by Sharma et al. [26]. In this study two workload management approaches were investigated: (1) a row-based thermal management to remove local hot spots and (2) a regional-based thermal management for reducing larger hot regions which may be due to a CRAC failure. Moore et al. [27]

developed two heuristics-based thermal aware workload management algorithms showing the possibility of reducing the cooling cost by using workload management. Tang et al. [28] proposed a task scheduler to minimize the hot air recirculation. The incoming tasks are distributed in a way that the temperature at the servers inlet is maintained below a defined threshold, while the cold air supply temperature is maximized. Different thermal aware workload management algorithms that employ an abstract heat flow model have been investigated to improve the cooling energy efficiency [29]-[31]. Shrivastava et al. [32] used a genetic algorithm in combination with a neural network-based algorithm to optimize the cooling performance of a group of servers.

Optimizing the physical parameters of the DC room is another area of improving the cooling energy efficiency. The effect of parameters such as gaps between the racks, under-floor obstructions, plenum height and open area of perforated tiles on the cooling efficiency was investigated and guideline for each parameter was provided by Patankar et al. [4]. Nada et al. [33] investigated the effect of cooling unit layout arrangement on thermal performance of DCs. Schmidt et al. [34] studied the effect of physical parameters, including cooling units location in the room, racks density, racks layout, and gaps between racks on the temperature and air distribution deficiency. The effect of climatic condition and DC location on the power consumption was examined by Song et al. [35]. Lyu et al. [36] evaluated the effect of enclosed aisle on cooling efficiency and temperature distribution in small scale DCs and showed that enclosure improves the energy efficiency. Cho et al. [37] presented analysis of the economic performance of seven cooling strategies which are the combinations of widely used DC cooling systems. Iyengar et al. [38]

developed a power consumption calculator for DCs and then investigated the effect of chiller setpoint and outdoor air temperature on the power consumption and cooling energy efficiency. A comprehensive cost model for DC ownership and operation was developed by Patel et al. [39]. This model evaluates inefficiencies in the DC infrastructure and shows cost improvement possibilities due to implementation of smart cooling techniques and strategies. Huang et al. [40] investigated the temperature distribution in 3 airflow patterns for a typical DC by computational fluid dynamics (CFD) simulation. The cooling performance of these airflow patterns was compared using indices like Index of Mixing and Return Temperature Index.

Despite the intuitive logic that predicts improved airflow distribution with row- and rack-based architectures over room-based systems [41], the mechanism of the reduction in cooling energy consumption has not been explained. The literature related to optimizing the DC cooling power consumption that discusses the influence of workload distribution, ITE configurations, cooling unit layouts, aisle separation and containment, and physical dimensions on cooling system efficacy is generally limited to room-based cooling applications. These prior investigations do not identify how changing the cooling architecture influences airflow features and the energy consumed by cooling systems.

2.2 Thermal modeling and temperature prediction of DCs

DC temperature prediction tools are required for design, control, fault prediction, and thermal aware workload management. Thermal models are necessary to examine DC designs and evaluate changes to the DC before implementation. Patel et al. [42] discussed the importance of this topic for high power density computer rooms. A series of DC thermal simulations that used CFD are reviewed by Rambo and Joshi [43]. The applications of the reviewed models vary from air flowrate prediction of the perforated floor tiles to evaluating the efficiency of different DC cooling strategies and configurations. Validation studies for CFD simulations of DCs are not widely provided in the literature due to the complexity of the air flow and temperature distribution in DCs.

A large pool of literature reports extensive CFD simulations for specific components of DC cooling system. Schmidt et al. [44] predicted the air flow through perforated floor tiles using experimentally validated CFD modeling. Further, it was used to study the effect of tile open area and raised floor heights on the airflow and temperature distribution. Gondipalli et al. [45] developed transient CFD simulations using transient boundary conditions to capture the fluctuations of rack inlet air temperature without experimental validation. Shrivastava et al. [46] compared experimental measurements and numerical simulation results for a large DC. The reported mean of absolute difference was 4ºC with a standard deviation of 3.3ºC. The higher deviations from the experimental data were in the area with higher IT load density.

In CFD simulation reported in the literature, usually the IT racks are considered simply as a black box that adds heat to the system. The airflow enters from the front of the server and then reappears at the back of the server rack with an appropriate increase in the temperature. It has been investigated whether the simplified modeling of the server racks in the CFD causes a considerable deviation from measurements or not [47]. The mentioned method of modeling has been compared with a more detailed modeling method to see if the temperature and airflow in a DC is influenced because of the simplified server modeling.

It is reported that there is not a considerable deviation in the results obtained by the different server modeling methods [47]. $k-\varepsilon$ model is well known in the literature as a suitable turbulence model for DCs [47]. It is demonstrated that buoyancy should be considered in the DC CFD simulations [48].

Rambo and Joshi [49], [50] developed temperature prediction tools using proper orthogonal decomposition (POD). Samadiani et al. [51] predicted the DC temperature distribution as a function of cooling unit air flowrate using data sets obtained from a group of temperature sensors and validated by experimental measurements. The average error was 0.7ºC, with a limited number of data points. They also presented a POD-based reduced order model [52] with enhanced flux matching process. Reduced order models have also been employed for transient DC temperature prediction. For example, Ghosh and Joshi [53] proposed a reduced order modeling framework of transient DC temperature prediction. Such statistical technique employs energy balance equations in conjunction with heat flux and/or surface temperature to generate a thermal model. This method has poor extrapolative accuracy when prediction is beyond the input parameter state.

Hamann et al. [54] developed a model by combining measurements obtained from a 3D mapping technology and real-time sensor data. They used this concept for implementing an interactive energy management solution.

Employing machine learning method especially artificial neural network (ANN) to predict DC temperature and airflow distribution is well established in the literature. These models need a dataset usually generated through CFD simulations or experiments to train the model [55]-[60]. Data-driven models are usually coupled with a black or gray box zonal modeling to predict temperature and airflow rate in a DC. Many studies have used black box machine learning-based models for thermal prediction of DCs [55], [56], [61], [62]. Black box data-driven modeling has been employed because of its rapidity, but the physical aspects of the system are totally ignored in this method. Gray box data-driven modeling is a more intelligent method that partially captures the internal physics [63]. Li et al. [64] developed a 2D gray box zonal model to predict the temperature distribution at the servers intake for a raised-floor DC, where the required data for this model were obtained experimentally. A rapid CFD and lumped capacitance hybrid model can predict server inlet temperature fluctuations due to transient events, such as server shutdown, chilled water interruption, and failure of the computer room air handlers [65]. However, the model requires CFD simulations for each case to determine unknown parameters and index values. As another example, a three-dimensional pressurized zonal model for room-based cooling with a raised floor can be employed to predict the temperature distribution [66]. Here, the characteristic dimension is typically limited to ∼1 m, which is too large to accurately predict temperatures at server inlets. Furthermore, the model requires information about mass flowrates through computationally expensive CFD simulations. In both examples, obtaining real-time temperature distributions is unfeasible.

With both POD, and all machine learning approaches, empirical parameters must be trained using sample datasets that are obtained either from CFD simulations or experiments. This poses two challenges. First, the development of training datasets that are statistically significant is nontrivial. Based on the numbers of input and output parameters, the corresponding number of simulations can easily range from $\sim 10^2$-10^3, requiring computational time of the order of days for typical 3D DC simulations, as well as dedicated access to supercomputing clusters. Performing so many specific experiments is also generally impractical. The second limitation is that test data are similar to the training data. Hence, when the physical configuration differs from one used to obtain training data, the algorithms must extrapolate, which degrades performance and reliability.

2.3 Metrics and performance evaluation

Multiple performance metrics and guidelines have been proposed for DCs [67], where an overview of them was provided by Schmidt et al. [68]. They concluded there is a considerable potential to save energy in DC cooling because most of the DCs require cooling power consumption up to fifty percent of their ITE load. To do so, thermal data of DCs should be analyzed, correlated and understood.

The American Society of Heating, Refrigerating and Air Conditioning Engineers (ASHRAE) has published guidelines for DCs which are widely accepted in the DC industry as a reference. The ASHRAE 2011 Thermal Guidelines [69] recommends that the temperature at the intake of servers should be in the range of 18ºC to 27ºC. Dimensionless parameters for thermal design and performance evaluation of large DCs are proposed by Sharma et al. [70]. To provide better understanding about convective heat transfer in DCs, they proposed two main indices, i.e., Supply Heat Index (SHI) and Return Heat Index (RHI). Herrlin [71], [72] and VanGilder et al. [73] proposed additional metrics for DC thermal performance evaluation at the rack level. A summary of thermal metrics for data centers reviewed by Capozzoli et al. [74] is provided in Table 2-1. More detailed such as formula can be found in [74].

Table 2-1: Summary of thermal metrics for DCs.

Index	Information provided	Input Measures	Benchmark
SHI	Recirculation extent within cold aisles	Airflow supply, inlet and outlet temperatures	Target: 0 Good: < 0.2
RHI	Effectiveness utilization of cold airflow	Airflow return, supply and outlet temperatures	Target: 1 Good: >0.8
$\mathbf{RCI_{lo}}$	Rack cooling condition in respect of cold threshold values	Rack intake air temperatures distribution	Ideal: 100 Good: >96 Poor: <90
$\mathbf{RCI_{Hi}}$	Rack cooling condition in respect of hot threshold values	Rack intake air temperatures distribution	Ideal: 100 Good: >96 Poor: <90
β Index	Presence of recirculation and over heating	Local airflow inlet supply and outlet temperatures	Target: 0
NP	Airflow infiltration into underfloor plenum	Airflow plenum, supply and return temperatures	-
BP	Bypass extent within data center	Plenum airflow, return and outlet temperatures	Ideal: 0 Good: <0.05 Acceptable: 0.05-0.2
R	Recirculation extent within cold aisles	Airflow supply, inlet and outlet temperatures	Ideal: 0 Good: <0.2
RTI	Presence of recirculation or bypass phenomena	Airflow return, supply and outlet temperatures	Ideal: 100 Good: 95-105

2.4 References

[1] A. Shehabi, “United States Data Center Energy Usage Report, LBNL-1005775,” no. June, pp. 1–66, 2016.

[2] K. Ebrahimi, G. F. Jones, and A. S. Fleischer, "A review of data center cooling technology, operating conditions and the corresponding low-grade waste heat recovery opportunities," Renewable and Sustainable Energy Reviews, vol. 31, pp. 622-638, 2014.

[3] N. El-Sayed, I. A. Stefanovici, G. Amvrosiadis, A. A. Hwang, and B. Schroeder, "Temperature management in data centers: Why some (might) like it hot," ACM SIGMETRICS Performance Evaluation Review, vol. 40, no. 1, pp. 163-174, 2012.

[4] S. V. Patankar, "Airflow and cooling in a data center," Journal of Heat transfer, vol. 132, no. 7, p. 073001, 2010.

[5] H. M. Daraghmeh and C.-C. Wang, "A review of current status of free cooling in datacenters," Applied Thermal Engineering, vol. 114, pp. 1224-1239, 2017.

[6] J. Rambo and Y. Joshi, "Modeling of data center airflow and heat transfer: State of the art and future trends," Distributed and Parallel Databases, vol. 21, no. 2, pp. 193-225, 2007.

[7] J. Cho, J. Yang, and W. Park, "Evaluation of air distribution system's airflow performance for cooling energy savings in high-density data centers," Energy and Buildings, vol. 68, pp. 270-279, 2014.

[8] K. Dunlap and N. Rasmussen, “Choosing Between Room, Row, and Rack-based Cooling for Data Centers,” Schneider Electra. White Pap. 130, p. 18, 2012.

[9] “White Papers - WP 55 - The Different Types of Air Distribution for IT Environments.” .

[10] A. Capozzoli and G. Primiceri, "Cooling systems in data centers: State of art and emerging technologies," Energy Procedia, vol. 83, pp. 484-493, 2015.

[11] A. Capozzoli, G. Serale, L. Liuzzo, and M. Chinnici, "Thermal metrics for data centers: A critical review," Energy Procedia, vol. 62, pp. 391-400, 2014.

[12] J. Cho and B. S. Kim, “Evaluation of air management system’s thermal performance for superior cooling efficiency in high-density data centers,” Energy Build., vol. 43, no. 9, pp. 2145–2155, 2011.

[13] K. Wu, "A comparative study of various high-density data center cooling technologies," The Graduate School, Stony Brook University: Stony Brook, NY., 2008.

[14] B. Fakhim, M. Behnia, S. Armfield, and N. Srinarayana, "Cooling solutions in an operational data centre: A case study," *Applied thermal engineering,* vol. 31, no. 14, pp. 2279-2291, 2011.

[15] Y. Fulpagare and A. Bhargav, "Advances in data center thermal management," *Renewable and Sustainable Energy Reviews,* vol. 43, pp. 981-996, 2015.

[16] H. Zhang, S. Shao, H. Xu, H. Zou, and C. Tian, "Free cooling of data centers: A review," *Renewable and Sustainable Energy Reviews*, vol. 35, pp. 171-182, 2014.

[17] J. B. Marcinichen, J. A. Olivier, and J. R. Thome, "On-chip two-phase cooling of datacenters: Cooling system and energy recovery evaluation," *Applied Thermal Engineering*, vol. 41, pp. 36-51, 2012.

[18] The Green Grid, “The Green Grid metrics: Describing data center power efficiency,” technical committee white paper, The Green Grid, February 2007.

[19] V. Avelar and D. A. A. French, “PUE: A comprehensive examination of the metric,” white paper, The Green Grid, October 2012.

[20] C. Bash, C. Patel, and R. Sharma, “Dynamic thermal management of air cooled data centers,” in *10th Intersociety Conference on Thermal and Thermomechanical Phenomena in Electronics Systems (ITherm)*, pp. 8 pp. –452, June 2006.

[21] M. Iyengar, R. Schmidt, and J. Caricari, “Reducing energy usage in data centers through control of room air conditioning units,” in *12th IEEE Intersociety Conference on Thermal and Thermomechanical Phenomena in Electronic Systems (ITherm)*, pp. 1–11, June 2010.

[22] T. Boucher, D. Auslander, C. Bash, C. Federspiel, and C. Patel, “Viability of dynamic cooling control in a data center environment,” in *9th Intersociety Conference on Thermal and Thermomechanical Phenomena in Electronic Systems (ITherm)*, vol. 1, pp. 593 –600, June 2004.

[23] K. Chen, D. M. Auslander, C. E. Bash, and C. D. Patel, “Local temperature control in data center cooling: Part i, correlation matrix,” tech. rep., HP Laboratories Palo Alto, 2006.

[24] K. Chen, C. E. Bash, D. M. Auslander, and C. D. Patel, “Local temperature control in data center cooling: Part ii, statistical analysis,” tech. rep., HP Laboratories Palo Alto, 2006.

[25] K. Chen, D. M. Auslander, C. E. Bash, and C. D. Patel, “Local temperature control in data center cooling: Part iii, application,” tech. rep., HP Laboratories Palo Alto, 2006.

[26] R. Sharma, C. Bash, C. Patel, R. Friedrich, and J. Chase, “Balance of power: dynamic thermal management for internet data centers,” *IEEE Internet Computing*, vol. 9, pp. 42–49, Jan.-Feb. 2005.

[27] J. Moore, J. Chase, P. Ranganathan, and R. Sharma, "Making scheduling "cool": Temperature-aware resource assignment in data centers," in *2005 USENIX Annual Technical Conference,* April 2005.

[28] Q. Tang, S. Gupta, and G. Varsamopoulos, "Thermal-aware task scheduling for data centers through minimizing heat recirculation," in *IEEE International Conference on Cluster Computing 2007*, pp. 129–138, Sept. 2007.

[29] T. Mukherjee, Q. Tang, C. Ziesman, S. K. S. Gupta, and P. Cayton, "Software architecture for dynamic thermal management in datacenters," in *2nd International Conference on Communication Systems Software and Middleware (COMSWARE)*, pp. 1–11, 2007.

[30] N. Vasic, T. Scherer, and W. Schott, "Thermal-aware workload scheduling for energy efficient data centers," in *7th International Conference on Autonomic Computing (ICAC)*, (New York, NY, USA), pp. 169–174, ACM, 2010.

[31] T. Scherer, "Modeling and control for energy efficient data centers," mathesis, ETH Zurich, 2009.

[32] S. Shrivastava, J. VanGilder, and B. Sammakia, "Optimization of cluster cooling performance for data centers," in *11th Intersociety Conference on Thermal and Thermomechanical Phenomena in Electronic Systems (ITerm)*, pp. 1161 –1166, May 2008.

[33] S. A. Nada and M. A. Said, "Effect of CRAC units layout on thermal management of data center," *Appl. Therm. Eng.*, vol. 118, pp. 339–344, 2017.

[34] R. Schmidt and I. Madhusudan, "EFFECT OF DATA CENTER LAYOUT ON RACK INLET AIR TEMPERATURES," *ASME InterPACK '05 July 17-22, San Fr. California, USA*, pp. 1–9, 2005.

[35] Z. Song, X. Zhang, and C. Eriksson, "Data Center Energy and Cost Saving Evaluation," *Energy Procedia*, vol. 75, pp. 1255–1260, 2015.

[36] C. Lyu, G. Chen, S. Ye, and Y. Liu, "Enclosed aisle effect on cooling efficiency in small scale data center," *Procedia Eng.*, vol. 205, pp. 3789–3796, 2017.

[37] K. Cho, H. Chang, Y. Jung, and Y. Yoon, "Economic analysis of data center cooling strategies," *Sustain. Cities Soc.*, vol. 31, pp. 234–243, 2017.

[38] M. Iyengar and R. Schmidt, "Analytical Modeling for Thermodynamic Characterization of Data Center Cooling Systems," *J. Electron. Packag.*, vol. 131, no. 2, p. 021009, 2009.

[39] C. D. Patel and A. J. Shah, "Cost Model for Planning , Development and Operation

of a Data Center," *Internet Syst. Storage Lab. HP Lab. Palo Alto*, vol. 107, pp. 1–36, 2005.

[40] Z. Huang, K. Dong, Q. Sun, L. Su, and T. Liu, "Numerical Simulation and Comparative Analysis of Different Airflow Distributions in Data Centers," *Procedia Eng.*, vol. 205, pp. 2378–2385, 2017.

[41] K. Dunlap and N. Rasmussen, "Choosing Between Room, Row, and Rack-based Cooling for Data Centers," *Schneider Electr. White Pap. 130*, p. 18, 2012.

[42] C. D. Patel, R. Sharma, C. E. Bash, and A. Beitelmal, "Thermal considerations in cooling large scale high compute density data centers," in *8th Intersociety Conference on Thermal and Thermomechanical Phenomena in Electronic Systems (ITherm)*, pp. 767–776, 2002.

[43] J. Rambo and Y. Joshi, "Reduced-order modeling of turbulent forced convection with parametric conditions," *International Journal of Heat and Mass Transfer*, vol. 50, no. 3-4, pp. 539–551, 2007. Bibliography 107.

[44] R. R. Schmidt, K. C. Karki, K. M. Kelkar, A. Radmehr, and S. V. Patankar, "Measurements and predictions of the flow distribution through perforated tiles in raised-floor data centers," in *Pacific Rim/ASME International Electronic Packaging Technical Conference and Exhibition (IPACK)*, 2001.

[45] S. Gondipalli, M. Ibrahim, S. Bhopte, B. Sammakia, B. Murray, K. Ghose, M. Iyengar, and R. Schmidt, "Numerical modeling of data center with transient boundary conditions," in *12th IEEE Intersociety Conference on Thermal and Thermomechanical Phenomena in Electronic Systems (ITherm)*, pp. 1–7, June, 2010.

[46] S. Shrivastava, M. Iyengar, B. Sammakia, R. Schmidt, and J. VanGilder, "Experimental-numerical comparison for a high-density data center: Hot spot heat fluxes in excess of 500 w/ft2," *IEEE Transactions on Components and Packaging Technologies*, vol. 32, pp. 166–172, March 2009.

[47] Zhang X, VanGlider JW, Iyengar M, Schmidth RR. Effect of Rack Modeling Detail on the Numerical Results of a Data Center Test Cell. Proceedings of the 11th IEEE ITHERM Conference; 2008 May 28-31; Orlando, USA.

[48] Adbdelmaksoud WA, Khalifa HE, Dang TQ, Schmidt RR, Iyengar M. Improved CFD Modeling of a Small Data Center Test Cell. Proceedings of the 12th IEEE ITHERM Conference; 2010 June 2-5; Las Vegas, USA.

[49] J. Rambo and Y. Joshi, "Reduced order modeling of steady turbulent flows using the pod," in *2005 ASME Summer Heat Transfer Conference*, 2005.

[50] J. D. Rambo, *Reduced-order Modeling of Multiscale Turbulent Convection: Application to Data Center Thermal Management*. PhD thesis, Department of Mechanical Engineering 2006, Georgia Institute of Technology, Atlanta, GA, 2006.

[51] E. Samadiani, Y. Joshi, H. Hamann, M. Iyengar, S. Kamalsy, and J. Lacey, "Reduced order thermal modeling of data centers via distributed sensor data," in *ASME/Pacific Rim Technical Conference on Packaging and Integration of Electronic and Photonic Systems, MEMS and NEMS (InterPACK)*, 2009.

[52] E. Samadiani and Y. Joshi, "Proper orthogonal decomposition for reduced order thermal modeling of air-cooled data centers," *Journal of Heat Transfer*, vol. 132, no. 7, 2010.

[53] R. Ghosh and Y. Joshi, "Error estimation in pod-based dynamic reduced-order thermal modeling of data centers," *International Journal of Heat and Mass Transfer*, vol. 57, no. 2, pp. 698 – 707, 2013.

[54] H. F. Hamann, T. G. van Kessel, M. Iyengar, J.-Y. Chung, W. Hirt, M. A. Schappert, A. Claassen, J. M. Cook, W. Min, Y. Amemiya, V. L´opez, J. A. Lacey, and M. O'Boyle, "Uncovering energy-efficiency opportunities in data centers," *IBM Journal of Research and Development*, vol. 53, pp. 10:1–10:12, May 2009. Paper 10.

[55] Song, Z., B.T. Murray, and B. Sammakia, *Airflow and temperature distribution optimization in data centers using artificial neural networks.* International Journal of Heat and Mass Transfer, 2013. 64: p. 80-90.

[56] Athavale, J., Y. Joshi, and M. Yoda. *Artificial neural network-based prediction of temperature and flow profile in data centers*. in *2018 17th IEEE Intersociety Conference on Thermal and Thermomechanical Phenomena in Electronic Systems (ITherm)*. 2018. IEEE.

[57] Moore, J., et al. *Datacenter workload monitoring, analysis, and emulation*. in *Eighth Workshop on Computer Architecture Evaluation using Commercial Workloads*. 2005.

[58] Moore, J., J. Chase, and P. Ranganathan. *Consil: Low-cost thermal mapping of data centers*. in *the First Workshop on Tackling Computer Systems Problems with Machine Learning (SysML)*. 2006.

[59] Moore, J., J.S. Chase, and P. Ranganathan. *Weatherman: Automated, online and predictive thermal mapping and management for data centers*. in *2006 IEEE international conference on Autonomic Computing*. 2006. IEEE.

[60] De Lorenzi, F. and C. Vömel, *Neural network-based prediction and control of airflow in a data center*. Journal of Thermal Science and Engineering Applications, 2012. 4(2): p. 021005.

[61] Athavale, J., M. Yoda, and Y. Joshi, *Comparison of data-driven modeling approaches for temperature prediction in data centers.* International Journal of Heat and Mass Transfer, 2019. 135: p. 1039-1052.

[62] Song, Z., B.T. Murray, and B. Sammakia. *Multivariate prediction of airflow and temperature distributions using artificial neural networks*. in *ASME 2011 Pacific Rim Technical Conference and Exhibition on Packaging and Integration of Electronic and Photonic Systems*. 2011. American Society of Mechanical Engineers.

[63] Acharya, S. and V. Pandya, *Bridge between Black Box and White Box–Gray Box Testing Technique.* International Journal of Electronics and Computer Science Engineering, 2012. **2**(1): p. 175-185.

[64] Li, L., et al. *Thermocast: a cyber-physical forecasting model for datacenters*. in *Proceedings of the 17th ACM SIGKDD international conference on Knowledge discovery and data mining*. 2011. ACM.

[65] H. S. Erden, H. E. Khalifa, and R. R. Schmidt, “A hybrid lumped capacitance-CFD model for the simulation of data center transients,” *HVAC R Res.*, vol. 20, no. 6, pp. 688–702, 2014.

[66] Z. Song, B. T. Murray, and B. Sammakia, “A compact thermal model for data center analysis using the zonal method,” *Numer. Heat Transf. Part A Appl.*, vol. 64, no. 5, pp. 361–377, 2013.

[67] H. F. Hamann, M. Schappert, M. Iyengar, T. van Kessel, and A. Claassen, “Methods and techniques for measuring and improving data center best practices,” in *11th Intersociety Conference on Thermal and Thermomechanical Phenomena in Electronic Systems (ITherm)*, 2008.

[68] R. R. Schmidt, E. E. Cruz, and M. K. Iyengar, “Challenges of data center thermal management,” *IBM Journal of Research and Development*, vol. 49, no. 4/5, pp. 709–723, 2005.

[69] ASHRAE TC 9.9, “2011 thermal guidelines for data processing environments expanded data center classes and usage guidance.” technical committee white paper, ASHRAE, 2011.

[70] R. K. Sharma, C. E. Bash, and R. D. Patel, “Dimensionless parameters for evaluation of thermal design and performance of large-scale data centers,” in *In 8th ASME/AIAA Joint Thermophysics and Heat Transfer Conf*, 2002.

[71] M. K. Herrlin, “Rack cooling effectiveness in data centers and telecom central offices: The rack cooling index (rci),” *ASHRAE Transactions*, vol. 111, 2005.

[72] M. K. Herrlin, “Airflow and cooling performance of data centers: Two performance metri,” *ASHRAE Transactions*, 2008.

[73] J. VanGilder and S. Shrivastava, “Capture index: An airflow-based rack cooling performance metric,” *ASHRAE Transactions*, vol. 113, pp. 126–136, 01 2007.

[74] A. Capozzoli, G. Serale, L. Liuzzo, and M. Chinnici, “Thermal metrics for data centers: A critical review,” *Energy Procedia*, vol. 62, pp. 391–400, 2014.

3 Problem statement and research objectives

Row- and rack-based cooling architectures for DCs have been made available only recently, especially for high density DCs. Studies comparing the benefits of row-based with room-based cooling architectures are scarce and only provide qualitative comparisons of the reduction in average air temperature which is difficult to translate readily in terms of total system energy consumption. Extensions of these results to enclosed rack-based architectures, and comparison with room- and row-based architectures are not reported widely in the literature. Therefore, the first objective of this research is comparing the characteristic airflow and temperature distributions for the three, room-, row- and rack-based, cooling architectures using computational fluid dynamics (CFD) simulations that inform thermodynamic models of cooling power consumption.

The dynamics of airflow in room-based cooling architecture, which is widely reported in the literature, is inertia dominated. However, row- and rack-based cooling architectures with enclosure have pressure-driven flow field. Thereby, it is essential to characterize the transport dynamics for enclosed distributed cooling architectures. The second objective of this research is to develop an understanding of airflow, pressure, and temperature distribution within a confined DC environment that employs rack mountable cooling units (RMCUs).

Any effort to improve thermal performance of DCs, e.g., thermal aware workload distribution, employing model-based control methods, and fault detection requires a real-time temperature prediction tool. Developing temperature prediction tools for enclosed

DCs with row- and rack-based cooling architectures is another undiscovered area in thermal management of DCs. The available temperature prediction methods have four main limitations: (1) they are only applicable to traditional DCs, (2) they are data driven-based requiring a large number of sample datasets obtained either from CFD simulations or experiments, which increases the computational or experimental cost, (3) when the physical configuration differs from the one used to obtain training data, the algorithms must extrapolate, which degrades performance and reliability, (4) they cannot capture all effective parameters. Therefore, the third objective is to propose an original parameter-free transient zonal model to obtain real-time temperature distributions inside a typical DC that is confined within an enclosure cooled by row- or rack-based cooling units with separated cold and hot chambers.

4 Influence of Cooling Architecture on Data Center Power Consumption

This chapter is reproduced from *"Influence of Cooling Architecture on Data Center Power Consumption"*, ***Hosein Moazamigoodarzi***, *Peiying Jennifer Tsai, Souvik Pal, Suvojit Ghosh and Ishwar K. Puri, Published in Energy, 2019.* The author of this thesis is the first author and the main contributor of this publication.

4.1 Abstract

Almost thirty percent of the power consumed by data centers (DCs) is attributable to the cooling of IT equipment (ITE). There are opportunities to reduce a DC's energy budget by considering alternatives to traditional cooling methods, which experience inherent airflow deficiencies due to hot air recirculation and cold air bypass. Minimizing these two air distribution problems results in more effective cooling, but the two effects are manifest differently in the three conventional DC cooling architectures, i.e., (a) room-based, (b) row-based, and (c) rack-based cooling. Despite the intuitive logic that predicts improved cooling air distribution within row- and rack-based architectures that include shorter airflow pathlengths compared to room-based systems that have longer paths, the mechanism through which improvements translate into energy savings is not well understood. Therefore, we present methodologies that resolve the characteristic airflow and temperature distributions for three cooling architectures using computational fluid dynamics. These results inform thermodynamics models of the power consumptions that are required to cool these three architectures. The analysis reveals that row- and rack-based

architectures reduce cooling power by much as 29% over a room-based architecture. Adding an enclosure within row- and rack-based architectures to separate the hot and cold airflows provides further 18% reduction in cooling power. This analysis facilitates better DC design from a cooling power consumption perspective.

Key words: Data Center, Distributed cooling, power consumption, Row-based, Rack-based.

4.2 Introduction

The electrical power consumed by the IT equipment (ITE) in a data center (DC) is converted into heat, which must be removed. This heat removal is typically equivalent to almost thirty percent of the power consumed by a DC [1]–[4]. Although liquids offer significantly higher heat transfer capabilities, most DCs use air cooling due to the simplicity of its application and handling [1]–[5]. An air-cooled DC can contain thousands of ITE items, each with a cold air inlet and hot air outlet, thereby making airflow distribution inside a DC complex [6]. The design and control of these air paths significantly influences the cooling efficacy.

Air cooling has two major distribution problems, hot air recirculation and cold air bypass [7]–[9]. When cold air supply to the ITE is insufficient, the hot air exhausted from servers is recirculated to ITE inlets by fans inside the servers, increasing the inlet air temperatures. Bypass occurs when a portion of the cold airflow returns to the cooling unit without contributing to server cooling. While minimizing these air distribution issues leads to more effective cooling, simultaneously reducing the energy consumed for cooling, the two effects manifest differently in the three conventional DC cooling architectures, namely,

(a) room-based cooling, where cold air is delivered directly to the room through arrangements such as raised floors and hot air return plenums, (b) row-based cooling, where the cooling unit is located between IT racks or mounted above them so that cold air is delivered to a row of racks, and (c) rack-based cooling, where the cooling unit is integrated entirely within a single IT rack [6], [10].

A DC cooling system must accomplish two tasks simultaneously, i.e., (1) remove heat from hot air issuing from the ITE and (2) distribute cold air to it. For room-, row- and rack-based cooling architectures, the first task is identical since the cooling system capacity must match the total power consumed by the ITE. The second task, distribution of cold air to the ITE, is however performed differently for room-, row- and rack-based cooling. Airflow paths are shorter and more predictable for row- and rack-based architectures than for room-based systems since they are isolated from room constraints in the former case.

Despite the intuitive logic that predicts improved airflow distribution with row- and rack-based architectures over room-based systems [6],[11], the mechanism of the reduction in cooling energy consumption has not been explained. This analysis is required if DC operators are to make informed decisions while selecting a particular DC designer. The literature related to DC power consumption and cooling optimization that discusses the influence of workload distribution, ITE configurations, cooling unit layouts, aisle separation and containment, and physical dimensions on cooling system efficacy is generally limited to room-based cooling applications [12]–[25]. These prior investigations do not identify how changing the cooling architecture influences airflow features and the energy consumed by cooling systems.

Studies comparing the benefits of row-based solutions with room-based cooling [6], [11] are scarce and only provide qualitative comparisons of the reduction in average air temperature at server inlet and of the return temperature index, both of which are difficult to translate readily in terms of total system energy consumption. Extensions of these results to enclosed rack-based solutions, such as the inclusion of a rack mountable cooling unit (RMCU) within each enclosed IT rack, and comparison with room and row-based architectures are not reported widely in the literature. This lack of guidance is significant considering the rapid emergence of single rack data centers for edge computing, where rack mountable cooling solutions offer a more attractive deployment and maintenance choice. Therefore, we compare the characteristic airflow and temperature distributions for the three, room-, row- and rack-based, cooling architectures using computational fluid dynamics (CFD) simulations that inform thermodynamics models of cooling power consumption.

4.3 Methodology

We consider a 200 kW DC room that employs air handler units (CRAHs), water to air heat exchangers, fans, valves, and enclosures for which the heat rejection map is shown in Figure 4-1. Cold air flow through the servers transfers heat to the CRAHs, cold water flow in the CRAHs extracts heat from the DC room and transfers it to an air-cooled chiller, while the chiller releases the heat to the ambient. There are other possibilities for implementing cooling, e.g., using a water-cooled chiller and cooling tower instead of an air-cooled chiller, or placing the refrigeration cycle inside the DC room in the form of an air conditioner, but these are not considered herein. While the selected configuration may not be the most energy efficient for all possible cases, our purpose is to compare the cooling power consumption by the three different cooling architectures. Such an overall analysis is independent of the specific choice of cooling configuration. Certainly, some of the results would change by considering other cooling strategies like using CRACs instead of CRAHs but considering all possible cooling strategies is not within the scope of a single study. For this reason, we compare the architecture-based power consumption for chilled water-based DCs which are commonly used around the word. Furthermore, regardless of the cooling strategy, whether CRAH or CRAC, two parameters with most influence on the cooling efficiency are the same for different cooling strategies, i.e., (1) the required cold air flowrate and (2) the difference between the cooling unit setpoint and maximum server intake temperature. Even by considering just chilled water based DCs, we are comparing the effect of DC cooling architectures on these two parameters which are not dependent on the type of cooling system (CRAH or CRAC).

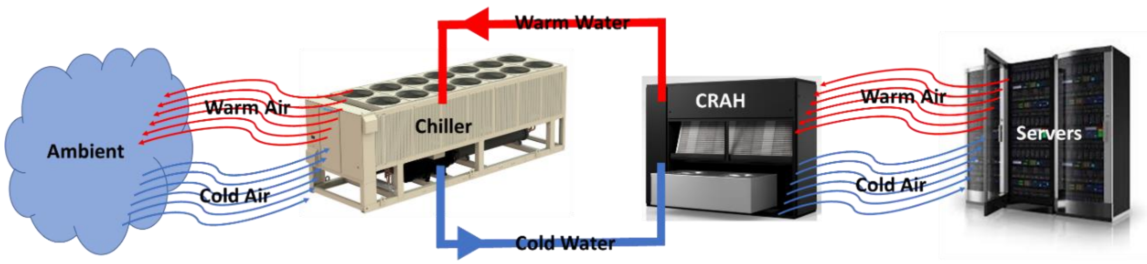

Figure 4-1: Heat dissipation route from the heat source to the ambient.

For a selected configuration, the primary energy consuming components include (1) server fans, (2) CRAHs blowers, (3) chilled water pumps and (4) the chiller. Item 1 is similar for the three architectures while item 3 consumes at most 3% of total cooling power [26] so that even for a 30% difference in water pumping power, the difference in total cooling power is less than 1%, which is negligible. Thus, we only compare items 2 and 4 above for room-, row-, and rack-based cooling.

To calculate the energy consumption of the CRAH blowers and the chiller, we must determine (1) total heat rejection from ITEs (assumed to be 200 kW), (2) total CRAH air flowrate and CRAH (3) setpoints, (4) return air temperatures and (5) chilled water flowrates, (6) chilled water temperature entering these CRAHs, and (7) the ambient air temperature. To compare the three cooling architectures, we consider the two scenarios presented in Table 4-1 with the restriction that all server intake air temperatures are lower than 26.5ºC.

Table 4-1**:** The two scenarios use to compare cooling architectures [27]–[30].

Scenario	CRAH setpoints	CRAH air flowrates	Maximum inlet air temperature of servers
1	Same for three architectures (17ºC)	Different for three architectures	26.5ºC
2	Different for three architectures	Same for three architectures	26.5ºC

Since the setpoint is specified for scenario 1, the CRAH air flowrates and their return air temperatures are determined using CFD. For scenario 2, the CRAH air flowrate, which is identical for the three architectures, the CRAH setpoints, and their return air temperatures are also determined with CFD. For both scenarios, the chilled water flowrates in the CRAHs and their water inlet temperatures are calculated using the $\varepsilon - NTU$ method by specifying the type and size of the heat exchanger inside these CRAHs. The room-, row-, and rack-based cooling architecture for the DC room case study are shown in Figure 4-2.

All configurations considered in this section are uncontained and there is no enclosure. The effect of enclosure and containment is considered in the later section.

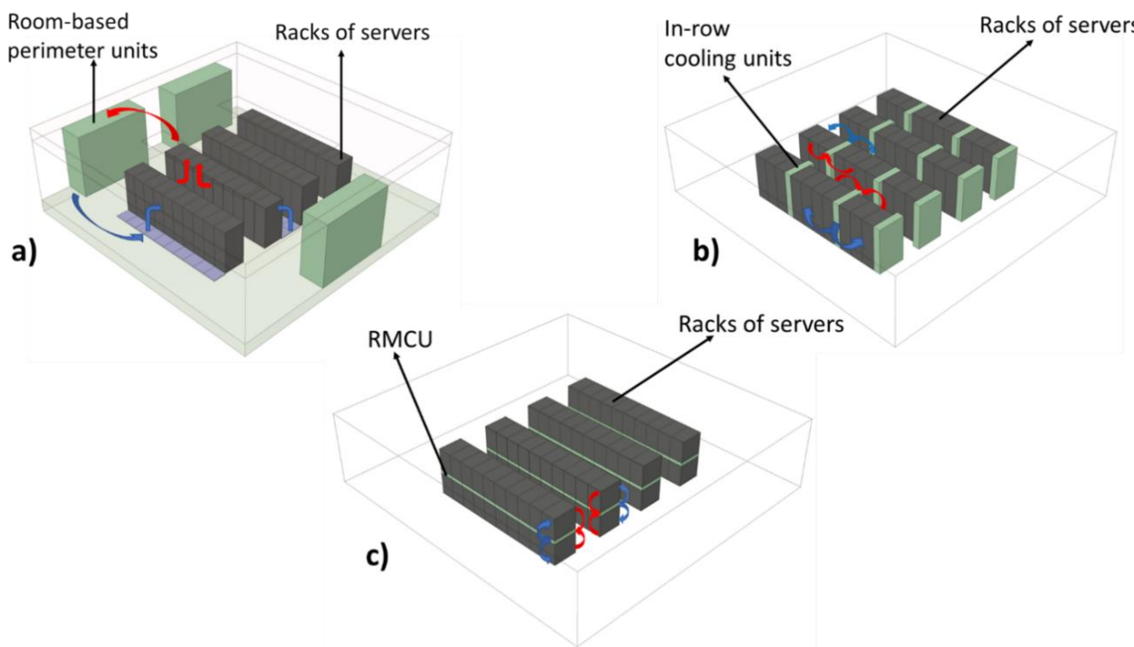

Figure 4-2: Geometry of three architectures for the case study DC room: a) room-based, b) row-based, and c) rack-based. All configurations considered in this section are uncontained and there is no enclosure.

4.3.1 CFD simulations

The CFD simulations are performed using ANSYS Fluent with the temperatures and turbulent flow field modeled through the energy equations and the realizable $k - \varepsilon$ model, which is the most commonly used turbulent model in data center modeling [31]–[36]. A grid independence analysis is performed to ensure the minimum node count required for accuracy. Three meshes, coarse, medium, and fine, are investigated with node count of 1.6 million, 2.3 million, and 4.7 million, respectively. The fine mesh is selected for all the simulations based on the root mean square of the temperature differences for 43 monitoring points to be less than 1°C [37]. Whereas the IT load is included in the simulation, the heat load of the building, being a small fraction of the IT load, is neglected. The simulation for room-based cooling includes three CRAHs in a DC room that has a raised floor design. Cold air from the CRAHs passes through the underfloor plenum, entering the room through perforated tiles. We are aware of the additional momentum source when modeling perforated tiles [38]. In order to capture it, additional designated zones on top of the tiles with a height usually equaling that of the under-rack gap must be defined. The perforated tiles are modeled as porous zones to account for the resistance without introducing regions with a momentum source. Warm air exiting the servers returns to the CRAHs through the hot air plenum placed above the room. The racks are arranged in four rows. Each row consists of 10 racks with individual heat loads and airflows. The backs of two adjacent rows, from where hot air leaves the servers, are placed facing each other, leading to two hot aisles and three cold aisles. Each rack has an IT load of 5 kW distributed over 20 servers and an airflow rate of 0.39 m^3/s, where each server consumes 0.0195 m^3/s [39]. For row-based cooling, twelve CRAHs are employed in the DC room with three CRAHs per row. The cold air release from the CRAHs flows directly to the cold aisle through their front panels and draw in hot air from the hot aisle through their back panels. For rack-based cooling, each rack is equipped with a single CRAH, resulting in forty CRAHs in the DC room. The CRAHs release cold air directly in front of servers through their front panels and draw in hot air from the backs of the servers through their back panels. For all three cooling architectures, the IT load and airflow are similar for a server rack.

The racks are modeled using a recirculation boundary condition, which employs the first law of thermodynamics to determine the rack exhaust temperature based on a specified heat load and flow rate. Recirculation boundary condition is applicable when a specific amount of heat is removed by a volume that emulates a device whose airflow is known *a priori*. This type of boundary condition is implemented in pairs, i.e., for every recirculation inlet boundary of the domain, there is a recirculation outlet associated with it. The exhaust hot air temperature, which depends on the heating load and flowrate inside the domain as well as the temperature of the cold air supply, is obtained from the CFD simulations. Cooling units are modeled as mass flow inlets and pressure outlets for the cold air supply zones and return air zones, respectively. For the steady-state analysis, cooling air flow rates, rack flow rates, rack heat loads, and supply air temperatures are fixed. Uniform airflows are applied at the rack and cooling unit inlets and outlets to focus on the macroscopic analysis of the different data center cooling architectures. The clearance or gap between the bottom of the rack and the floor may cause air leakages if not properly sealed, and rack manufacturers apply various measures to ensure that this leakage is minimized [40]. Since the geometrical simplification omitting the under-rack gap region has widely accepted [31], [32], [34]-[37], we have followed the same approach to perform CFD simulations to conduct like-for-like comparisons. For containments, two-inch gaps between racks with depths equal to those of the racks are considered due to the noticeable pressure differences between the hot and cold containments. These gaps are modeled as porous zones (Figure 4-8) using the power-law model for the resistance,

$$dp = -C_0 |v|^{C_1},$$

Where dp denotes the pressure drop across the porous zone, $|v|$ the velocity magnitude, and *the* empirical coefficients $C_0=11$ and $C_1=1.15$ are determined from our experimental results.

To validate the accuracy of the CFD simulations, experiments are performed for one specific configuration [41]. The validation case comprises five IT racks and two in-row cooling units that are contained by an enclosure. The positions of the CRAHs and IT racks, IT load of each rack, CRAH air flowrate and their setpoints are presented in Figure 4-3. The deviation of CFD temperature predictions from experimental measurements is defined by $\delta = T_{CFD} - T_{EXP}$. Figure 4-4 demonstrates δ for various locations in the front and back chambers, for which the maximum values for the front and back chambers are 0.6ºC and 1.7ºC, respectively. This confirms the relevance and accuracy of the CFD simulations. The higher δ in the back chamber arises due to the obstructing cable bundles there, which are not considered in the simulations.

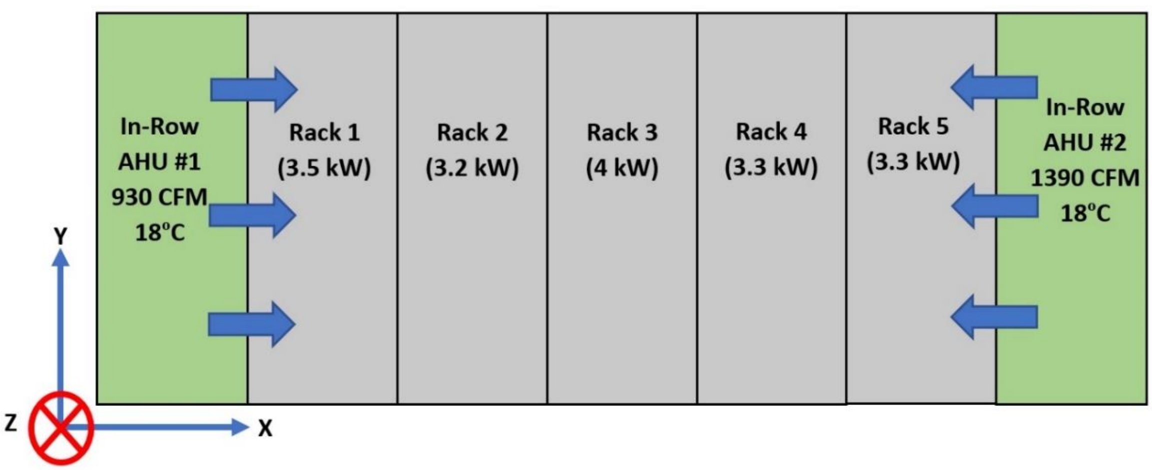

Figure 4-3: Configuration of the validation case (front view), including two CRAHs and five IT racks, IT load of each rack, air flowrate of the CRAHs and their setpoints.

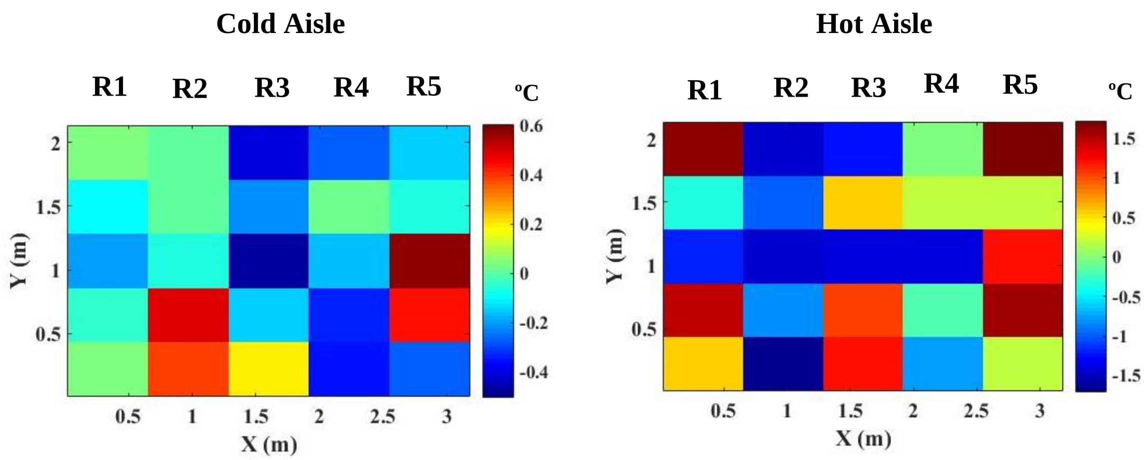

Figure 4-4: The values of δ at different locations in the front and back chambers.

4.3.2 Chilled water temperature and flowrate

After determining the air flowrate, supply air temperature, and return air temperature for each CRAH from the simulations, the chilled water characteristics, e.g., water flowrate and water inlet temperature can be calculated. CRAHs contain an air to water heat exchanger to extract the heat from the warm air. To calculate the required water flowrate and inlet temperature, the sizes of the heat exchangers, types of heat exchangers, and characteristics of heat exchanger fins must be known. Since optimization of heat exchanger size and fins for CRAHs would greatly increase the complexity of this study, we use fin characteristics and the sizes of heat exchangers that are currently available in the market. The required steady state water flowrate and inlet temperature are calculated using the $\varepsilon - NTU$ method. Heat exchanger details, such as size, fin type and water flowrate, are presented in Table 4-2. The water flowrate is specified based on available cooling units and the water inlet temperature is calculated with the $\varepsilon - NTU$ method [42], [43].

Table 4-2: Heat exchanger characterization [44],[45].

Architecture	Heat exchanger type	Heat exchanger size (m^3)	Water flowrate (m^3/s)
Room-based	Finned tube with *louvered fins*	0.20 × 1.50 × 2.25	0.0032
Row-based	Finned tube with *louvered fins*	0.20 × 0.70 × 2.00	0.0009
Rack-based	Plate-fin with *straight fins*	0.35 × 0.30 × 0.12	0.0004

4.3.3 Power consumption

The power consumed by the refrigeration system in the chiller is a function of the heat load at its evaporator, the temperature of fluid entering the condenser, the desired set point temperature of the water leaving the evaporator, and other operating and design parameters including the loading of the chiller with respect to its rated capacity. While there are several analytical models available in the literature to characterize chiller operation, the Gordon–Ng model is selected for its simplicity and ease since readily available data can fit model coefficients. The Gordon–Ng model has the form [26],

$$y = a_1x_1 + a_2x_2 + a_3x_3, \text{ where} \tag{4.1}$$

$$x_1 = T_{co}/Q_c, \tag{4.2}$$

$$x_2 = (T_{ci} - T_{co})/(T_{ci} \times Q_c), \tag{4.3}$$

$$x_3 = ([(1/COP) + 1] \times Q_c)/T_{ci}, \text{ and} \tag{4.4}$$

$$y = [(1/COP) + 1] \times (T_{co}/T_{ci}) - 1. \tag{4.5}$$

The COP, or coefficient of performance, is the ratio of the evaporator heat load to the electrical power consumption by the compressor, T_{ci}, and T_{co} denote the fluid temperatures in units of K entering the condenser and leaving the evaporator, respectively, and the chiller heat load expressed in kW is Q_c. Data for Q_c, COP, T_{ci}, and T_{co} are obtained from manufacturer test information for a s200 kW chiller [46] for the chiller model,

$$y = 0.05x_1 + 84.31x_2 + 0.072x_3. \quad (4.6)$$

Equation (4.6) allows us to determine the compressor power consumption once the total cooling load, evaporator temperature and condenser temperature are known.

Based on commercially available CRAHs, fans are selected for the three architectures, details for which are presented in Table 4-3. Manufacturer information is available for fan curves and fan power consumption in the form of data sheets that provide relations between power consumption, pressure drop, and air flowrate. The pressure drop across the heat exchanger inside the CRAHs can be determined based on the fin characteristics, air flowrate, heat exchanger size, and pressure drop correlations. Thereafter, using the fan data sheets, the total power consumption of the fans can be calculated.

Table 4-3: Fan characteristics [47]–[49].

Architecture	Number of fans per CRAH	Fan type	Section area (m^2)	Maximum air flowrate (m^3/s)
Room-based	3	EC backward curved	0.630 × 0.630	4.25
Row-based	5	EC backward curved	0.255 × 0.255	0.57
Rack-based	3	DC, Axial	0.130 × 0.130	0.24

4.4 Results and discussion

4.4.1 Airside parameters

The air flowrates required and the average return air temperatures for all cases are calculated from the CFD simulations and presented in Table 4-4. The results presented in this section are for uncontained architectures. For scenario 1, changing the architecture from room- to rack-based, the airflow required of the CRAHs decreases by 50% because the cold air path from the cooling unit to the ITE is shortened. The respective path lengths are (A) ~10 m, (B) ~1 m and (C) ~0.1 m. For case A-1, the air flowrate of the CRAHs should be increased to remove hot spots and maintain the inlet temperatures for all servers lower than 26.5ºC. Distributed cooling architectures (B-1 and C-1) require lower cold air flowrates.

For the second scenario, moving from room- to rack-based cooling allows the CRAH setpoint to increase by 5ºC. Since distributed cooling architectures require lower cold air flowrates, maintaining the same air flowrate for all architectures results in an oversupply of cold air for cases B-2 and C-2. This extra air flowrate produces higher pressures at server inlets than at their exhausts, eliminating recirculation. This increases bypass and produces a more uniform temperature profile in front of servers, eliminating undesirable hot spots, allowing higher CRAH setpoints, thus reducing cooling cost. Figure 4-5 demonstrates the differences in the required air flowrates and setpoints for the three cooling architectures.

Table 4-4: calculated air flowrates and temperatures by CFD for three architectures under two scenarios are presented.

Case	Scenario	Architecture	CRAH setpoint (ºC)	CRAH air flowrate (m^3/s)	Maximum air temperature at server's intake (ºC)	Average return air temperature to the CRAHs (ºC)
A-1	1	Room-based	17	26.6	26.5	23.4
B-1	1	Row-based	17	18.8	26.5	26.3
C-1	1	Rack-based	17	13.4	26.5	29.8
A-2	2	Room-based	15	18.8	26.5	24.3
B-2	2	Row-based	17	18.8	26.5	26.3
C-2	2	Rack-based	20	18.8	26.5	29.4

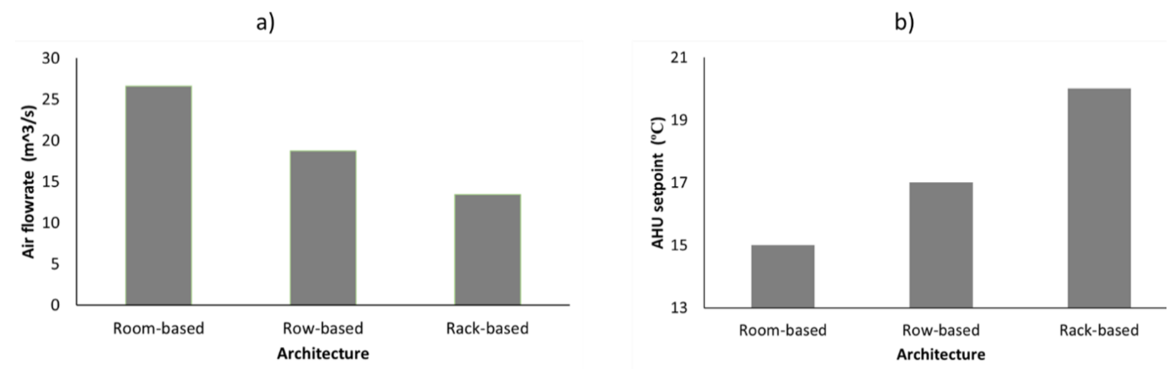

Figure 4-5: Comparison of the required air flowrate and setpoint to maintain the inlet air temperature of all the servers lower than 26.5ºC for the cases reported in Table 4-4. (a) Scenario 1 for same setpoints but different air flowrates. (b) Scenario 2 for same air flowrates but different setpoints.

Recirculation and bypass either lower or raise the air flowrate. Bypass occurs when a portion of the cold air exiting the cooling unit does not reach the servers. For instance, in open space, i.e., with no containment, the cold airflow from the cooling unit can be assumed to have the form of a jet [50]. If the jet does not expand significantly, it reaches the servers without entrainment, but this is of course not the case in practice. The more the entrainment the greater the bypass. The jet entrainment is a function of Re^{-1}[50]. For jet flow, an effective dimensionless number reflecting the amount of bypass is $\sqrt{\mu/\rho\bar{V}L}$, where ρ and μ are the density and dynamic viscosity of air respectively, $\bar{V}$ the jet velocity exiting the cooling unit, and L the distance from the jet source. We realize that this is an approximation since the cold airflow of the cooling unit can be considered as a jet only for open spaces with no containment.

In addition to jet entrainment, the bypass is influenced by the ratio of the mass flowrate through the cooling unit $\dot{m}_{CU}$ and that through the servers $\dot{m}_{IT}$. The higher the value of $\dot{m}_{CU}$, the higher the bypass because there is more cold airflow that is not drawn by the ITEs. However, as $\dot{m}_{IT}$ increases, the ITEs draw more airflow, lowering bypass. The second dimensionless ratio influencing bypass is therefore $\dot{m}_{CU}/\dot{m}_{IT}$.

The third ratio includes the influence of geometry. As air travels from the cooling unit to the ITEs, the longer the distance L, the greater the possibility that the flow deviates in the form of bypass from a desired path. The cross section area of the server inlets is the target destination for the cold air stream. Thus, as server inlet cross section area are enlarged, the lower the bypass. Accordingly, the geometric dimensionless ratio is L^2/A_{IT}.

The fourth factor influencing bypass is the angle α between the normal vectors orthogonal to the cooling unit exhaust and the server inlet. When the cooling unit and servers are placed face to face in front of one another, $\alpha = \pi$ and bypass is minimized. The dimensionless angle between these normal vectors is assumed to have the form $\theta = (\alpha + 2k\pi)/(2k\pi + \pi)$, where k denotes a positive integer. Here, k is a tool to control the magnitude of changes of θ when α changes. This ensures that the influence of changes in θ does not surpass the influence of changes in other factors discussed above. We arbitrarily select a desirable value of k = 2. When the cooling unit and servers are placed in front of each other, this dimensionless angle equals unity and lower values indicate increasing misalignment between the cooling unit and servers.

In order to present a dimensionless number which can represent the influence of all of these parameters on bypass, we combine the above four dimensionless factors, i.e.,

$$B = \sqrt{\frac{\mu}{\rho \bar{V} L}} \times \frac{\dot{m}_{CU}}{\dot{m}_{IT}} \times \frac{L^2}{A_{IT}} \times \frac{(\pi + 2k\pi)}{(\alpha + 2k\pi)} \tag{4.7}$$

Lower values of B, which is inversely proportional to $Re = \mu/(\rho\bar{V}L)$ imply lower bypass. If the cooling unit exhaust is placed in front of the server entrance, or $L = 0$ and $\alpha = \pi$, there is no bypass. Bypass increases by increasing $\dot{m}_{CU}/\dot{m}_{IT}$. Changing the architecture from room- to rack-based cooling reduces B because L is considerably shortened. Other dimensionless indices are available in the literature, e.g., return heat index (RHI), rack cooling index (RCI), and recirculation index (RI), but all of these are based on the effect of recirculation and bypass and not on the cause of these effects [51]–[54]. Moreover, while these indices are based on the temperature distribution within the DC room, which in fact results from recirculation and bypass, Eq. (4.7) represents the causes of these phenomena.

Recirculation occurs when part of the hot air exiting the servers does not reach the cooling unit. It depends on $\dot{m}_{CU}$, $\dot{m}_{IT}$, cross section area of the cooling unit inlet A_{CU}, distance between the cooling unit inlet and server exhausts L', angle between the normal vectors orthogonal to the cooling unit entrance and the servers exhaust α', velocity of the jet emerging from the servers $\bar{V}'$, and ρ and μ. By applying the above methodology, the dimensionless number characterizing recirculation,

$$R = \sqrt{\frac{\mu}{\rho \bar{V}' L'}} \times \frac{\dot{m}_{IT}}{\dot{m}_{CU}} \times \frac{L'^2}{A_{CU}} \times \frac{(\pi + 2k\pi)}{(\alpha' + 2k\pi)} \tag{4.8}$$

Again, *R* is inversely proportional to *Re*. The lower the value of *R* the lower is the recirculation, but R increases with decreasing $\dot{m}_{CU}/\dot{m}_{IT}$, denoting the challenge for reducing bypass and recirculation simultaneously. Changing from room- to rack-based cooling reduces *R* because L' is shortened. Values of *B* and *R* for all six cases are reported in Table 4-5. To analyze the relative importance of R and B on energy consumption, we examine their influence on the CRAH air flowrate and setpoint, the two primary determinants of power consumption, as shown in Figure 4-6.

Table 4-5: Bypass Number *B* and Recirculation Number *R*.

Case	Scenario	Architecture	CRAH setpoint (ºC)	CRAH air flowrate (m^3/s)	*B* $(\times 10^9)$	*R* $(\times 10^4)$
A-1	1	Room-based	17	26.6	37	85
B-1	1	Row-based	17	18.8	25	45
C-1	1	Rack-based	17	13.4	5	18
A-2	2	Room-based	15	18.8	32	93
B-2	2	Row-based	17	18.8	25	45
C-2	2	Rack-based	20	18.8	6	11

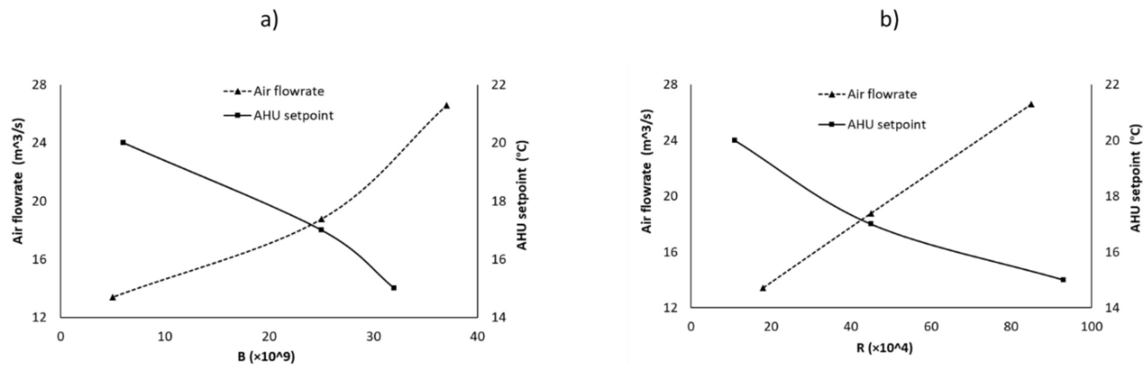

Figure 4-6: Influence of Bypass Number B and Recirculation Number R on the required CRAH air flowrate and setpoint. These two parameters are the primary determinants of power consumption.

4.4.2 Chilled water

The temperature of the chilled water entering the CRAHs, required to calculate chiller power consumption, is a function of the total heat transfer rate, return air temperature, supply air temperature or setpoint, air flowrate and water flowrate. Since these parameters are known, the water inlet temperature is calculated using the $\varepsilon - NTU$ method. The chilled water characteristics of the three cooling architectures are presented in Table 4-6.

For scenario 1, even though all cases have the same setpoint, the distributed cooling architectures implemented for cases B-1 and C-1 transfer heat with warmer chilled water, leading to lower cooling costs. Because the number of CRAHs required in distributed architectures is larger, this results in a higher total chilled water flowrate, improving cooling efficacy. Hence, the water inlet temperature can be increased, reducing chilling energy cost. For scenario 2, the water inlet temperature is different due to two reasons. First, the CRAHs have different setpoints which influence the required water inlet temperature and, second, the total water flowrates and heat exchanger types for the three architectures are different. To increase the efficacy of a room-based architecture and reduce cooling cost, one solution is to increase the required chilled water temperature by increasing the total water flowrate. However, there is a limit on the water flowrate inside a heat exchanger, particularly its piping loop.

Table 4-6: chilled water characterization of three cooling architectures.

Case	Scenario	Architecture	CRAHs setpoint (ºC)	CRAHs air flowrate (m^3/s)	Water temperature entering the CRAHs (ºC)	CRAHs water flowrate (m^3/s)
A-1	1	Room-based	17	26.6	7.4	0.0032
B-1	1	Row-based	17	18.8	9.8	0.0009
C-1	1	Rack-based	17	13.4	13.7	0.0004
A-2	2	Room-based	15	18.8	6.5	0.0032
B-2	2	Row-based	17	18.8	9.8	0.0009
C-2	2	Rack-based	20	18.8	16.5	0.0004

4.4.3 Power consumption

Based on Eq. (4.6) and Table 4-3, the power consumption of the chiller and the fans for the three cooling architectures are presented in Figure 4-7. For scenario 1, cases B-1 and C-1 provide up to 29% reduction in power consumption over case A-1. The rack-based architecture has the best efficacy. For all cooling solutions, the largest contribution to the power consumption is from the compressor in the chiller refrigeration cycle. For scenario 1, moving from room- to rack-based cooling, chiller power consumption decreases because the required water inlet temperature increases. The power consumption by fans for case A-1 is significantly higher than for other architectures because they must provide a higher 26.6 m^3/s air flowrate compared to cases B-1 and C-1 for which the flowrates are respectively 18.8 and 13.4 m^3/s. Although case C-1 has a lower air flowrate compared to case B-1, a similar amount of power is consumed in both cases because fan efficiencies measured as the volume flow per unit energy consumption decrease with a reduction in fan size [55]–[57]. For the same air flowrates, rack-based fans consume more power due to their smaller sizes. Furthermore, the size limitation of rack-based CRAHs leads to the requirement for a deeper heat exchanger. The pressure drop across it is consequently higher, resulting in a higher fan power consumption to draw in a specified air flowrate.

For scenario 2, cases B-2 and C-2 provide up to 12% reduction in the power consumption as compared to case A-2. The row-based architecture has the best efficacy. The differences in chiller power consumption for this second scenario are higher because the setpoints of the CRAHs are different and required water inlet temperatures, i.e., 6.5, 9.8, and 16.5 ºC, are markedly different for the three room-, row- and rack-based cooling architectures. Besides, fan power consumption for case C-2 is higher due to the use of smaller fans.

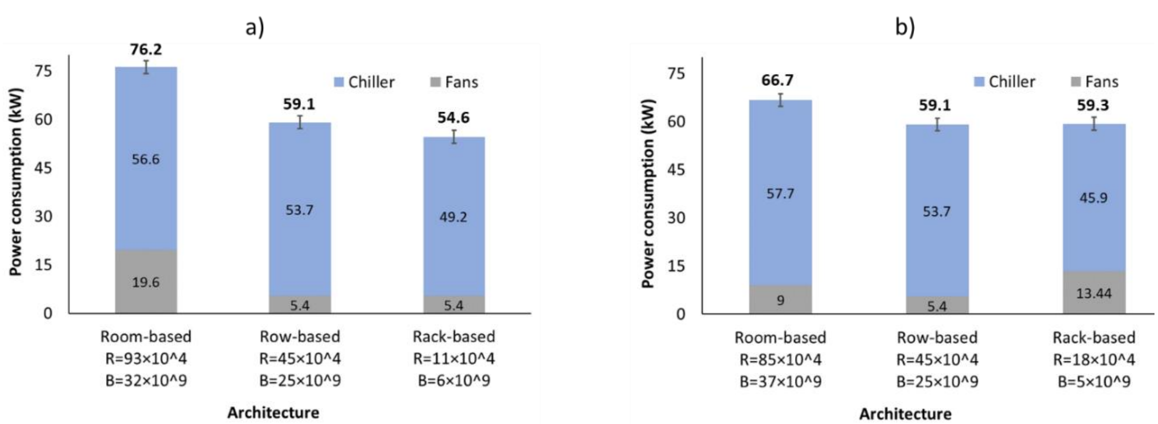

Figure 4-7: Comparison of power consumption for the three cooling architectures described in Table 4-6. (a) Scenario 1 for the same setpoints but different air flowrates. (b) Scenario 2 for the same air flowrates but different setpoints. The values of *R* and *B* for each case are presented to demonstrate their relative influence on power consumption.

4.4.4 Effect of containment

Containment isolates the hot air exhaust of the ITE from its cold air intake, providing an additional benefit for reducing recirculation regardless of architecture. Therefore, a distributed cooling architecture with containment is expected to be the most energy efficient configuration. We examine the power consumption of enclosed room-, row- and rack-based cooling to understand the influence of enclosures that separate the hot and cold airflows on power consumption. The geometries of the enclosed row- and rack-based cooling architectures for a case study DC room are shown in Figure 4-8. For the row and rack-based architectures, we assume that the front and back chambers are separated by placing dense commercially available brushes in gaps, which are modeled in Ansys Fluent as a porous media. While there are various methods for separating the hot and cold airflows for room-based architecture, we select “hot aisle containment” since it is a common configuration for room-based architectures [58]–[61].

The required air flowrates and setpoints for all architectures are presented in Figure 4-9. For Scenario 1, the required air flowrates for all three architectures are lower. Here, since the front and back chambers are separated, both recirculation and bypass are minimized. For the required airflowrate, the rack-based solution uses the minimum (12.5 m^3/s) while the room-based solution requires the maximum amount (15 m^3/s). Adding an enclosure reduces the required air flowrate by 46% for the room-based, 24% for the row-based and 8% for the rack-based cooling architecture compared to their values for open architecture. So, the maximum reduction in required air flowrate by adding containment is observed for room-based architectures.

By using an enclosure for scenario 2, the CRAH setpoint for all three architectures are improved. Adding enclosures that separate the chambers reduces recirculation and bypass resulting in more uniform temperature profiles in the front chamber and diminishing hotspot formation. Therefore, the difference between the setpoint temperature and the maximum server intake temperature decreases so that then the CRAH setpoint can be at a higher temperature. The rack-based solution has the highest setpoint (25.3 ºC) while the room-based solution has the lowest setpoint (22 ºC). The CRAH setpoints for room-, row- and rack-based architectures can be maintained at an additional 7, 8 and 5ºC higher, respectively compared to their values for open architecture.

To compare the three architectures, regardless of their cooling unit characteristics, such as fan size and heat exchanger type, we examine just the flowrates and setpoints shown in Figure 4-9. In general, we can conclude that, based on airflow characteristics, the rack-based architecture is best for eliminating bypass and recirculation. Comparing the power consumption required by these three architectures, we must consider their cooling units characteristics, which are different for each type of CRAH.

In essence, an enclosure that separates chambers reduces power consumption because of a lower required air flowrate and higher CRAH setpoint. The power consumption for all cases that are considered is presented in Figure 4-10. The best solution for Scenario 1 is rack-based cooling with an enclosure, while for Scenario 2 it is the row-based architecture within an enclosure. However, the rack-based cooling architecture could have the best efficacy for energy consumption if more energy efficient smaller fans were to become available.

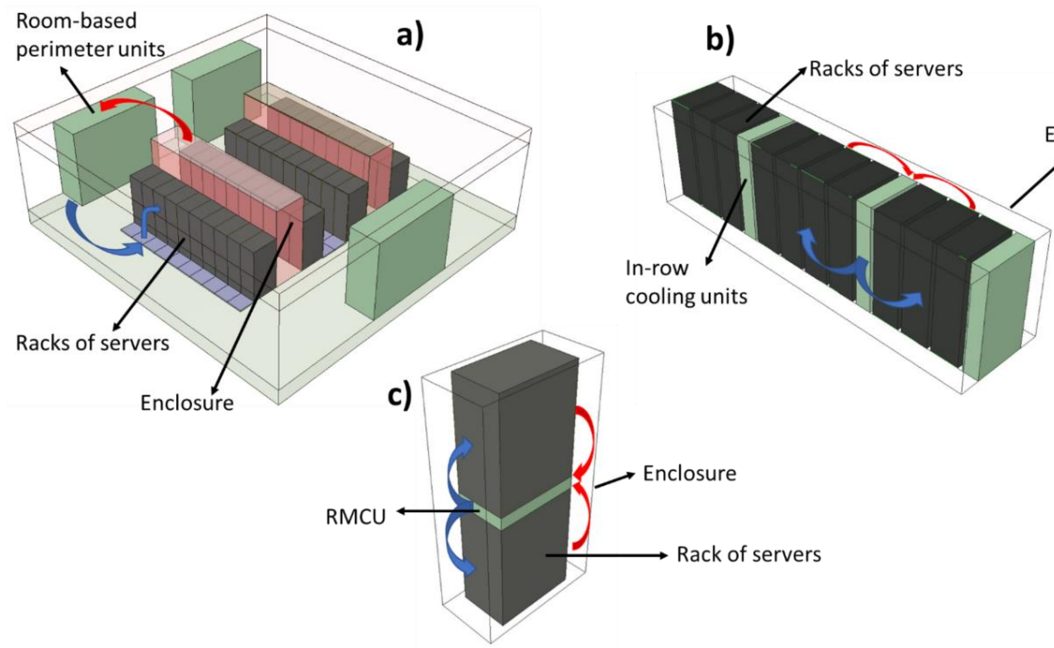

Figure 4-8: Geometry of three architectures that include enclosures for a case study DC room: (a) room-based architecture, (b) row-based architecture, and (c) rack-based architecture.

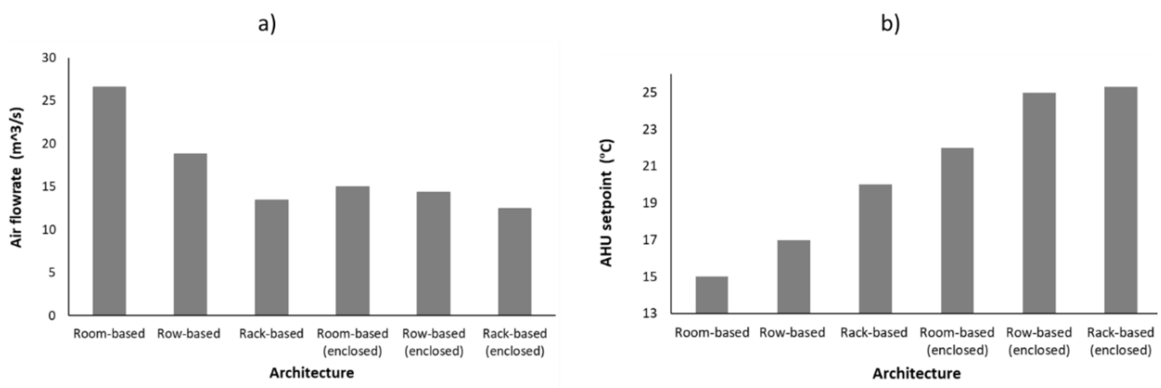

Figure 4-9: Comparison of air flowrates and setpoints for enclosed architectures with the open architectures for two scenarios. (a) Scenario 1 for same setpoints but different air flowrates. (b) Scenario 2 for same air flowrates but different setpoints.

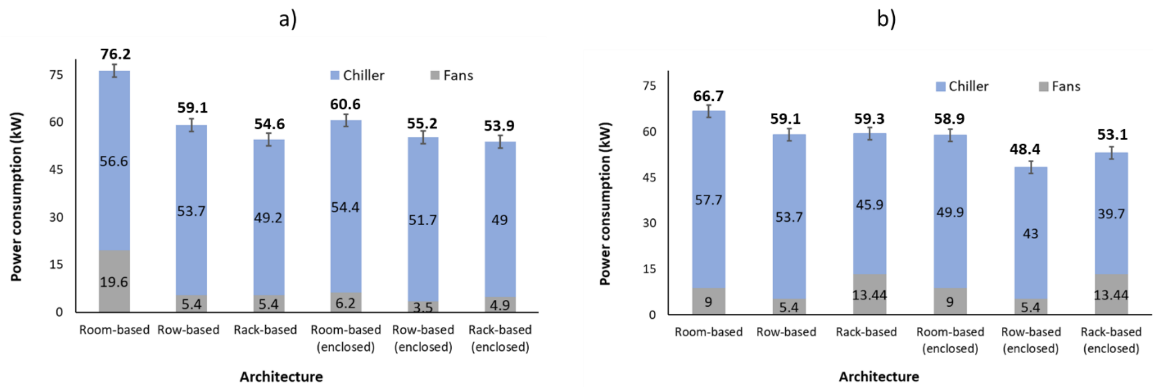

Figure 4-10: Comparison of power consumption for enclosed architectures with the open architectures for two scenarios. (a) Scenario 1 for the same setpoints but different air flowrates. (b) Scenario 2 for the same air flowrates but different setpoints.

We note that the power consumption calculations for the room- and row-based architectures are general and valid for common room- and row-based solutions, but the corresponding calculation for the rack-based architecture is valid only for rack mountable cooling units. We have selected rack mountable cooling units for the rack-based architecture for the following reasons: (1) This is the only rack-based solution which can fit within an isolated IT cabinet. Other possible rack-based configurations, such as rear door cooling, require air transfer to the room. Our motivation for the study is based on our interest in modular data centers, which do not allow any air transfer to the room. (2) Since our research is translational, our commercial collaborator (CINNOS) produces rack mountable cooling units. To be immediately helpful to industry, our intention is to compare the rack mountable solution with other cooling architectures. (3) The rack mountable cooling unit is a new solution for modular data centers. While not yet common, it has the potential for wider future use since it helps further overcomes the space limitations that make modular data centers desirable.

The dimensionless numbers presented in the previous section $\boldsymbol{B}$ and $\boldsymbol{R}$ are applicable for open environments, where jet-like airflows dominate, but not for enclosed environments. However, when there is containment, momentum is a lesser factor since there is a pressure driven flow through the resistances [62], [63]. A simplified mechanical resistance circuit for DCs with containment is illustrated in Figure 4-11. Obviously, this simplified circuit cannot represent all flow patterns of an enclosed DC, but it does show the basic flow for the three architectures with containment. The description of each resistance is provided in the figure caption.

If the air flows through the paths $R_2 \rightarrow R_3 \rightarrow R_4 \rightarrow R_5$, there is no bypass and recirculation, but if there is any airflow through R_1 there will be either bypass or recirculation. If the airflow through $R_1$is from the cold chamber to the hot chamber, there is bypass and if it is from the hot chamber to the cold chamber, there is recirculation. By increasing the quality of separation between the chambers by increasing R_1, the amount of bypass and recirculation are reduced.

Essentially, for an enclosed DC, the ratio $(R_2 + R_3 + R_4 + R_5)/R_1$ determines the intensity of bypass and recirculation. The implication of Figure 4-11 is that the rack-based architecture has lowest $(R_2 + R_3 + R_4 + R_5)/R_1$ while the room-based architecture has the highest.

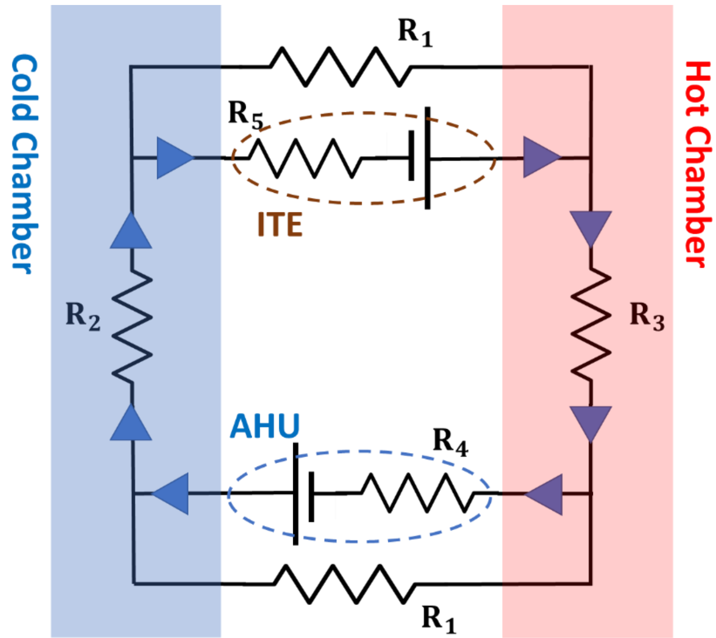

Figure 4-11: Simplified mechanical resistance circuit for DCs with containment. R1: The mechanical resistance due to the separation between the cold and hot chambers. R2: The mechanical resistance between the CRAH outlet and the ITE inlet. R3: The mechanical resistance between the ITE outlet and the CRAH inlet. R4: The mechanical resistance across the CRAH, mainly due to the heat exchanger. R5: The mechanical resistance across the ITE. The two power supplies are the fans inside the CRAH and the ITE.

4.5 Conclusion

We compare the power consumption of three DC cooling architectures. Row- and rack-based distributed cooling architectures are more energy efficient as compared to the conventional room-based architecture. Adding enclosures within distributed cooling architectures reduces their cooling cost further. These energy savings occur due to significant reductions in recirculation and bypass.

We find that, (1) for a constant temperature setpoint, distributed cooling architectures require up to a 50% lower cold air flowrate, (2) for constant airflow, distributed cooling architectures increase the CRAH setpoint by as much as 5ºC, (3) the dimensionless number *B* representing bypass decreases to one-seventh for the rack-based configuration as compared to room-based cooling, (4) the dimensionless number *R* representing recirculation decreases to one-ninth for rack-based cooling as compared to its value for the room-based configuration, (5) distributed cooling architectures enable an increase in the water temperature entering the CRAHs by 6ºC, (6) row- and rack-based architectures facilitates a 29% reduction in cooling power consumption, and (7) adding an enclosure within the distributed cooling architecture results in an additional 18% energy savings.

Beside improving energy efficiency, distributed cooling architectures, both row- and rack-based, have lower initial cost and are more easily maintained, with greater agility and manageability. Considering all of the above aspects, employing enclosed distributed cooling architectures is the best choice from a DC energy consumption perspective.

4.6 Acknowledgment

This research was supported by the Natural Sciences and Engineering Research Council (NSERC) of Canada under a collaborative research and development (CRD) project titled: Adaptive Thermal Management of Data Centers. We also thank our colleagues from CINNOS Mission Critical Incorporated who provided insight and expertise that greatly assisted the research.

4.7 References

[1] J. Dai, M. M. Ohadi, D. Das, and M. G. Pecht, "Optimum Cooling of Data Centers, Application of Risk Assessment and Mitigation Techniques", Springer Science Business Media, New York, 2014, DOI: 10.1007/978-1-4614-5602-5.

[2] K. Ebrahimi, G. F. Jones, and A. S. Fleischer, “A review of data center cooling technology, operating conditions and the corresponding low-grade waste heat recovery opportunities,” *Renew. Sustain. Energy Rev.*, vol. 31, pp. 622–638, 2014.

[3] H. M. Daraghmeh and C. C. Wang, “A review of current status of free cooling in datacenters,” *Appl. Therm. Eng.*, vol. 114, pp. 1224–1239, 2017.

[4] N. El-Sayed, I. A. Stefanovici, G. Amvrosiadis, A. A. Hwang, and B. Schroeder, “Temperature management in data centers: Why some (might) like it hot,” *Sigmetrics ’12*, no. TECHNICAL REPORT CSRG-615, pp. 163–174, 2012.

[5] M. K. Patterson, “The effect of data center temperature on energy efficiency,” *2008 11th IEEE Intersoc. Conf. Therm. Thermomechanical Phenom. Electron. Syst. I-THERM*, pp. 1167–1174, 2008.

[6] K. Dunlap and N. Rasmussen, “Choosing Between Room, Row, and Rack-based Cooling for Data Centers,” *Schneider Electr. White Pap. 130*, p. 18, 2012.

[7] J. Cho and B. S. Kim, “Evaluation of air management system’s thermal performance for superior cooling efficiency in high-density data centers,” *Energy Build.*, vol. 43, no. 9, pp. 2145–2155, 2011.

[8] J. Cho, J. Yang, and W. Park, “Evaluation of air distribution system’s airflow performance for cooling energy savings in high-density data centers,” *Energy Build.*, vol. 68, no. PARTA, pp. 270–279, 2014.

[9] S. V. Patankar, “Airflow and Cooling in a Data Center,” *J. Heat Transfer*, vol. 132, no. 7, p. 073001, 2010.

[10] N. Rasmussen, “The Different Types of Air Distribution for IT Environments”, White paper 55, APC By Scenider Electric.

[11] Z. Huang, K. Dong, Q. Sun, L. Su, and T. Liu, “Numerical Simulation and Comparative Analysis of Different Airflow Distributions in Data Centers,” *Procedia Eng.*, vol. 205, pp. 2378–2385, 2017.

[12] E. Pakbaznia and M. Pedram, “Minimizing data center cooling and server power costs,” *Proc. 14th ACM/IEEE Int. Symp. Low power Electron. Des. - ISLPED ’09*, p. 145, 2009.

[13] S. A. Nada and M. A. Said, “Effect of CRAC units layout on thermal management of data center,” *Appl. Therm. Eng.*, vol. 118, pp. 339–344, 2017.

[14] Z. Song, X. Zhang, and C. Eriksson, “Data Center Energy and Cost Saving Evaluation,” *Energy Procedia*, vol. 75, pp. 1255–1260, 2015.

[15] C. Lyu, G. Chen, S. Ye, and Y. Liu, “Enclosed aisle effect on cooling efficiency in small scale data center,” *Procedia Eng.*, vol. 205, pp. 3789–3796, 2017.

[16] H. . Rong, H. . Zhang, S. . Xiao, C. . Li, and C. . Hu, “Optimizing energy

consumption for data centers," *Renew. Sustain. Energy Rev.*, vol. 58, pp. 674–691, 2016.

[17] H. Hamann, M. Iyengar, and M. O'Boyle, "The impact of air flow leakage on server inlet air temperature in a raised floor data center," *2008 11th IEEE Intersoc. Conf. Therm. Thermomechanical Phenom. Electron. Syst. I-THERM*, pp. 1153–1160, 2008.

[18] S. Bhopte, D. Agonafer, R. Schmidt, and B. Sammakia, "Optimization of Data Center Room Layout to Minimize Rack Inlet Air Temperature," *J. Electron. Packag.*, vol. 128, no. 4, p. 380, 2006.

[19] K. Cho, H. Chang, Y. Jung, and Y. Yoon, "Economic analysis of data center cooling strategies," *Sustain. Cities Soc.*, vol. 31, pp. 234–243, 2017.

[20] A. Habibi and S. K. Halgamuge, "A Review on e ffi cient thermal management of air- and liquid-cooled data centers : From chip to the cooling system," *Appl. Energy*, vol. 205, no. March, pp. 1165–1188, 2017.

[21] C. D. Patel and A. J. Shah, "Cost Model for Planning , Development and Operation of a Data Center," *Development*, vol. 107, pp. 1–36, 2005.

[22] A. Capozzoli and G. Primiceri, "Cooling systems in data centers: State of art and emerging technologies," *Energy Procedia*, vol. 83, pp. 484–493, 2015.

[23] A. H. Beitelmal and C. D. Patel, "Thermo-fluids provisioning of a high performance high density data center," *Distrib. Parallel Databases*, vol. 21, no. 2–3, pp. 227–238, 2007.

[24] R. K. Sharma, C. E. Bash, C. D. Patel, R. J. Friedrich, and J. S. Chase, "Balance of Power: Dynamic Thermal Management for Internet Data Centers," *IEEE Internet Comput.*, vol. 9, no. 1, pp. 42–49, 2005.

[25] L. Silva-llanca, A. Ortega, and K. Fouladi, "Determining wasted energy in the airside of a perimeter-cooled data center via direct computation of the Exergy Destruction," *Appl. Energy*, vol. 213, no. January, pp. 235–246, 2018.

[26] M. Iyengar and R. Schmidt, "Analytical Modeling for Thermodynamic Characterization of Data Center Cooling Systems," *J. Electron. Packag.*, vol. 131, no. 2, p. 021009, 2009.

[27] Pelley, S., Meisner, D., Wenisch, T.F., Van Gilder, J.W. "Understanding and abstracting total data center power". In: Workshop on Energy Efficient Design (WEED), (2009).

[28] Schmidt, R., "Effect of Data Center Characteristics on Data Processing Equipment Inlet Temperatures", Proc. ASME Pacific Rim Technical Conf. and Exhibition on Integration and Packaging of MEMS, NEMS, and Electronic Systems Collocated with the ASME Heat Transfer Summer Conf., pp. 1097–1106, 2001.

[29] Schmidt, R., and Iyengar, M., "Effect of Data Center Layout on Rack Inlet Air Temperatures", Proc. ASME Pacific Rim Technical Conf. and Exhibition on Integration and Packaging of MEMS, NEMS, and Electronic Systems Collocated with the ASME Heat Transfer Summer Conf., pp. 517–525,2005.

[30] ASHRAE TC9.9 Mission Critical Facilities, Technology Spaces, and Electronic Equipment, Thermal Guidelines for Data Processing Environments, American Society of Heating, Refrigeration, and Air-conditioning Engineers, Inc., 2011. http://tc99.ashraetcs.org.

[31] Y. Fulpagare and A. Bhargav, "Advances in data center thermal management," *Renew. Sustain. Energy Rev.*, vol. 43, pp. 981–996, 2015.

[32] W. A. Abdelmaksoud, H. E. Khalifa, T. Q. Dang, R. R. Schmidt, and M. Iyengar, "Improved CFD modeling of a small data center test cell," *2010 12th IEEE Intersoc. Conf. Therm. Thermomechanical Phenom. Electron. Syst.*, pp. 1–9, 2010.

[33] C. Buratti, D. Palladino, and E. Moretti, "Prediction of Indoor Conditions and Thermal Comfort Using CFD Simulations: A Case Study Based on Experimental Data," *Energy Procedia*, vol. 126, pp. 115–122, 2017.

[34] B. Durand-Estebe, C. Le Bot, J. N. Mancos, and E. Arquis, "Data center optimization using PID regulation in CFD simulations," *Energy Build.*, vol. 66, pp. 154–164, 2013.

[35] N. M. S. Hassan, M. M. K. Khan, and M. G. Rasul, "Temperature monitoring and CFD analysis of data centre," *Procedia Eng.*, vol. 56, pp. 551–559, 2013.

[36] C. Gao, Z. Yu, and J. Wu, "Investigation of airflow pattern of a typical data center by CFD simulation," *Energy Procedia*, vol. 78, pp. 2687–2693, 2015.

[37] E. Cruz and Y. Joshi, "Inviscid and Viscous Numerical Models Compared to Experimental Data in a Small Data Center Test Cell," *J. Electron. Packag.*, vol. 135, no. 3, p. 030904, 2013.

[38] M. Seymour, S. Davies, "What is a Valid Data Center Model? An Introduction to Calibration for Predictive Modeling", Future Facilities' White Paper FFL-007 Revision 1.0

[39] H. Moazamigoodarzi, S. Pal, S. Ghosh, and I. K. Puri, "Real-time temperature predictions in IT server enclosures," *Int. J. Heat Mass Transf.*, vol. 127, pp. 890–900, 2018.

[40] Wan, J., Gui, X., Kasahara, S., Zhang, Y., & Zhang, R. (2018). "Air Flow Measurement and Management for Improving Cooling and Energy Efficiency in Raised-Floor Data Centers: A Survey". IEEE Access, 6, 48867–48901.

[41] W. A. Abdelmaksoud, H. E. Khalifa, T. Q. Dang, B. Elhadidi, and L. Hall,

"EXPERIMENTAL AND COMPUTATIONAL STUDY OF PERFORATED FLOOR TILE IN DATA CENTERS," *2010 12th IEEE Intersoc. Conf. Therm. Thermomechanical Phenom. Electron. Syst.*, pp. 1–10, 2010.

[42] R. K. Shah and D. P. Sekulic, *Fundamentals of Heat Exchanger Design*. John Wiley & Sons, 2003.

[43] E. Hochsteiner, D. V. Segundo, A. Levati, V. Cocco, and S. Coelho, "Thermodynamic optimization design for plate- fi n heat exchangers by Tsallis JADE," International Journal of Thermal Sciences., vol. 113, pp. 136–144, 2017.

[44] Product Data Sheet, *RITTAL*, CRAC Precision climate control units for data centres, Model Number:3300.387, 2014.

[45] Product Data Sheet, *RITTAL*, TopTherm LCP Rack/Inline CW, Model Number: 3311.130/3311.530, 2015.

[46] Product Data Sheet, *YORK*, Air-Cooled Scroll Chillers With Brazed Plate Heat Exchangers, Style: E, Model: YCAL.

[47] Product Data Sheet, *ebm-papst* , EC centrifugal fan, Model Number: R3G250-RO40-A9, 2012.

[48] Product Data Sheet, *ebm-papst* , EC centrifugal fan RadiPac, Model Number: R3G450-PI86 -01, 2016.

[49] Product Data Sheet, *Delta Electronics, Inc*, Model Number: THD1348HE, Specification for Approval, 2017.

[50] P. K. KUNDU, I. M. COHEN, and D. R. DOWLING, *FLUID MECHANICS*, FIFTH EDIT. Academic Press is an imprint of Elsevier.

[51] S. M. Hoseyni, B. Norouzi-Khangah, M. B. Mohammadsadeghi-Azad, and S. M. Hoseyni, "Performance assessment of cooling systems in data centers; Methodology and application of a new thermal metric," *Case Stud. Therm. Eng.*, vol. 8, pp. 152–163, 2016.

[52] M. K. Herrlin, "Rack cooling effectiveness in data centers and telecom central offices: The Rack Cooling Index (RCI)," *ASHRAE Trans.*, vol. 111 PART 2, pp. 725–731, 2005.

[53] R. Tozer, C. Kurkjian, M. salim, "Air management management metrics in Data Centers" *ASHRAE*, CH-09-009, 2009.

[54] J. VanGilder, S. Shrivastava, "Capture Index: an airflow-based rack cooling performance metric " *ASHRAE*, DA-07-014, 2007.

[55] T. Mathson and M. Ivanovich, "AMCA ' s Fan Efficiency Grades : Answers to Frequently Asked Questions." AMCA International, 2011. www.amca.org.

[56] "A closer look at fan eficciency Look", providing insights for today's HVAC system

designer, Engineering Newsletter. volume 43 –3 Trane, 2014.

[57] “AMCA Standard 205 , Energy Efficiency Rating for Fans,” Technical news, BULLETIN. No. 30. 2014.

[58] J. Niemann, K. Brown, and V. Avelar “Impact of Hot and C old Aisle Containment on Data Center Temperature and Efficiency”, White paper 135, APC By Scenider Electric.

[59] Y. Xu and Z. Gao, “Analyzing the Cooling Behavior of Hot and Cold Aisle Containment in Data Centers,” Fourth Int. Conf. Emerg. Intell. Data Web Technol., no. 2011, pp. 685–689, 2013.

[60] R. Zhou, Z. Wang, C. E. Bash, and A. Mcreynolds, “MODELING AND CONTROL FOR COOLING MANAGEMENT OF DATA CENTERS,” Proceedings of the ASME International Mechanical Engineering Congress & Exposition, 2011, USA.

[61] R. Schmidt, A. Vallury, and M. Iyengar, “ENERGY SAVINGS THROUGH HOT AND COLD AISLE CONTAINMENT CONFIGURATIONS FOR,” Proceedings of the ASME Pacific Rim Technical Conference & Exposition on Packaging and Integration of Electronic and Photonic Systems, 2011, USA.

[62] J. VanGilder, S. Shrivastava, “A FLOW-NETWORK MODEL FOR PREDICTING RACK COOLING IN CONTAINMENT SYSTEMS,” Proceedings of the ASME InterPACK Conference 2009, USA.

[63] J. W. Vangilder, “A Hybrid Flow Network-CFD Method for Achieving Any Desired Flow Partitioning Through Floor Tiles of a Raised-Floor Data Center,” pp. 1–6, 2019.

5 Performance of A Rack Mountable Cooling Unit in an IT Server Enclosure

This chapter is reproduced from *"Performance of A Rack Mountable Cooling Unit in an IT Server Enclosure", **Hosein Moazamigoodarzi**, Souvik Pal, Douglas Down, Mohammad Esmalifalak and Ishwar K. Puri, Published in Thermal Science and Engineering Progress, 2019.* The author of this thesis is the first author and the main contributor of this publication.

5.1 Abstract

Almost thirty percent of the power consumption in a data center (DC) is attributable to the cooling of IT equipment (ITE). This offers opportunities to reduce a DC's energy budget by considering alternatives to traditional cooling methods, such as perimeter or in-row air-conditioners, which suffer from inherent airflow deficiencies, e.g., hot air recirculation and cold air bypass. Due to these deficiencies, not enough cold air is supplied to the ITE, leading to hot spots that reduce equipment life significantly. Rack mountable cooling units (RMCUs), i.e., air-handlers mounted within the same enclosure containing the ITE, do not face this problem due to their proximity to servers. However, a proper understanding of airflow and temperature distribution inside an enclosure containing an RMCU has not yet been developed, preventing its widespread adoption. We investigate the temperature and airflow for various ITE configurations to determine the efficacy of an RMCU inside an enclosed rack. Experiments reveal that the principal factor influencing the temperature distribution is the leakage of warm air through passive servers, a hitherto unreported facet, which is dependent on the locations of these servers, IT load density and distribution, and

cold chamber depth. This is also illustrated through a neural network model. The results help us to devise a design strategy to optimize ITE configurations with desirable temperature distributions, and to inform server workload assignments.

Key words: Rack mountable cooling units – IT enclosure - flowrate mismatch - ITE configurations – warm air leakage – temperature distribution.

Nomenclature

DC	Data center	RMCU	Rack mountable cooling unit
ITE	IT equipment	RCI	Rack cooling index
SHI	Supply heat index	RTI	Return temperature index
RHI	Return heat index	P_c	Pressure of the cold chamber
ΔP_1	Pressure difference induced by RMCU	P_h	Pressure of the hot chamber
ΔP_2	Pressure difference induced by servers	R_1	Airflow resistance across the heat exchanger
R_3	Airflow resistance against the leakage flow	R_2	Airflow resistance across the servers
R_4	Airflow resistance against the vertical airflow in the cold and hot chambers	a	Depths of the cold chamber
$ASTD$	Active Server Temperature Distribution		

5.2 Introduction

US data centers (DCs) consumed about 70 billion kilowatt-hours of electricity in 2014, the most recent year examined, representing 2 percent of the country's total energy consumption [1]. At a minimum, the energy density for DCs is ten times that of residential or office buildings. Since all of the electrical energy consumed by the ITE is eventually dissipated into heat, the thermal management system must remove this heat from the DC and release it into ambient air [2]. About 30% or more of the energy consumed in DCs is typically used to cool IT equipment (ITE) through cooling systems that maintain their safe, consistent and reliable operation [3],[4]. The ITE must be maintained within a designed operating temperature range (18-27ºC). Overshooting a maximum specified temperature negatively impacts the operation and health of the ITE. High temperatures, particularly variations in those temperatures, reduce ITE life span [5].

DCs generally operate with air cooling systems that experience two significant air distribution problems, i.e., hot air recirculation and cold air bypass, which reduce the cooling efficiency [6],[7]. If the cold air supply to the ITE is insufficient, the hot air exhausted from servers is recirculated to the ITE inlets by the fans inside the servers, increasing the overall inlet air temperature. Bypass occurs when part of the cold airflow returns to the cooling unit without contributing at all to server cooling [8],[9]. Hence, to safeguard the ITE, the cooling airflow is typically set to two times the required amount, leading to an increase in cooling energy consumption [10], [11].

There are three conventional DC cooling architectures [11], [12], namely, (a) room-based cooling, where cold air is delivered directly to the room through arrangements such as raised floors and hot air return plenums, (b) row-based cooling, where the cooling unit delivers cold air to a row of racks, and (c) rack-based cooling, where the cooling unit is integrated entirely within a single IT rack. The cold air path from the cooling unit to the ITE shortens, where the respective path lengths are, (a) (~10 m), (b) (~1 m) and (c) (~0.1

m). Confinement, which isolates the hot air exhaust of the ITE from its cold air intake, reduces recirculation for all three approaches. Logically, therefore, a cooling unit placed in an enclosed rack with separated hot and cold chambers should be the most promising strategy for improving cooling effectiveness for the following reasons. First, while traditional cooling methods typically set the cooling airflow to two times that drawn by the ITE, while in the proposed solution the cooling airflow can be equal to or even less than the airflow drawn by the ITE, because recirculation and bypass are minimized. Hence, for a specific IT load, placing the cooling unit within an enclosed rack with separated hot and cold chambers lowers energy consumption. Second, the shorter cold air path from the cooling unit to the ITE results in a smaller pressure drop, requiring less energy to pump the air from the cooling unit to the ITE. Third, since the cold air path from the cooling unit to the ITE is shorter, any heat gain from the ambient to the cold air is minimized, improving efficiency. Finally, since the warm air path from the ITE to the cooling unit is also shorter, the heat loss to the ambient (or the ventilated spaces) is smaller, reducing the heat load elsewhere in the facility. This also increases the capacity of the heat exchanger because the cooling unit now receives warmer air.

A recent solution in rack-based cooling is the rack mountable cooling unit (RMCU) with dimensions similar to those of a server so that it can be conveniently mounted anywhere inside a rack [13]–[16]. All RMCUs integrated with an enclosed rack have four main parts: the air handler inside the enclosure, the servers, the cold and hot chambers. Mass and heat transfer between these parts are totally different from conventional DC environments. However, the RMCU has remained conceptual. Examples of practical implementations are unavailable in the literature, primarily due to a still poor understanding of the air supply management and cooling in a system that would integrate RMCUs and ITE in a confined rack. Instead, the discussion of airflow and cooling in DCs has been limited to room-based cooling architectures, mostly employing computational fluid dynamics (CFD) simulations. Use of CFD to examine the thermal behavior of DCs is well established, with examples including thermal performance assessment of air management and cooling systems [17], [18], investigating airflow uniformity through perforated tiles in raised floor DCs [19], studying the influence of airflow leakage on temperature distribution [20], and using CFD simulations as input datasets for artificial neural network training to optimize airflow and temperature distribution in DCs [21]**.** There are, however, few corresponding experimental investigations. The few that exist are for idealized DC environments, e.g., to ascertain whether heterogeneous temperature distribution can be controlled by varying the cold air flow rates along servers [22], determine the influence of aisle containment on bypass and power consumption [23], and investigating thermal management solutions performance for different arrangements of cold aisle containment [24].

The effect of airflow imbalance in a high-density DC has been experimentally and numerically investigated [25]. Different metrics, such as the rack cooling index (RCI), return temperature index (RTI), and supply heat index and return heat index (SHI/RHI) are used to evaluate cooling performance [8], [10], [18], [19], [26]. Various room-based arrangements and configurations to reduce recirculation and improve thermal efficiency have also been proposed [22], [27]–[29]. However, the understanding developed through these studies cannot be extended to rack-based cooling in an enclosed environment because of the very different transport dynamics induced by the geometry and configuration of an enclosed rack. Currently there are no studies on airflow and temperature distributions inside an enclosed rack employing RMCU with separated hot and cold chambers.

The central theme of this investigation is, therefore, to develop an understanding of airflow and cooling within a confined rack environment that employs RMCUs. This comprehension is essential for the IT community to efficiently manage workload without producing ITE hot spots. A popular proposition to reduce DC energy consumption is to turn off idle servers that do not perform any useful task but still generate heat. Herein, we hypothesize that those switched off, i.e., passive, servers will short circuit the thermal isolation within an enclosure, defeating its primary purpose and significantly increasing the probability of hot-spot formation. Experimental validations of this hypothesis are presented.

Our main goals are (1) explaining airflow, pressure and temperature distributions inside the enclosure, (2) exploring the consequences of passive servers on the temperature distribution and prescribing configurations, (3) characterizing how the transport and resulting temperature distribution at the intake and exhaust of the ITE are influenced by (a) positional variations of the ITE, (b) workload distribution, (c) IT load density, and (d) cold aisle depth, and (4) developing a steady state machine learning based temperature prediction tool for this architecture by using the available experimental datasets. The result of this study is not limited to this specific case and is applicable to the operation of any type of RMCU installed in any type of enclosed rack with separated hot and cold chambers.

5.3 Experimental Methods

An RMCU with 5 kW cooling capacity is designed and fabricated, and is schematically shown in Figure 5-1. The size of the unit corresponds to a $3U$ server (5.25×17.5×30 in^3). IT servers have specific heights: $N \times 1.75"$ $(N = 1,2, \dots , 6)$ and are categorized based on the value of N. Thus, the height of a $3U$ server is 5.25 in. The unit employs a heat removal module in the form of a plate-fin heat exchanger that transfers heat to a chilled water loop. Cold water for the RMCU is supplied from a building chilled water system. An IT rack containing 30 servers is prepared and installed within an enclosure with the RMCU mounted at the bottom. The hot and cold chambers in the rack are separated. Air inside the rack is confined, i.e., there is no air leakage from the rack to ambient or vice versa. Three groups of Maxim Integrated DS18B20 digital temperature sensors (with 0.5ºC accuracy) are mounted in the rack, the first group is placed immediately in front of the servers at their intakes (T_1), the second along the middle of the depth of the cold chamber (T_2), and the third along the middle of the lateral depth of the hot chamber. An Arduino Mega ATmega1280-based microcontroller is used to read temperatures. Each group of sensors is distributed across the height.

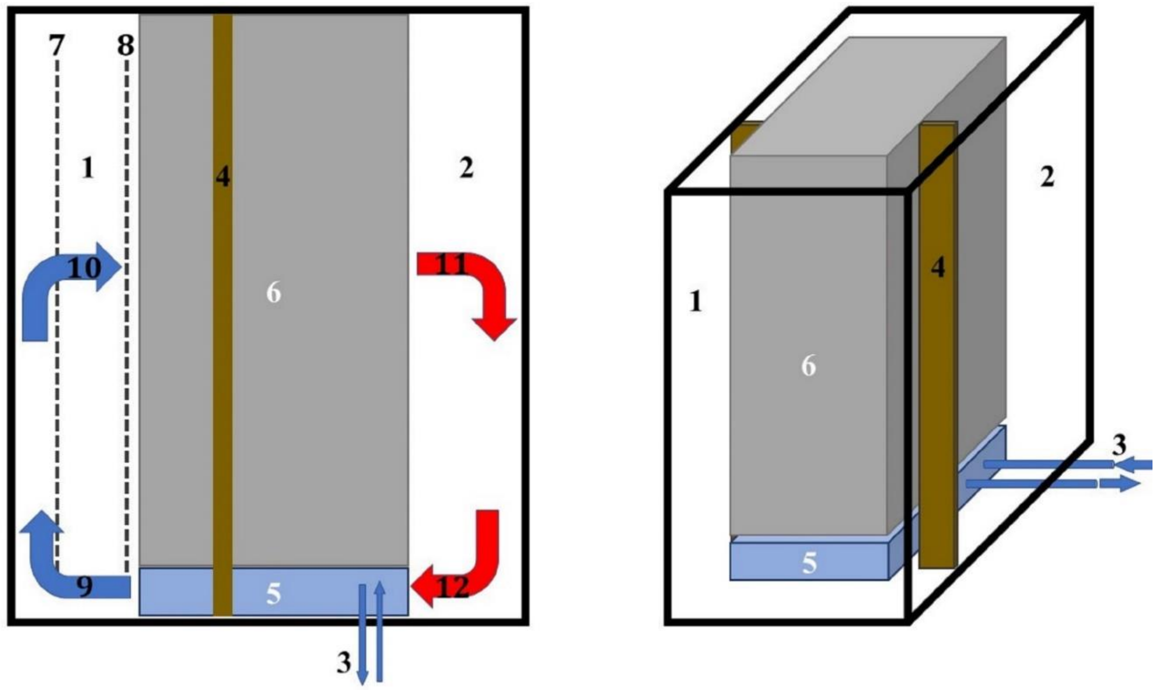

Figure 5-1: Schematic of the experimental setup. 1: cold chamber, 2: hot chamber, 3: water inlet and outlet pipes, 4: insulation between hot and cold chamber, 5: RMCU, 6: servers, 7: location of first group of temperature sensors, 8: location of second group of temperature sensors, 9: cold air exiting RMCU, 10: cold air entering servers, 11: warm air exiting servers, 12: warm air entering RMCU.

To measure the airflow through the RMCU and the servers, a Kanomax TABmaster™ 6710 Flow Capture Hood with 0.00235 m^3s^{-1} accuracy is used. A differential pressure sensor with an accuracy of 0.2 mm of water is deployed to detect the pressure difference between the cold and hot chambers across the height. A FLIR ONE Pro thermal camera records temperature contours for a specific area in the cold chamber. Servers are powered by a single phase 208 V power source. Since the control system within the RMCU is deactivated, its water and air flowrates are constant for all tests. The inlet temperature of cold water is 13ºC. The RMCU air and water flowrates are 0.18406 m^3s^{-1} and 0.00377 m^3s^{-1}, respectively.

The experimental procedure is as follows:

1. Flowrates in the RMCU and a sample server are measured in an unrestricted open space using the Flow Capture Hood.
2. 20 servers (4.9 KW) and the RMCU are turned ON. Then, the pressure difference at five different heights along the rack is measured.
3. Temperature sensors are mounted and connected to the Arduino.
4. Servers that are assigned to be active in each experiment are similarly loaded and the RMCU is activated.
5. After the rack system reaches a steady state, all temperatures are recorded.
6. One of the cases is repeated with the temperature sensors replaced by a thermal camera to record the temperature contour for a specific area in the cold chamber.

5.4 Results and discussion

5.4.1 Airflow, pressure, and temperature distribution in an enclosure

A schematic of the airflow in an RMCU enclosure is shown in Figure 5-2. In the cold chamber, the cold air flows from the bottom of the rack towards its top. There are two prime movers, the fans inside the RMCU and those in the servers. Server fans draw cold air from the cold chamber to the hot chamber, removing heat from the servers and transporting it to the hot chamber. The RMCU draws hot air from the hot chamber, extracts heat from it and then releases it to the cold chamber.

Warm air leakage from the hot chamber to the cold chamber is a function of the pressure difference between the two chambers, which is induced by the rack geometry and a mismatch between the flowrates of the two prime movers. The prime mover inside the RMCU increases the air pressure P_c at its exhaust, i.e., to the cold chamber, while the prime movers in the servers increase the pressure P_h at their exhausts, i.e., to the hot chamber. The actual pressures in the chambers are determined by a balance between these two competing effects along with the pressure drops along the flow directions in the respective chambers, as indicated in Figure 5-2. Thus, at any height in the enclosure, the pressure difference, $\Delta P = P_h - P_c$, determines the direction of leakage flow through the passive servers. If the flowrate from the RMCU is greater than the total flowrate through the servers, the resulting pressure difference ΔP is negative, i.e., cold air leaks through the servers to the hot chamber. However, this is of secondary concern, since, in this case, the entire cold chamber is at the supply air temperature of the RMCU, ensuring desirable cooling. Therefore, we only investigate the reverse scenario, when the total flowrate from servers is greater than from the RMCU, i.e., ΔP is positive, which leads to leakage of warm air into the cold chamber.

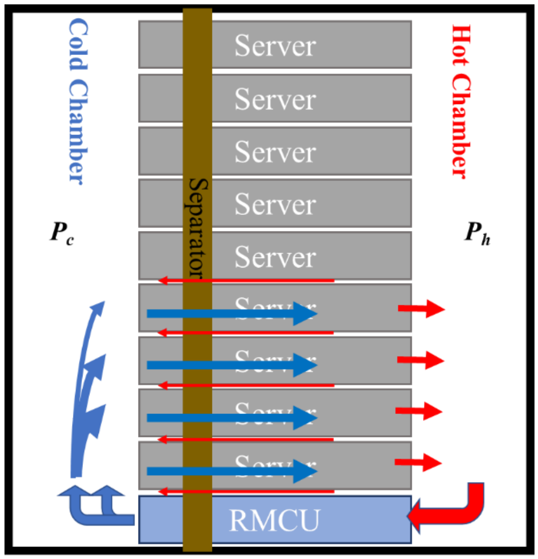

Figure 5-2: Schematic of the airflow distribution inside an enclosure. In the cold chamber (on the left), cold air exits the RMCU and is drawn in by the servers. In the hot chamber (on the right), hot air exits the servers and is drawn into the RMCU. There is leakage airflow from the hot to the cold chamber.

Due to this warm air leakage, the measured mean temperatures in the cold chamber for all experiments are between 22-25ºC, which are higher than the 17ºC supply air temperature from the RMCU. The local cold chamber temperature gradually increases at locations that are further removed from the RMCU. This temperature increase occurs due to two reasons, (1) the leaked warm air gradually mixes with the cold air stream, and (2) the air also gains ambient heat through the enclosure walls. The measured temperatures in the hot chamber are between 35-39ºC. The exhausts of the servers and the RMCU are respectively the hottest and coldest points in the two air chambers. All reported temperatures are at steady state, since the relatively rapid initial transients in the RMCU and enclosure are neglected. Temperature distributions at the server inlets and along the middle of the lateral depth of the cold chamber are presented hereafter, but only the average temperature of the hot chamber is reported since the temperature gradient there is negligible.

A simplified flow-resistance network for the airflow inside the enclosure is presented in Figure 5-3. For simplicity of illustration, just four active servers and two passive servers are considered in this diagram. The RMCU is considered as a power supply (ΔP_1) and the airflow resistance across the heat exchanger is assumed to be in series (R_1). Similarly, active servers are represented as a single power supply (ΔP_2) with an airflow resistance (R_2), but their power supplies (essentially, their fans) increase the pressure in the reverse direction. Passive servers are simply considered to be a resistance (R_2). Since separating the cold and hot chambers completely is unfeasible, there is usually airflow leakage between the chambers. The resistance against this airflow is the leakage resistance (R_3), which we assume to be distributed along the rack. The third airflow resistance in the enclosure lies along the height in the cold and hot chambers (R_4).

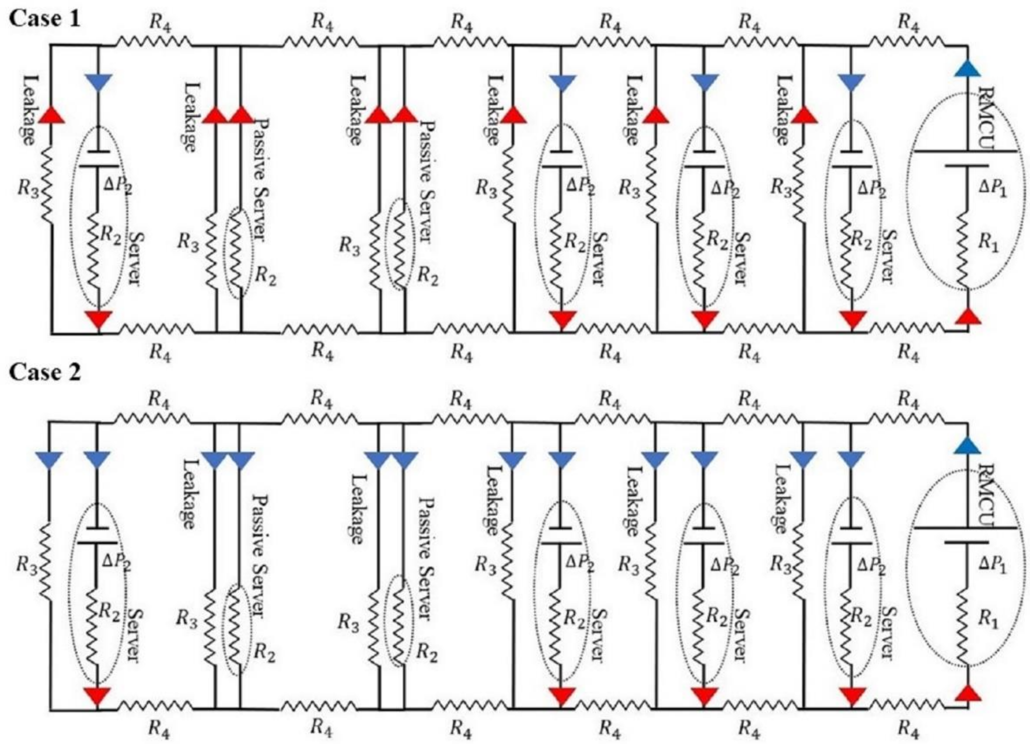

Figure 5-3: Simplified flow-resistance network inside the enclosure. Case 1: The total airflow through the active servers is greater than the RMCU airflow. Case 2: The total airflow through the active servers is lower than the RMCU airflow.

The airflows are functions of $\mathrm{R_1}$, $\mathrm{R_2}$, $\mathrm{R_3}$, $\mathrm{R_4}$, $\Delta \mathrm{P_1}$ and $\Delta \mathrm{P_2}$. Here, $\Delta \mathrm{P_1}$ is an order of magnitude larger than $\Delta \mathrm{P_2}$, $\mathrm{R_3} > \mathrm{R_1} > \mathrm{R_2}$. where these resistances are of the same order of magnitude, but $\mathrm{R_4}$ is much smaller than the other resistances because the characteristic dimension of the front chamber is an order of magnitude larger than the dimensions of the heat exchanger and server air channels. At a critical value of $\Delta \mathrm{P_1}$ ($\Delta \mathrm{P_1^c}$) there is a minimal airflow due to leakage and backflow through the passive servers. Table 5-1 shows two possible conditions for $\Delta \mathrm{P_1}$ that produce different airflows within the rack. Similarly, when $\Delta \mathrm{P_1}$ is constant, there is a critical value for the number of active servers ($\mathrm{N_s^c}$) that leads to minimum leakage and backflow, as shown in Table 5-2.

Table 5-1: Two possible conditions for pressure difference induced by RMCU.

Condition	The hot and cold chamber's pressure comparison	Airflow condition
$\Delta P_1 < \Delta P_1^c$	$P_{cold} < P_{hot}$	hot air recirculation through passive servers and leakages (Case 1, Figure 5-3)
$\Delta P_1 > \Delta P_1^c$	$P_{cold} > P_{hot}$	cold air bypass through passive servers and leakages (Case 2, Figure 5-3)

Table 5-2: Two possible conditions for the numbers of active servers.

Condition	The hot and cold chamber's pressure comparison	Airflow condition
number of active servers $> N_s^c$	$P_{cold} < P_{hot}$	hot air recirculation through passive servers and leakages (Case 1, Figure 5-3)
number of active servers $< N_s^c$	$P_{cold} > P_{hot}$	cold air bypass through passive servers and leakages (Case 2, Figure 5-3)

5.4.2 Effect of passive servers

Servers that are not powered cannot draw in air because their internal fans are not operating. These passive servers behave like porous ducts. Our first observation is the effect of these passive servers on the inlet temperatures of active servers and the average temperature of the cold chamber. To understand the influence of passive servers on the temperature distribution, two different configurations are investigated. In the first, the rack is occupied by a combination of active servers and blanking panels, the latter blocking airflow through unoccupied slots and maintaining isolation between hot and cold zones (Configuration 1 in Figure 5-4). In the second case, the blanking panels are replaced by passive servers (Configuration 2 in Figure 5-4). For both cases the IT load is 4.9 kW, which corresponds to 20 active servers. The temperature distributions recorded by sensor groups 1 and 2 for the two configurations are shown in Figure 5-4. The introduction of passive servers in the second configuration produces significant temperature increases at the inlets of active servers and in the cold chamber. The average temperatures of the hot chamber for Configurations 1 and 2 are 37.6 and 39.6ºC, respectively.

Passive servers behave as a porous medium**,** allowing warm air in the hot chamber to pass through backwards into the cold chamber, producing recirculation of the hot air to the cold side. Hence, replacing passive servers with blanking panels is recommended, but this is not possible when servers must be turned on/off in real time in response to varying IT load. The leakage, or recirculation, through the passive servers is induced by the pressure difference between the cold and hot chambers, which is produced by the mismatch between the flowrates of the RMCU and servers. The flowrates for a single server and the RMCU are 0.01415 m^3s^{-1} and 0.18406 m^3s^{-1}, respectively. Since 20 active servers are used in this test, there is a considerable mismatch between the airflow supplied by the RMCU and the total airflow demand for all servers, inducing a pressure difference across the cold and hot chambers, causing the leakage that leads to recirculation. This phenomenon has been hitherto unreported for the ITE contained in enclosed racks.

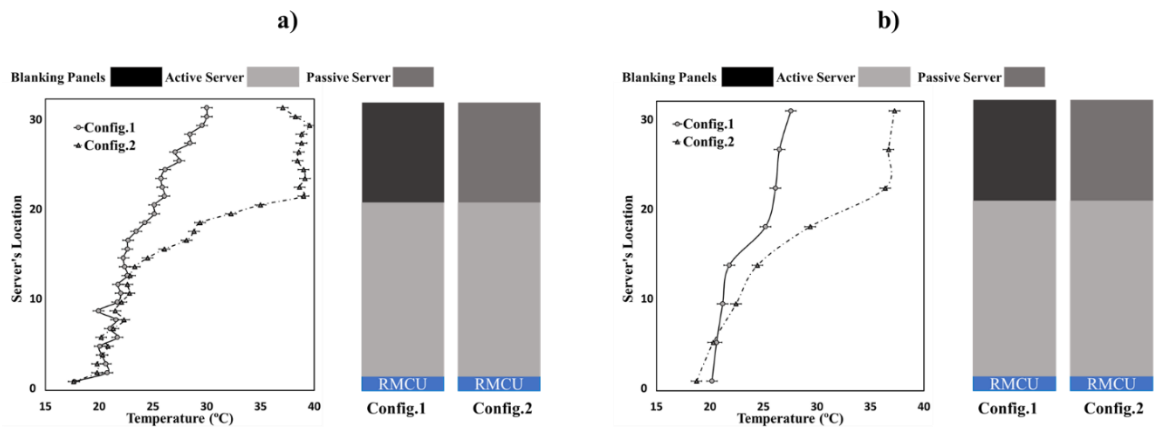

Figure 5-4: Temperature distributions at server inlets (a) and along the middle of the depth of the cold chamber (b) for two server configurations. Configuration 1: combination of active servers and blanking panels. Configuration 2: combination of active and passive servers. The total IT load for both configurations is 4.9 kW and active servers are located at the bottom.

Replacing passive servers with blanking panels increases the airflow resistance within the passive servers (R_2 in Figure 5-3), which results in lower hot air recirculation. In this case, the pressure difference between the hot and cold chambers increases and the mismatch between the RMCU and server flowrates decreases. Recirculation through passive servers does not depend on their location. This is confirmed by repeating the previous test, but by changing the locations of passive servers and blanking panels. Active servers are moved to the middle of the rack. The temperature distributions recorded by sensor groups 1 and 2 for the two configurations are presented in Figure 5-5. The average temperatures of the hot chamber for Configurations 1 and 2 are 38 and 38.8ºC, respectively. Figures 5-4 and 5-5 show that passive servers have essentially the same effect, i.e., they increase the inlet temperature of neighboring servers and the average cold chamber temperature, irrespective of their location.

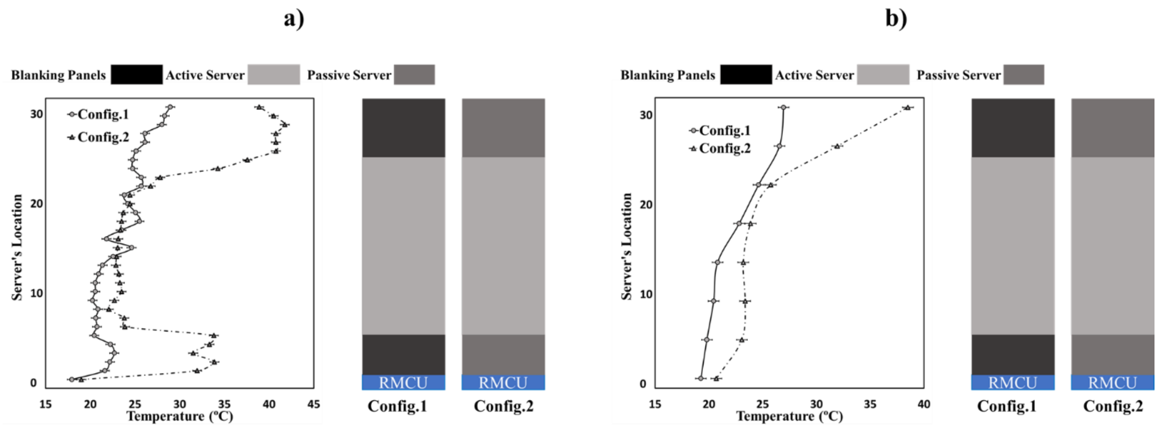

Figure 5-5: Temperature distributions at server inlets (a) and along the middle of the depth of the cold chamber (b) for two server configurations. Configuration 1: combination of active servers and blanking panels. Configuration 2: combination of active and passive servers. The total IT load for both configurations is 4.9 kW and active servers are located at the middle of the rack.

With traditional cooling methods, the cold airflow required to remove 1 kW heat load from the ITE is between 0.05663-0.08023 m^3s^{-1} [30], [31]. Our experiments show that use of an RMCU in an enclosed rack, lowers the required airflow to 0.03756 m^3s^{-1}, resulting in a reduction in energy consumption.

5.4.3 Airflow characterization through single passive server

The above experiments establish the presence of warm air recirculation through passive servers driven by a pressure difference across the cold and hot chambers. The average ΔP between the hot and cold chambers in Configuration 1 of Figures 5-4 and 5-5 is measured to be 9 Pa. To explore this further, experiments are performed to relate the airflow through a passive server and the pressure drop, results for which are presented in Figure 5-6. Based on this relation and the pressure difference across the chambers, the leakage flow through a passive server is evaluated to be 0.00377 m^3s^{-1}. Consequently, ~0.04147 m^3s^{-1} of warm air flows from the hot to the cold chamber, mixing with the cold air stream and forming hot spots, as observed in Figure 5-4.

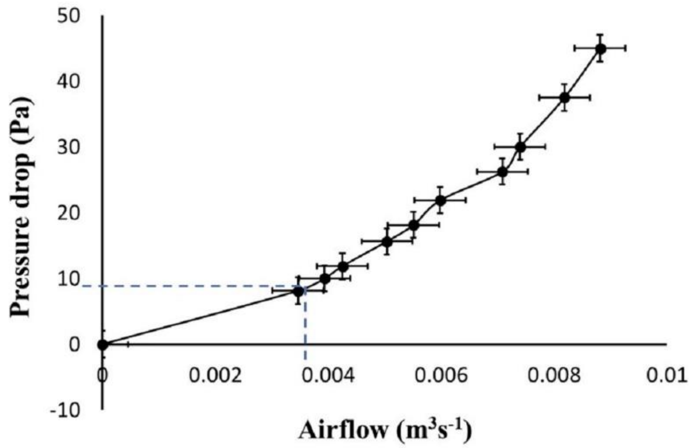

Figure 5-6: Relation describing the airflow through a passive server and pressure drop across it.

Configuration 2 of Figure 5-5-a reveals a rapid temperature change at the server inlets, the magnitude of which increases moving upward along the rack height. In contrast, the temperature distribution presented for the front chamber in Figure 5-5-b is monotonic, showing relatively small changes. The rapid local temperature increase at the inlets of passive servers is attributed to the leakage of warm air through them, forming a localized hot region. Nevertheless, cold air supplied by the RMCU can bypass this hot zone to reach those active servers that are placed above passive servers, while entraining air from the warmer zone, as shown in Figure 5-7. Here, since the warm leakage airflow (0.00377 m^3s^{-1}) is insufficient to impede the cold air flow, the temperatures at the inlets of the neighboring active servers increase. Further validation is obtained by mounting an FLIR ONE Pro thermal camera inside the cold chamber to record temperatures at the inlets of passive servers, which are presented in Figure 5-7. These temperature contours confirm that warm air leakage through passive servers influences the inlet temperatures of neighboring active servers but is not sufficiently dominant to increase the temperature along the middle of the depth of the cold chamber.

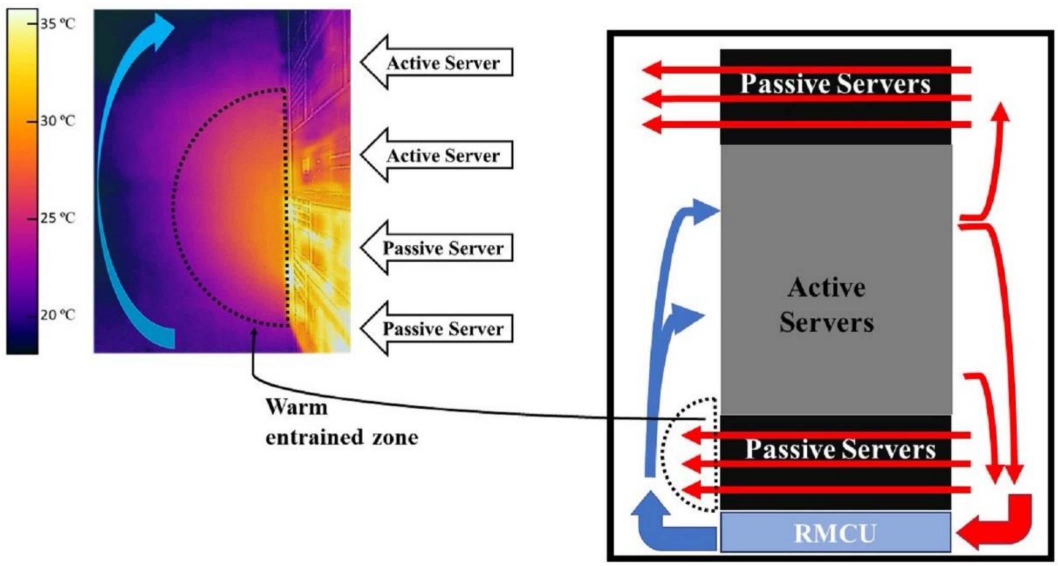

Figure 5-7: Schematic of the influence of passive servers on the airflow and temperature distribution (on the right) and temperature contour in the cold chamber obtained with a thermal camera (on the left). The contours correspond to Configuration 1 in Figure 5-5.

5.4.4 Effect of IT load density

Next, we investigate the impact of IT load density on the temperature distribution and airflow inside an enclosed rack that contains an integrated RMCU. Three configurations with different IT load densities are investigated, where the total IT load for all configurations is 3.4 kW but the number of active servers varies. The temperature distributions recorded by sensor groups 1 and 2 for three different IT load densities are presented in Figure 5-8. The number of active servers in Configurations 1, 2, and 3 are 9, 12, and 14, respectively, with average hot chamber temperatures of 31.9ºC, 31.9ºC, and 34.5ºC, respectively.

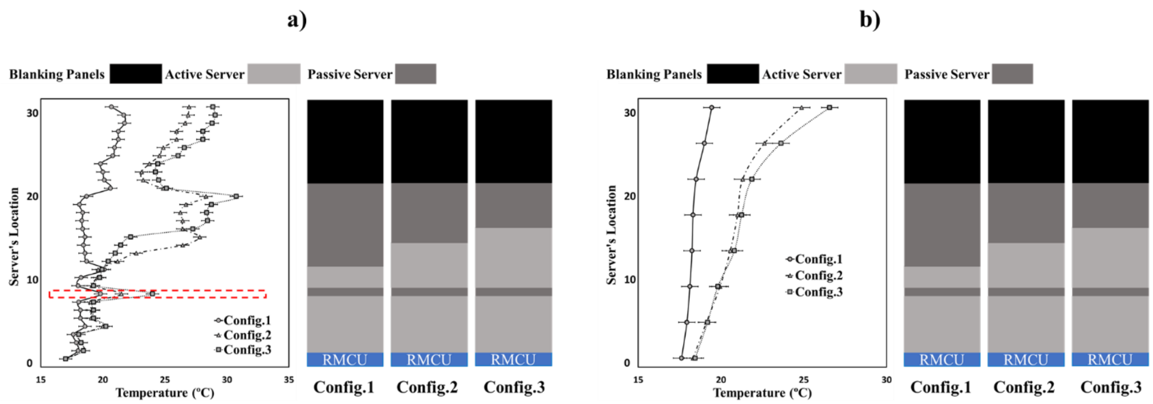

Figure 5-8: Temperature distributions at server inlets (a) and along the middle of the depth of the cold chamber (b) for three IT load densities. Configuration 1: highest IT load density with 9 active servers. Configuration 2: intermediate IT load density with 12 active servers. Configuration 3: lowest IT load density with 14 active servers. The total IT load for all three configurations is 3.4 kW.

Figure 5-8 indicate that the highest IT load density, when the same IT load is distributed among the lowest number of active servers leading to smaller overall air intake by these servers, results in a more uniform temperature distribution (Table 5-2). This reduction in server intake airflow produces a smaller airflow mismatch and thus a smaller pressure drop across the chambers. For Configuration 1, the total server airflow of 0.12742 m^3s^{-1} is lower than the RMCU airflow of 0.18406 m^3s^{-1}. Hence, there is no recirculation from the hot to cold chamber because the cold chamber is at a higher pressure. As the number of active servers increases, lowering the IT load density, recirculation occurs and increases with decreasing load density. In essence, the higher the IT load density the more uniform the temperature distribution. Configuration 3 of Figure 5-8 reveals that a single passive server does not influence its neighboring active servers since the warm airflow through a single passive server is insufficiently large to influence other active servers.

However, a group of passive servers can influence the inlet temperatures for a neighboring block of active servers.

Based on Figure 5-8, for a constant IT load, minimizing the number of active servers (or maximizing the number of passive servers) results in a more desirable temperature distribution, for which the number of active servers should be minimized. In order to minimize the power consumption, the number of active servers must again be minimized because turning on passive servers results in (1) increasing total IT power consumption, (2) increasing total system heat load which results in higher chiller power consumption, and (3) increasing the required cold air flowrate which increases fan power consumption. Table 5-3 provides a comparison of two scenarios. For Scenario 1, all servers are turned on. For Scenario 2, all idle servers are turned off. The power consumption to maintain the maximum intake temperature lower than 27ºC for both scenarios is reported in the table. For each scenario, the fan speed is first adjusted to keep the steady state temperature in front of the servers lower than 27ºC. Then, the RMCU fan power consumption and that for the chiller are measured at steady state. Table 5-3 shows that turning on passive servers not only does not save energy, but also results in more power consumption because typically idle IT servers (1) consume sixty percent of their maximum power consumption and (2) draw the same air flowrate as active servers.

Table 5-3: Effect on the power consumption of turning on passive servers. In both scenarios the intake temperature of all the servers is maintained to be lower than 27ºC. For Scenario 1, all servers are turned on. For Scenario 2, all idle servers are turned off.

Scenario	1	2
Number of active servers	14	10
Number of passive servers	0	4
Number of idle servers	4	0
IT power consumption (kW)	3.51	2.52
Fan power consumption (W)	540	420
Chiller power consumption (W)	875	625
Total energy consumption (W)	4925	3565

5.4.5 Effect of cold chamber depth

Because fluid flow resistance in the cold air stream is a function of the cold chamber depth, this depth also influences the temperature and airflow in an enclosed rack with an integrated RMCU. Hence, two different cold chamber depths are investigated to determine their influence on the temperature distribution. Both cases have identical IT loads and IT load distributions, and equal numbers of active servers. As shown in Figure 5-9, the depths of the cold chamber, denoted as a, are 19 cm and 13 cm for Cases 1 and 2, respectively, and the average temperatures of the corresponding hot chambers are 37.4 and 36.5ºC, respectively.

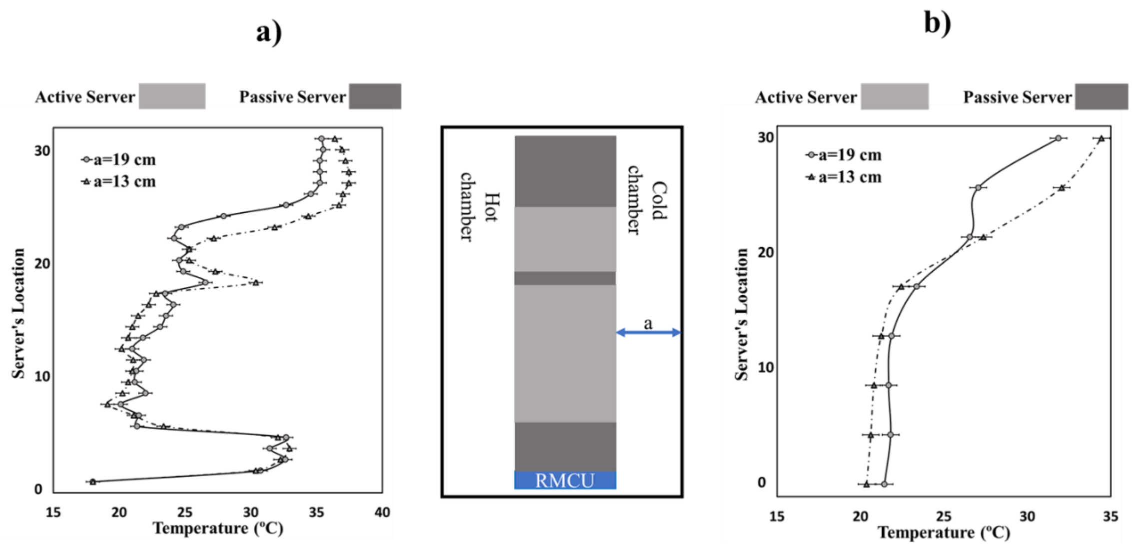

Figure 5-9: Temperature distributions at server inlets (a) and along the middle of the depth of the cold chamber (b) for two cold chamber depths. Case 1: cold chamber depth of 19 cm. Case 2: cold chamber depth of 13 cm. The total IT load for both cases is 4.9 kW and active servers are located at the middle of the rack.

For $a = 19$ cm, the average temperatures at the server inlets and the cold chamber are lower due to the smaller fluid flow resistance faced by the cold air stream exiting the RMCU. Figure 5-9 show that a larger cold chamber depth that lowers fluid flow resistance increases the cold air supply available to the top of the rack, reducing the local temperature there. In contrast, the smaller cold chamber depth offers higher resistance to the passage of the cold air, accumulating cold air at the bottom of the rack and thereby reducing the cold air supply to the top of the rack. Hence, as the depth of air passage is decreased during rack design, servers should be preferentially placed near the RMCU. As the depth of the cold chamber increases, passive servers have a diminishing influence on neighboring servers, resulting in more uniform temperature distributions. Increasing the cold chamber depth reduces the resistance against the airflow in the cold and hot chambers (R_4 in Figure 5-3), which results in a more uniform pressure along the rack height. Here, the cold air flowrate to the top server increases, and flowrates through the active server are more uniform.

5.4.6 Effect of IT load distribution

Since passive servers are a key determinant of the temperature distribution in the cold chamber, optimizing their location is important. We investigate scenarios for four IT load distributions, as shown in Figures 5-10 and 5-11, maintaining a total load of 4.9 kW with 20 active servers. The average temperatures of the hot chambers for Configurations 1, 2, 3 and 4 are 38.4, 37.8, 37.7 and 37.0ºC, respectively.

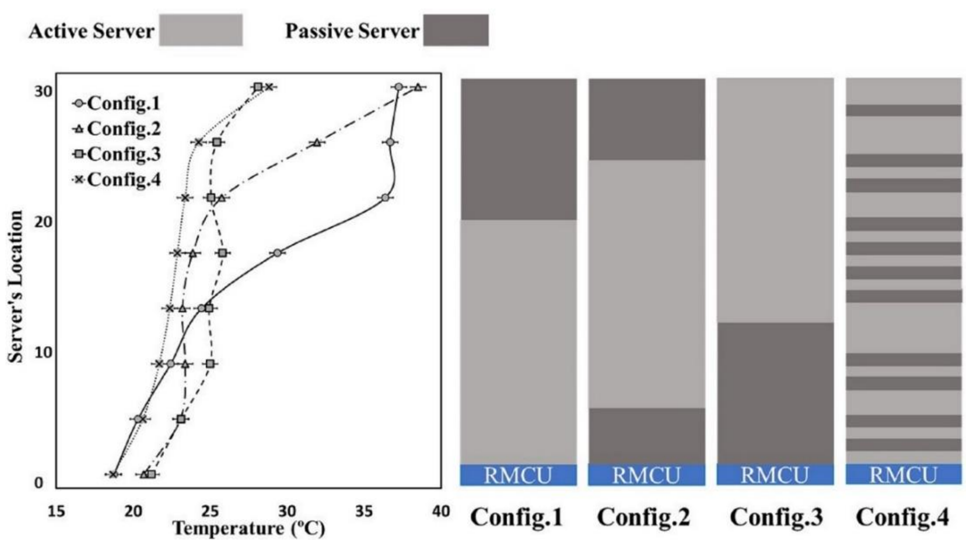

Figure 5-10: Temperature distributions along the middle of the depth of the cold chamber for four configurations. Configuration 1: IT load placed at the bottom. Configuration 2: IT load placed in the middle. Configuration 3: IT load placed at the top. Configuration 4: IT load distributed across the rack. The total IT load for all configurations is 4.9 kW.

Figures 5-10 and 5-11 reveal that, unlike the first two configurations, the distributed IT load for Configuration 4 and when the IT load is placed at the top of the rack (Configuration 3) both produce lower temperatures along the middle of the lateral depth of the cold chamber. When the IT load is distributed, the average temperature is lowest, and the cold chamber temperature does not exceed 36ºC. This is because the leakage airflow is now shared among all the distributed passive servers, resulting in spatially smaller warm zones (cf. Figure 5-7) that do not significantly influence their immediate neighbors. When the IT load is concentrated at the top of the rack in Configuration 3, a smaller number of active servers is influenced by the recirculation through the passive servers placed at the bottom of the rack. The smaller recirculation, i.e., smaller ΔP, can be attributed to a higher pressure at the RMCU exhaust. The best strategy to reduce recirculation is to place passive servers near the RMCU. Considering the cold chamber and server inlet temperatures, the worst configuration is when the IT load accumulates at the bottom of the rack because, in this case, passive servers are further removed from the RMCU and subjected to higher ΔP, resulting in higher backwards leakage that produces recirculation of the hot exhaust into the cold chamber. Accumulating the IT load in the middle is also undesirable because this creates two hot zones in the cold chamber, leading to a higher average temperature in that chamber.

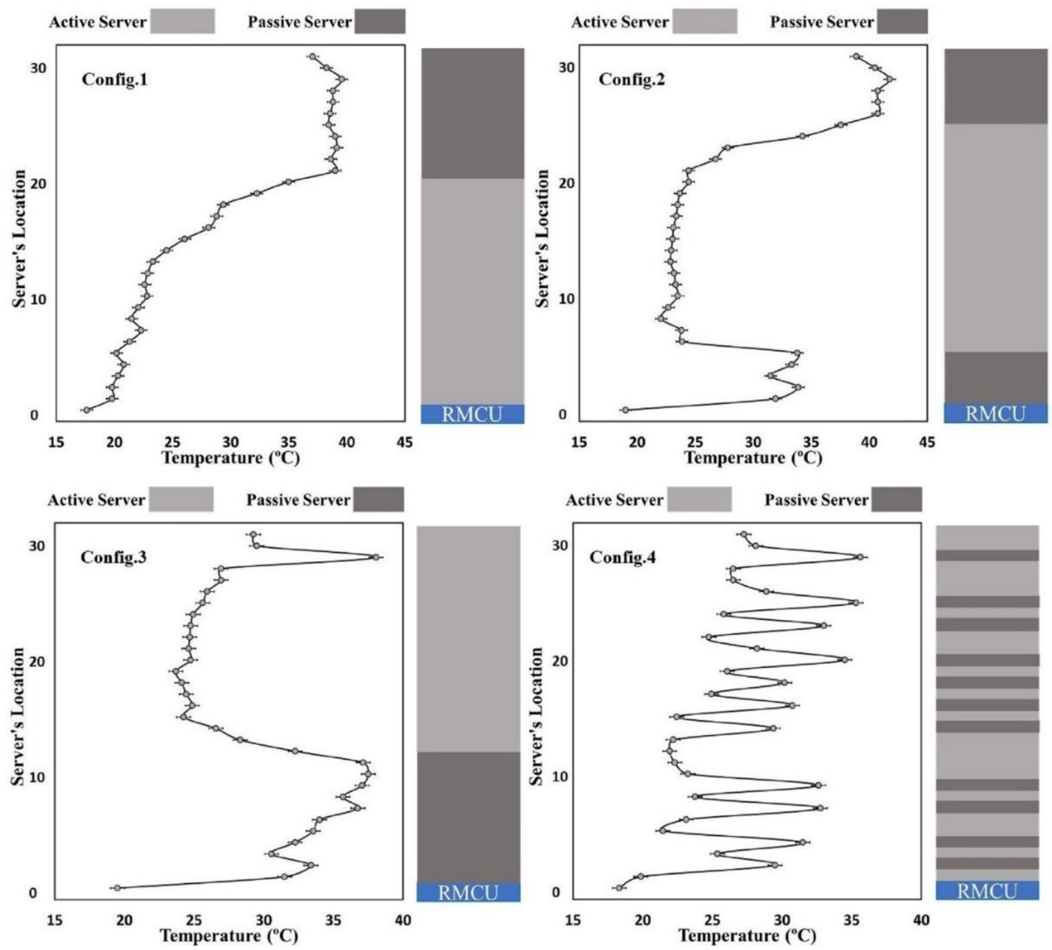

Figure 5-11: Temperature distributions at server inlets for four server configurations. Configuration 1: IT load placed at the bottom. Configuration 2: IT load placed in the middle. Configuration 3: IT load placed at the top. Configuration 4: IT load distributed across the rack. The total IT load for all configurations is 4.9 kW.

5.4.7 Quantitative Comparison of the Various Configurations

To this point, we have considered different ITE configurations and the resulting temperature distributions. A quantitative comparison of these configurations can be made by introducing a metric that scores the temperature distribution. The primary cooling requirement in a DC is to provide air to servers that is colder than a specific temperature. Additionally, a smaller temperature gradient along the height of the rack is desirable.

Therefore, our proposed metric, the Active Server Temperature Distribution, is based on the average temperature at the inlets of active servers $\bar{T}_{fa}$ and the standard deviation of active server inlet temperatures $\sigma_{T_{fa}}$,

$$ASTD = \bar{T}_{fa} + \sigma_{T_{fa}}.$$

The primary parameters that influence *ASTD* are the rack geometry and ITE configuration, e.g., number of active and passive servers, load density, cold chamber depth, presence of blanking panels and location of passive servers in the rack. The effects of different parameters on *ASTD* are presented in Figure 5-12. Distributing active servers along the rack lowers *ASTD*, a higher IT load density lowers it, replacing passive servers with blanking panels significantly improves the value of this metric, and larger cold chamber depths reduce it.

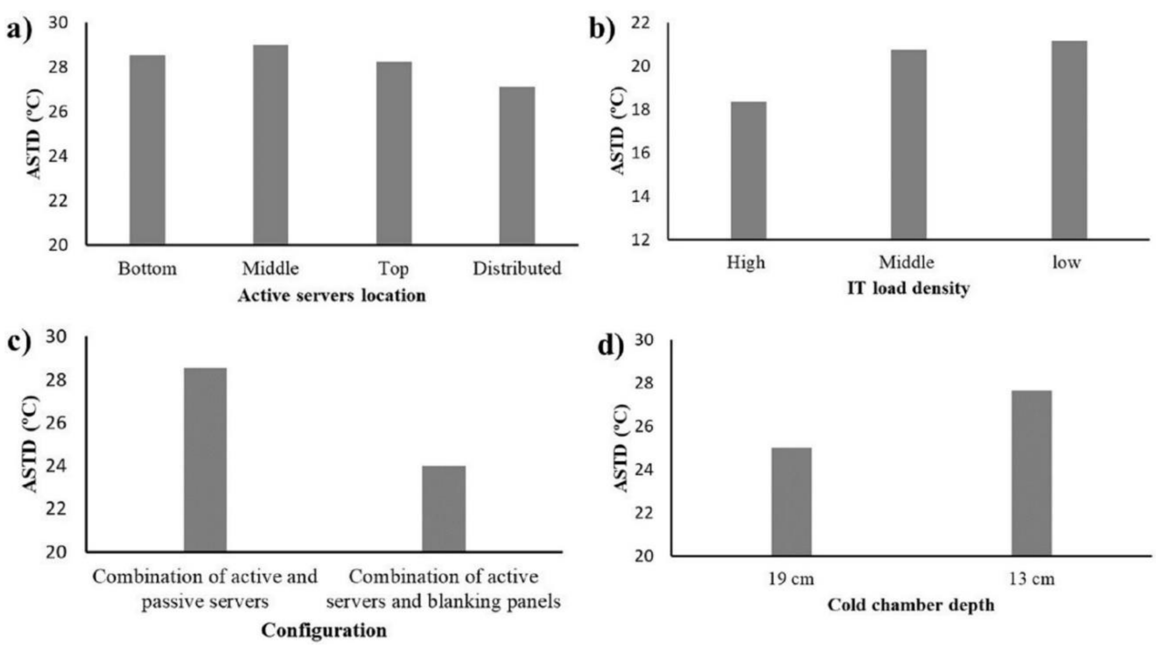

Figure 5-12: Effect of different parameters on ASTD. a) IT load distribution. b) IT load density. c) Passive servers and blanking panels. d) Cold chamber depth.

5.5 Conclusion

We investigate the temperature distribution and airflow inside an enclosed rack that is internally integrated with an RMCU. Experiments reveal effects due to passive servers, IT load density, IT load distribution and cold chamber depth that guide server configurations and rack geometry. A new metric, *ASTD*, is developed to assess RMCU performance. We find: (1) The amount of required cold airflow per unit IT load in the enclosed rack integrated with an RMCU is up to fifty percent lower than required cold airflow for traditional cooling systems. (2) Regardless of RMCU location, there is a temperature gradient in the cold chamber of an enclosed rack. (3) The pressure difference ∼10 Pa between the cold and hot chambers is a function of the server and RMCU flowrates. (4) Passive servers behave as porous ducts placed between the hot and cold chambers, allowing backward leakage of ∼0.00377 m^3s^{-1} of warm air from the hot chamber to the cold chamber. (5) Replacing passive servers with blanking panels provides a more uniform temperature distribution. (6) A higher IT load density is desirable, since it reduces the mismatch between the server and RMCU flowrates, leading to a more uniform temperature distribution. (7) A larger cold chamber depth results in lower fluid flow resistance for the cold airflow, leading to a more uniform temperature distribution in the cold chamber. (8) Distributing the IT load along the rack or accumulating it further from the RMCU produces a more favorable temperature distribution and reduces recirculation. (9) The *ASTD* based on the average temperature at the inlets of active servers and the standard deviation of active server inlet temperatures is a new and useful metric to evaluate RMCU performance in an enclosed rack.

This investigation proves the potential of placing an RMCU in an enclosed rack as a highly efficient cooling architecture, which requires almost 50% lower airflow as compared to traditional methods. However, to maximize the benefit, the system design and the server workload assignments must consider several factors that influence the leakage of warm air through the passive servers. This phenomenon has not been previously reported or investigated. In that context, we provide essential guidelines to optimize the ITE configuration based on a fundamental understanding of the airflow and temperature distribution inside an enclosure.

5.6 Acknowledgment

This research was supported by the Natural Sciences and Engineering Research Council (NSERC) of Canada under a collaborative research and development (CRD) project titled: Adaptive Thermal Management of Data Centers. We also thank our colleagues from CINNOS Mission Critical Incorporated who provided insight and expertise that greatly assisted the research.

5.7 References

[1] A. Shehabi, S. Smith, D. Sartor, R. Brown, M. Herrlin, “United States Data Center Energy Usage Report, LBNL-1005775”, BERKELEY NATIONAL LABORATORY, 2016.

[2] J. Dai, M. M. Ohadi, D. Das, and M. G. Pecht, "Optimum Cooling of Data Centers, Application of Risk Assessment and Mitigation Techniques", Springer Science Business Media, New York, 2014, DOI: 10.1007/978-1-4614-5602-5.

[3] K. Ebrahimi, G. F. Jones, and A. S. Fleischer, “A review of data center cooling technology, operating conditions and the corresponding low-grade waste heat recovery opportunities,” Renew. Sustain. Energy Rev., vol. 31, no. Supplement C, pp. 622–638, Mar. 2014.

[4] H. M. Daraghmeh and C.-C. Wang, “A review of current status of free cooling in datacenters,” Appl. Therm. Eng., vol. 114, no. Supplement C, pp. 1224–1239, Mar. 2017.

[5] N. El-Sayed, I. Stefanovici, G. Amvrosiadis, A. A. Hwang, and B. Schroeder, “Temperature management in data centers: Why some (might) like it hot,” Perform. Eval. Rev., vol. 40, Jan. 2012.

[6] “White Papers - WP 59 - The Different technologies for cooling data centers.” [Online]. Available: http://it-resource.schneider-electric.com/i/482944-wp-59-the-different-technologies-for-cooling-data-centers/1? [Accessed: 12-Oct-2017].

[7] J. Cho, J. Yang, and W. Park, “Evaluation of air distribution system’s airflow performance for cooling energy savings in high-density data centers,” Energy Build., vol. 68, no. Part A, pp. 270–279, Jan. 2014.

[8] A. Capozzoli and G. Primiceri, “Cooling systems in data centers: state of art and emerging technologies,” Energy Procedia, vol. 83, no. Supplement C, pp. 484–493, Dec. 2015.

[9] A. Capozzoli, G. Serale, L. Liuzzo, and M. Chinnici, “Thermal metrics for data centers: a critical review,” Energy Procedia, vol. 62, no. Supplement C, pp. 391–400, Jan. 2014.

[10] M. K. Patterson, “The effect of data center temperature on energy efficiency,” in 2008 11th Intersociety Conference on Thermal and Thermomechanical Phenomena in Electronic Systems, 2008, pp. 1167–1174.

[11] S. V. Patankar, “Airflow and cooling in a data center,” J. Heat Transf., vol. 132, no. 7, pp. 073001-073001-17, Apr. 2010.

[12] “White Papers - WP 55 - The Different types of air distribution for IT environments.” [Online]. Available: http://it-resource.schneider-electric.com/i/482974-wp-55-the-different-types-of-air-distribution-for-it-environments/7? [Accessed: 04-Nov-2017].

[13] “White Papers - WP 130 - Choosing between room, row, and rack-based cooling for data centers.” [Online]. Available: http://it-resource.schneider-electric.com/i/482320-wp-130-choosing-between-room-row-and-rack-based-cooling-for-data-centers/13? [Accessed: 04-Nov-2017].

[14] J. V. Smith, V. P. Hester, and W. A. Wylie, “Rack mountable computer component fan cooling arrangement and method,” US6801428 B2, 05-Oct-2004.

[15] R. J. Johnson, R. C. Pfleging, T. J. Anderson, and D. C. Kroupa, “Rack-mounted equipment cooling,” US6668565 B1, 30-Dec-2003.

[16] J. Smith, V. Hester, and W. Wylie, “Rack mountable computer component cooling method and device,” US20030221817 A1, 04-Dec-2003.

[17] J. Cho and B. S. Kim, “Evaluation of air management system’s thermal performance for superior cooling efficiency in high-density data centers,” Energy Build., vol. 43, no. 9, pp. 2145–2155, Sep. 2011.

[18] B. Norouzi-Khangah, M. B. Mohammadsadeghi-Azad, S. M. Hoseyni, and S. M. Hoseyni, “Performance assessment of cooling systems in data centers; Methodology and application of a new thermal metric,” Case Stud. Therm. Eng., vol. 8, no. Supplement C, pp. 152–163, Sep. 2016.

[19] J. W. VanGilder and R. R. Schmidt, “Airflow uniformity through perforated tiles in a raised-floor data center,” pp. 493–501, Jan. 2005.

[20] H. Hamann, M. Iyengar, and M. OBoyle, “The impact of air flow leakage on server inlet air temperature in a raised floor data center,” in 2008 11th Intersociety Conference on Thermal and Thermomechanical Phenomena in Electronic Systems, 2008, pp. 1153–1160.

[21] Z. Song, B. T. Murray, and B. Sammakia, “Airflow and temperature distribution optimization in data centers using artificial neural networks,” Int. J. Heat Mass Transf., vol. 64, no. Supplement C, pp. 80–90, Sep. 2013.

[22] S. A. Nada, A. M. A. Attia, and K. E. Elfeky, “Experimental study of solving thermal heterogeneity problem of data center servers,” Appl. Therm. Eng., vol. 109, no. Part A, pp. 466–474, Oct. 2016.

[23] M. Tatchell-Evans, N. Kapur, J. Summers, H. Thompson, and D. Oldham, “An experimental and theoretical investigation of the extent of bypass air within data centres employing aisle containment, and its impact on power consumption,” Appl. Energy, vol. 186, no. Part 3, pp. 457–469, Jan. 2017.

[24] S. A. Nada and K. E. Elfeky, “Experimental investigations of thermal managements solutions in data centers buildings for different arrangements of cold aisles containments,” J. Build. Eng., vol. 5, no. Supplement C, pp. 41–49, Mar. 2016.

[25] H. A. Alissa et al., “Analysis of airflow imbalances in an open compute high density storage data center,” Appl. Therm. Eng., vol. 108, pp. 937–950, Sep. 2016.

[26] “Servers and data centers energy performance metrics - ScienceDirect.” [Online]. Available:http://www.sciencedirect.com.libaccess.lib.mcmaster.ca/science/article/pii/S0378778814003594. [Accessed: 12-Oct-2017].

[27] D. W. Demetriou and H. E. Khalifa, “Energy modeling of air-cooled data centers: part I—the optimization of enclosed aisle configurations,” pp. 385–394, Jan. 2011.

[28] I.-N. Wang, Y.-Y. Tsui, and C.-C. Wang, “Improvements of airflow distribution in a container data center,” Energy Procedia, vol. 75, no. Supplement C, pp. 1819–1824, Aug. 2015.

[29] J. Rambo and Y. Joshi, “Modeling of data center airflow and heat transfer: state of the art and future trends,” Distrib. Parallel Databases, vol. 21, no. 2–3, pp. 193–225, Jun. 2007.

[30] “Airflow issues: silent enemy of efficient cooling,” Data Center Knowledge, 19-May,2011.Available:http://www.datacenterknowledge.com/archives/2011/05/19/airflow-issues-silent-enemy-of-efficient-cooling. [Accessed: 10-Nov-2017].

[31] “Current data center design,” slideblast.com. [Online]. Available: https: //slideblast.com/current-data-center design_595c74b21723dd37e515e0db.html.

6 Real-Time Temperature Prediction in IT Server Enclosures Integrated with RMCU

This chapter is reproduced from *"Real-Time Temperature Prediction in IT Server Enclosures", **Hosein Moazamigoodarzi**, Souvik Pal, Suvojit Ghosh and Ishwar K, Puri, Published in International Journal of Heat and Mass Transfer, 2018*. The author of this thesis is the first author and the main contributor of this publication.

6.1 Abstract

Current data center (DC) cooling architectures are inefficient due to (1) inherent airflow efficiencies and (2) their inability to spatiotemporally control cooling airflow and DC temperatures on demand. Rack-based cooling is a promising recent alternative since it provides more effective airflow distribution and is more amenable to rapid real-time control. A control scheme should be able to predict spatiotemporal temperature changes as the system configuration and parameters change, but a suitable method is not yet available. Existing approaches, such as proper orthogonal decomposition or machine learning are unsuitable because they require an inordinately large number of *a priori* simulations or experiments to generate a training dataset. We provide an alternative real-time temperature prediction tool which requires no *a priori* training for DC server enclosures into which a rack mountable cooling unit (RMCU) has been integrated. This new model is validated with experimental measurements and its applicability is demonstrated by separately evaluating the influence of varying IT server configuration, RMCU flowrate, step changes in system conditions, and interactions between multiple RMCUs. The resulting tool will

facilitate advanced control techniques and optimize design for any DC rack-based cooling architecture.

Key words: Rack mountable cooling units - Temperature prediction - Zonal method - Flowrate mismatch – Energy balance.

6.2 Introduction

A third of the energy provided to a conventional data center (DC) cools its IT equipment (ITE) [1]–[3]. Typically, traditional DCs use air cooling systems because of their relatively reliability, and lower capital and maintenance costs [4], [5]. Cooling units for delivering cold air are placed either along the server room perimeter or in-row along racks. These architectures contain two significant air distribution inefficiencies, i.e., hot air recirculation and cold air bypass [6]–[8]. Therefore, to protect the ITE, typically the provided cooling airflow equals two times the required amount [9].

To reduce redundant airflow, a rack-based cooling architecture that is integrated entirely within a single, IT rack is an alternative means for supplying cold air in close proximity to servers [10], [11]. A rack mountable cooling unit (RMCU) with dimensions similar to those of a server can be mounted conveniently inside a standard rack [12]–[14], considerably shortening airflow paths, lowering fan power and facilitating better airflow distribution [7], [11]. The shorter airflow path enables more rapid regulation of cooling in response to dynamically changing ITE demand. The faster cooling control eliminates large temperature fluctuations when there are rapid changes in IT load, significantly mitigating equipment failure [4]. However, this is possible only when control actions occur within a duration $t_e < \tilde{t}$, where the latter denotes the timescale over which significant DC thermal events occur. For realistic rack-based DC cooling, $\tilde{t} \sim 1$ s [15]–[17]. Real-time control in a rack mountable cooling architecture requires a rapid scheme to predict temperature. This is not yet possible since candidate methods, such as (1) proper orthogonal decomposition (POD), (2) machine learning, and (3) heuristic models, have limitations that prevent practical implementation.

Models based on POD and machine learning predict changes in DC temperature distribution faster than full-field simulations [18]–[21]. Machine learning methods to train model parameters are classified as black box or grey box. Black box approaches relate outputs, e.g., temperatures, to inputs through equations that ignore the flow physics [22]–[26]. In contrast, a grey box method considers some aspects of the physics while ignoring others. With both POD, and all machine learning approaches, empirical parameters must be trained using sample datasets that are obtained either from CFD simulations or experiments.

This poses two challenges. First, the development of training datasets that are statistically significant is nontrivial. Based on the numbers of input and output parameters, the corresponding number of simulations can easily range from $\sim 10^2$-10^3, requiring computational time of the order of days for typical 3D DC simulations, as well as dedicated access to supercomputing clusters. Performing so many specific experiments is also generally impractical. The second limitation of is that test data are similar to the training data. Hence, when the physical configuration differs from one used to obtain training data, the algorithms must extrapolate, which degrades performance and reliability.

In contrast, heuristic approaches express the physical behavior of the system through strategic simplifications of rigorous physical laws to predict air temperatures at discrete locations, such as server inlets and outlets [27]–[31]. However, simplification still requires empirical parameters. For instance, a rapid CFD and lumped capacitance hybrid model can predict server inlet temperature changes due to transient events, such as server shutdown, chilled water interruption, and failure of the computer room air handlers [29]. However, the model requires CFD simulations for each case to determine unknown parameters and index values. As another example, a three-dimensional pressurized zonal model for room-based cooling with a raised floor can be employed to predict the temperature distribution [28]. Here, the characteristic dimension is typically limited to ~ 1 m, which is too large to accurately predict temperatures at server inlets. Furthermore, the model requires information about mass flowrates through computationally expensive CFD simulations. In both examples, obtaining real-time temperature distributions is unfeasible.

Instead, we propose an original parameter-free transient zonal model to obtain real-time temperature distributions inside a typical DC IT rack that is contained within an enclosure cooled by an RMCU with separated cold and hot chambers. The model is based on mass and energy conservation relations for each zone within the enclosure. Because of its geometry, the flow field can be resolved using fluid mechanics principles, avoiding the need for CFD simulations, experiments or training of empirical parameters.

Our objectives are to (1) describe the application of the zonal transient model for a specific configuration, (2) validate the model with experimental results, (3) investigate the effect of RMCU operational parameters on the temperature distribution, (4) analyze the influence of IT load distribution on thermal performance, and (5) compare thermal performance when a single RMCU is used *versus* two RMCUs placed within the enclosure.

6.3 Methodology

6.3.1 System configuration

The zonal model is an intermediate method between full CFD simulations and multi-node lumped models to calculate temperatures. This method considers mass and energy transport in a space that is partitioned into a coarse number of zones to which conservation relations are applied. Physical quantities, such as temperature, are assumed uniform within a zone, eliminating spatial dependence. Hence, the partial differential equations for mass, momentum and energy conservation are reduced to a system of ordinary differential equations, significantly reducing solution time compared to CFD simulations. Various zonal models have been developed for HVAC and building energy management [28], [32]–[36].

The geometry and zones for a DC IT rack within an enclosure that is cooled by an RMCU are shown in Figure 6-1. Assuming no heat and mass transfer between the enclosure and the ambient, four control volumes are identified, i.e., (1) the cold chamber in front of each server, (2) the hot chamber at the back of each server, (3) each server itself, and (4) the RMCU. The RMCU is a heat removal module in the form of a plate fin heat exchanger that transfers heat to a chilled water loop supplied from an external chilled water system.

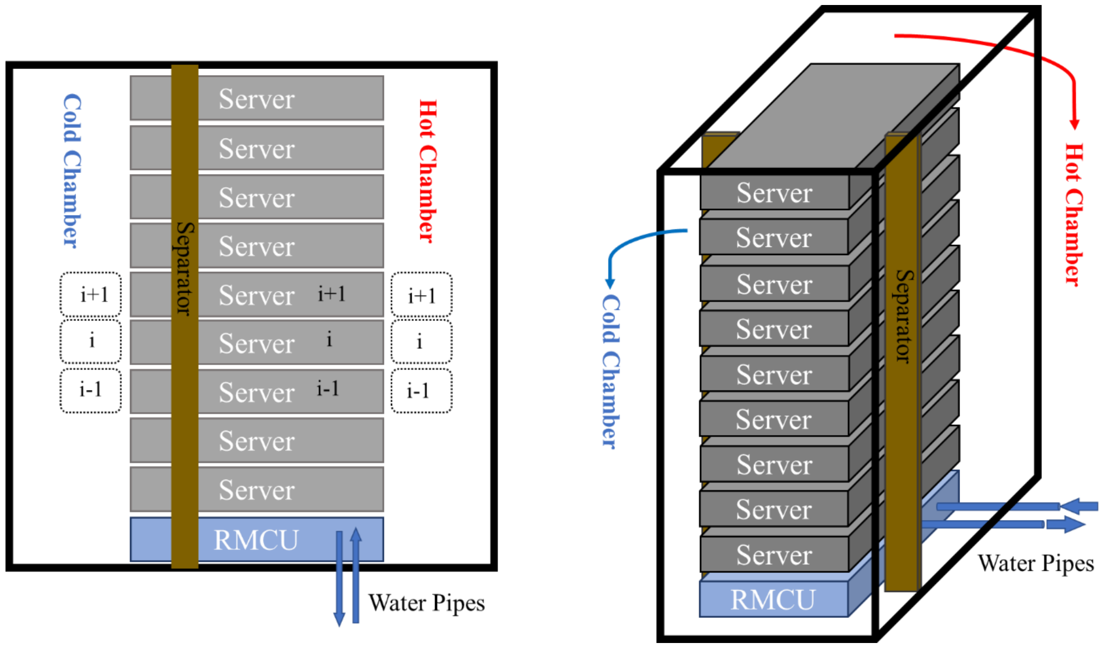

Figure 6-1: Schematic of the IT enclosure integrated with a single rack and an RMCU with separated cold and hot chambers. The zones (control volumes) in the front and back chambers are shown.

If the entering and exiting air flowrates for the zones are known, the energy balance for each zone can be solved. While a CFD simulation is required to determine the flowrates within a conventional DC room, for the architecture of Figure 6-1 these airflows are readily determined from mass conservation relations alone. Figure 6-2 depicts a schematic of the airflows within the enclosure, where there are two prime movers, the fans inside the RMCU and in the servers. Server fans draw in cold air from the cold chamber, remove heat from the servers and transport the warmer air to the hot chamber. The RMCU draws warm air from the hot chamber, extracts heat from it and releases cooled air into the cold chamber. A leakage airflow between the hot and cold chambers occurs due to the pressure difference between these two chambers $\Delta P = P_h - P_c$ induced by the rack geometry and mismatch between the flowrates of the RMCU and the servers.

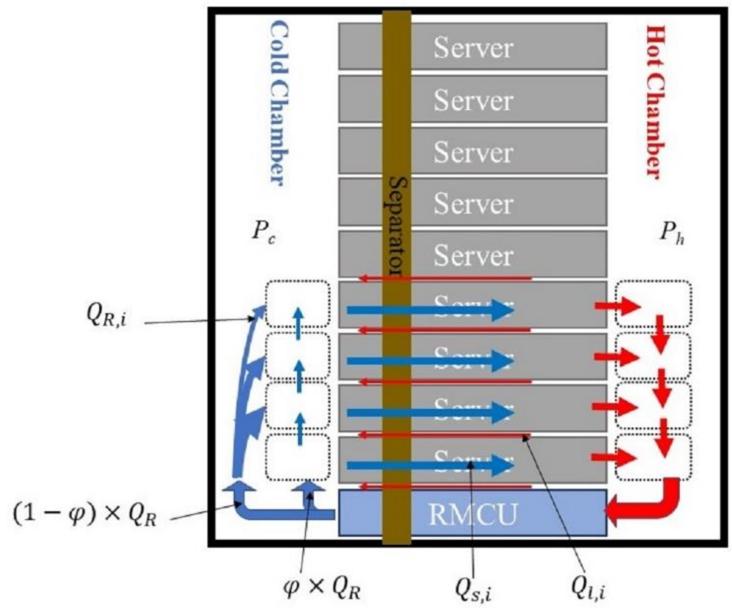

Figure 6-2: Schematic of the airflow distribution inside an enclosure. In the cold chamber (on the left), cold air exits the RMCU and is drawn into the servers. In the hot chamber (on the right), hot air exits the servers and is drawn into the RMCU. There is leakage airflow from the hot to the cold chamber.

6.3.2 Flow-resistance network representation

Considering the example of four active servers and two passive servers (i.e., servers that are not powered), the simplified airflow-resistance network inside the enclosure is presented in Figure 6-3. The RMCU is represented as a voltage source ΔP_1, and the airflow resistance R_1 across the heat exchanger is assumed to occur in series, where voltage is analogous to pressure while current is equivalent to airflow. Similarly, active servers are represented as a single voltage source ΔP_2 with an airflow resistance R_2. Passive servers are simply considered as another resistance R_2. The resistance against leakage airflow R_3 is assumed to be distributed along the rack. The airflow resistance along the height of the cold and hot chambers is denoted as R_4. Here, ΔP_1 is an order of magnitude larger than ΔP_2, and while $R_3 > R_1 > R_2$, all three resistances are of the same order of magnitude. R_4 is an order of magnitude smaller than these resistances because the characteristic dimension of the front chamber is an order of magnitude larger than the dimensions of the heat exchanger and the server air channels.

If the flowrate from the RMCU is lower than the total flowrate through the servers, the resulting pressure difference ΔP is positive, i.e., hot air leaks through the passive servers to the cold chamber, e.g., Case 1 in Figure 6-3. If the flowrate from the RMCU is greater than the total flowrate through the servers, the resulting pressure difference ΔP is negative, i.e., now cold air leaks through the passive servers to the hot chamber as shown through Case 2 in Figure 6-3.

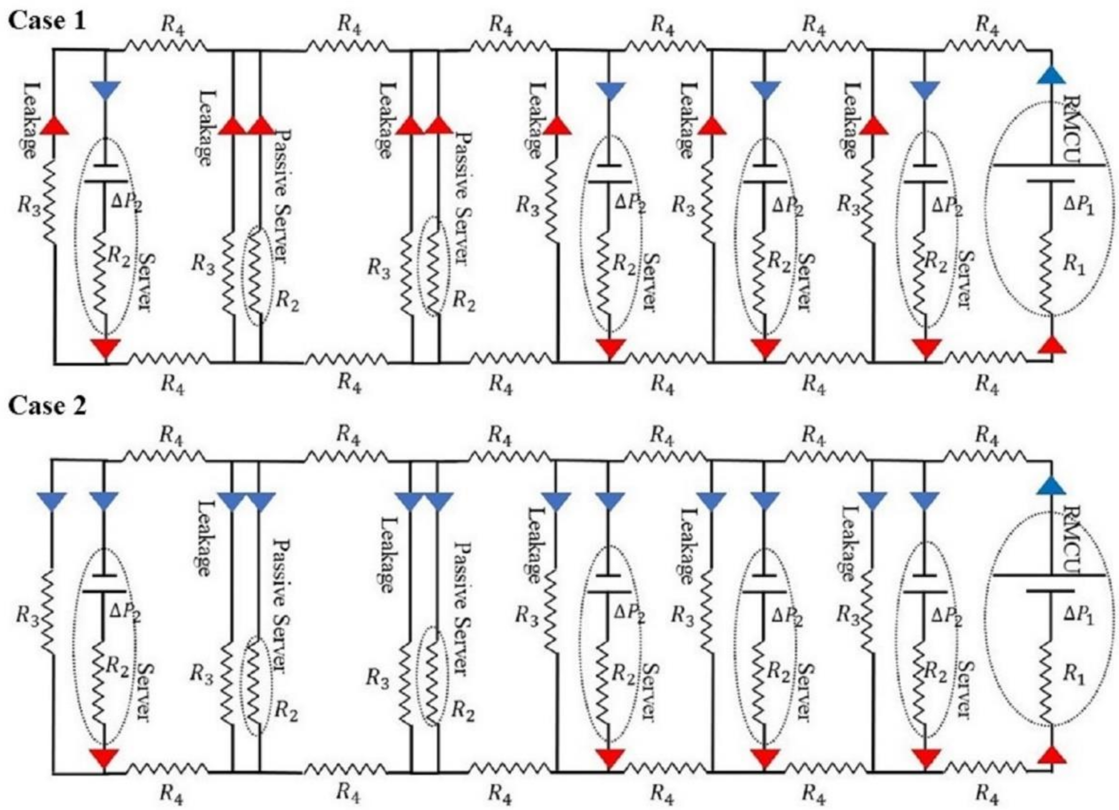

Figure 6-3: Simplified flow-resistance network inside the enclosure. Case 1: The total airflow through the active servers is greater than the RMCU airflow. Case 2: The total airflow through the active servers is lower than the RMCU airflow.

6.3.3 Calculating airflows

The airflow Q_R through the RMCU is determined by the control system, implying that the RMCU flowrate is solely a function of fan speed, which is justified by measuring the air flowrate through the RMCU for different pressure differences as follows using the experimental setup shown below. By using an extra fan, we produce pressure differences ($\Delta P = P_2 - P_1$) that simulate those between the hot and cold chambers. The fan speed inside the RMCU is held constant during measurements. While the pressure difference between the chambers for realistic cases is ≈10 Pa, in experiments ΔP has values as high as 20 Pa for constant RMCU flowrates.

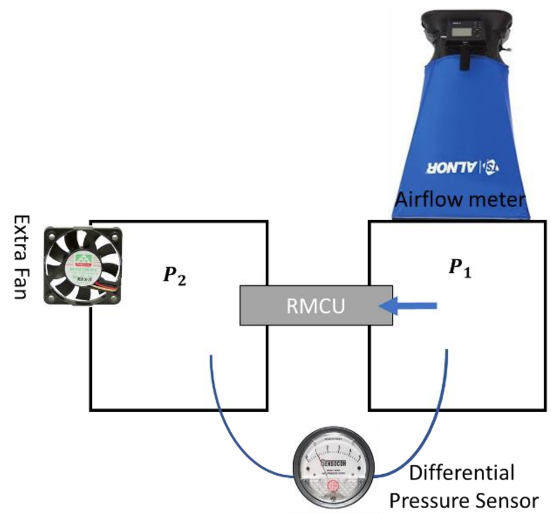

Figure 6-4: Experimental setup for measuring the air flowrate through the RMCU for different pressure differences.

Since the zones in the cold chamber do not occupy the entire chamber, as shown in Figure 6-2, we assume a cold airflow $Q_{R,i}$ directly from the RMCU into each zone. The cold airflow that exits the RMCU is divided into a portion that enters the cold chamber zone in front of the first server $\varphi \times Q_R$ and a remainder $(1-\varphi) \times Q_R$, that enters other cold chamber zones, as shown in Figure 6-2. This statement is justified by measuring the temperature profile in the cold chamber. An FLIR ONE Pro thermal camera is mounted inside the cold chamber to record temperatures at server inlets, as shown in Figure 6-5 below. These temperature contours confirm that while warm air leaks through passive servers and influences the inlet temperatures of neighboring active servers, it is not sufficient to increase the temperature along the middle of the depth of the cold chamber. Hence, part of the cold air stream from the RMCU remains unaffected and reaches the servers placed at the top of the rack. The measured temperature contours confirm that the control volume specified for the cold chamber should not occupy that entire chamber.

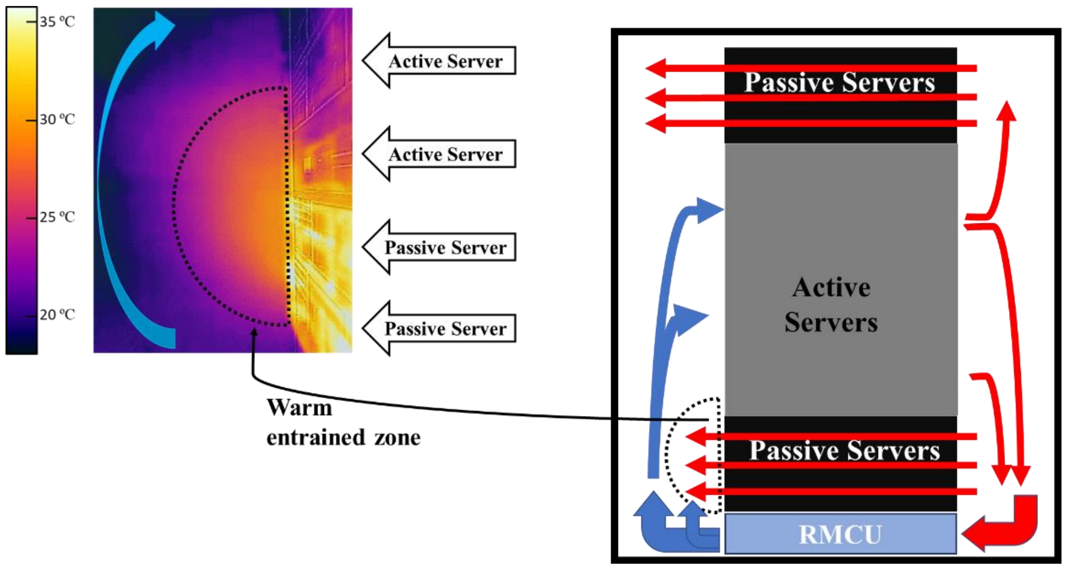

Figure 6-5: Schematic of the airflow distribution (on the right) and temperature contour in the cold chamber obtained with a thermal camera (on the left).

The airflow through each active server $Q_{s,i}$ is a function of the fan speed and pressure difference between the cold and hot chambers, $\Delta P = P_h - P_c$. However, if ΔP is lower than 10 Pa, the airflow is essentially a function of the fan speed alone. Hence, it is reasonable to assume that the airflow through each active server equals the measured airflow in open space. This is corroborated through measurements for an active server (cf. Figure 6-4 for an RMCU). The server fan speed is a function of the inlet air temperature, which in this case is the cold chamber zone temperature $T_{c,i}$. For example, the airflow through HP ProLiant DL360 G5 server is,

$$Q_{s,i}(m^3/s) = \begin{cases} 0.01415 & if \quad T_{c,i} < 25°C \\ 0.01415 + (T_{c,i} - 25) \times 0.00142 & if \quad 25°C < T_{c,i} < 35°C \end{cases} \tag{6.1}$$

Passive servers behave like porous ducts. Hence, their response to the pressure difference between the cold and hot chambers must be known to calculate the flowrates through them. Relationships for specific fan models are available. This is also corroborated by measuring flowrate and pressure drop for which results are presented in Figure 6-6.

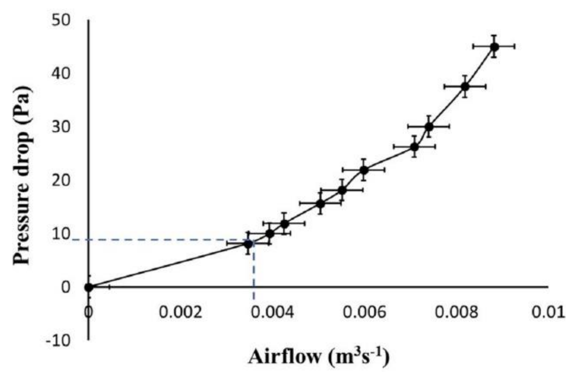

Figure 6-6: Relation describing the airflow through a passive server and the pressure drop.

Since the pressure difference between the cold and hot chambers is a function of the mismatch between the airflows of the RMCU and all active servers, these flowrates can be mapped to ΔP by a positive constant β which is a function of the enclosure geometry and the degree of isolation between the hot and cold chambers. Hence,

$$\Delta P = \beta(\sum_{\substack{Active \\ servers}} Q_{s,i} - Q_R) \tag{6.2}$$

This parameter must be calculated once by measuring ΔP, Q_R, and $\sum_{\substack{Active \\ servers}} Q_{s,i}$. In Figure 6-7, each cold chamber zone interacts with five airflows, namely, (1) air exchange between the zone of interest and the zone below that $Q_{in,i}$, (2) air exchange between the zone of interest and the zone above that $Q_{o,i}$, (3) air exchange with the corresponding server $Q_{s,i}$, (4) leakage airflow $Q_{l,i}$, and (5) cold air emerging from the RMCU $Q_{R,i}$. Assuming a linear reduction in $Q_{R,i}$ when the distance between the zone and the RMCU increases, the mass balance for each front zone is,

$$Q_{o,i} = Q_{in,i} + Q_{R,i} + Q_{l,i} - Q_{s,i}, \tag{6.3}$$

where,

$$Q_{R,i} = [(n-i)/n(n+1)]Q_R(1-\varphi) + [0.5/n]Q_R(1-\varphi) \qquad for\ i = 2, 3, \dots, n \tag{6.4}$$

and n an integer representing the number of zones. While a reduction in cold air from the RMCU ($\mathrm{Q_{R,i}}$) may not be linear in this context, selecting a linear relation does not cause a large error and, in any event, a different relationship can be inserted without difficulty. To determine the leakage airflow, the mass balance for the entire cold chamber,

$$\sum Q_{l,i} = \sum_{\substack{Active\\ servers}} Q_{s,i} - Q_R + \sum_{\substack{Passive\\ servers}} Q_{s,i}. \tag{6.5}$$

Since the total leakage airflow is distributed equally among all zones,

$$\sum Q_{l,i} = n \times Q_{l,i}. \tag{6.6}$$

Similarly, the mass balance for the hot chamber zones,

$$Q'_{o,i} = Q_{s,i} + Q'_{in,i} - Q_{l,i}. \tag{6.7}$$

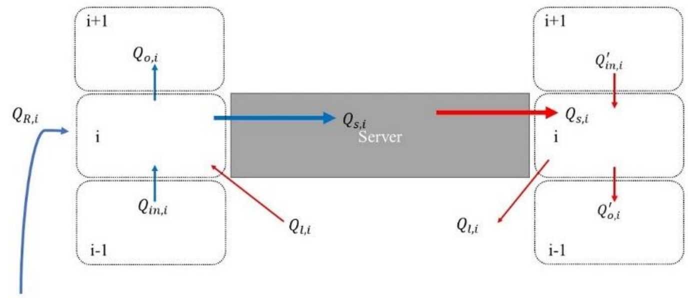

Figure 6-7: Airflows in the cold and hot chambers zones.

The inputs required for the model include server types, server states (On or Off and their utilization), type and size of the heat exchanger inside the unit, air and water flowrates of the RMCU, and initial temperatures. Since these inputs are readily identified or measured, they do not influence the reliability of the model. The algorithm used to calculate all airflows follows. (1) Determine $\sum_{\substack{Active \\ servers}} Q_{s,i}$ from the total number of active servers (Eq. (6.1)) and obtain Q_R as the model input, (2) determine the flowrate mismatch and the pressure difference between the chambers (Eq. (6.2)), (3) determine the flowrates of the passive servers using the fan system curve and ΔP, (4) determine the leakage flowrate for each zone (Eq. (6.5)) and (6.6)), (5) determine the cold air stream flow emerging from the RMCU (Eq. (6.4)), (6) determine $Q_{o,1}$ and use as $Q_{in,2}$ followed by calculating $Q_{o,i}$ for each zone in sequence, where $Q_{o,i} = Q_{in,i+1}$, and (7) determine $Q'_{o,n}$ and use as $Q'_{in,n-1}$, then calculate $Q'_{o,i}$ for each zone in sequence, i.e., $Q'_{o,i} = Q'_{in,i-1}$.

6.3.4 Formulation of energy balance equations

The energy balance equation for an active server is

$$\frac{X}{2}\left(\frac{dT_{e,i}}{dt}+\frac{dT_{c,i}}{dt}\right)=\rho_a c_{p,a} Q_{s,i}\left(T_{c,i}-T_{e,i}\right)+\dot{P}_s. \tag{6.8}$$

Here, $T_{e,i}$ denotes the server exhaust temperature, $T_{c,i}$ the temperature of the corresponding cold chamber zone, ρ_a air density, $c_{p,a}$ the specific heat of air, X the thermal mass of the server, which is available from the literature [37], and $\dot{P}_s$ the total power consumption of the corresponding server. For airflow within the RMCU,

$$\rho_a c_{p,a} V_a\left(\frac{dT_c}{dt}+\frac{dT_h}{dt}\right)=\rho_a c_{p,a} Q_R\left(T_h-T_c\right)-\frac{UA}{2}\left(T_h+T_c-T_{i,w}-T_{o,w}\right), \tag{6.9}$$

and for water flow within the RMCU,

$$\rho_w c_{p,w} V_w\left(\frac{dT_{i,w}}{dt}+\frac{dT_{o,w}}{dt}\right)=\rho_w Q_w c_{p,w}\left(T_{i,w}-T_{o,w}\right)+\frac{UA}{2}\left(T_h+T_c-T_{i,w}-T_{o,w}\right), \tag{6.10}$$

where, T_c denotes the air temperature at the RMCU exhaust, T_h the air temperature at the RMCU inlet, $T_{i,w}$ and $T_{o,w}$ the water inlet and outlet temperatures, Q_w the water flowrate, $c_{p,w}$ the specific heat of water, ρ_w the density of water, U the overall heat transfer coefficient inside the RMCU (a function of Q_R and Q_w), A the contact area on each fluid side, and V_a and V_w the air and water volumes inside the heat exchanger. The value of UA for an air to water heat exchanger, which has a strong dependence on the air flowrate but is a weak function of the water flowrate, can be expressed in terms of the RMCU air flowrate. For each cold chamber zone, the energy balance is

$$\rho_a c_{p,a} V_c \gamma\left(\frac{dT_{c,i}}{dt}\right)=\Phi_R+\Phi_i+\Phi_o+\Phi_l+\Phi_s. \tag{6.11}$$

For each hot chamber zone, the corresponding energy balance is

$$\rho_a c_{p,a} V_h \gamma\left(\frac{dT_{h,i}}{dt}\right)=\Phi_i'+\Phi_o'+\Phi_l'+\Phi_s', \tag{6.12}$$

where γ denotes a correction factor for the thermal masses of the cold and hot chambers zones, ϕ the energy exchange for the cold chamber zones, and ϕ' the energy exchange for the hot chamber zones. Table 6-1 presents expressions for each term in Equations (6.11) and (6.12) in terms of the temperature of the corresponding hot chamber zone $T_{h,i}$.

Table 6-1:Expressions for the terms in Equations 6.11 and 6.12

Equation 6.11		Equation 6.12	
ϕ_i		ϕ_i'	
$Q_{in,i} \geq 0$	$\rho_a c_{p,a} Q_{in,i} T_{c,i-1}$	$Q_{in,i}' \geq 0$	$\rho_a c_{p,a} Q_{in,i}' T_{h,i+1}$
$Q_{in,i} < 0$	$\rho_a c_{p,a} Q_{in,i} T_{c,i}$	$Q_{in,i}' < 0$	$\rho_a c_{p,a} Q_{in,i}' T_{h,i}$
ϕ_o		ϕ_o'	
$Q_{in,i} \geq 0$	$-\rho_a c_{p,a} Q_{o,i} T_{c,i}$	$Q_{o,i}' \geq 0$	$-\rho_a c_{p,a} Q_{o,i}' T_{h,i}$
$Q_{in,i} < 0$	$-\rho_a c_{p,a} Q_{o,i} T_{c,i+1}$	$Q_{o,i}' < 0$	$-\rho_a c_{p,a} Q_{o,i}' T_{c,i-1}$
ϕ_s(for passive servers)		ϕ_s'(for passive servers)	
$\Delta P \geq 0$	$-\rho_a c_{p,a} Q_{s,i} T_{h,i}$	$\Delta P \geq 0$	$\rho_a c_{p,a} Q_{s,i} T_{h,i}$
$\Delta P < 0$	$-\rho_a c_{p,a} Q_{s,i} T_{c,i}$	$\Delta P < 0$	$\rho_a c_{p,a} Q_{s,i} T_{c,i}$
ϕ_s(for active servers)		ϕ_s'(for active servers)	
$-\rho_a c_{p,a} Q_{s,i} T_{c,i}$		$\rho c_p Q_{s,i} T_{e,i}$	
ϕ_l		ϕ_l'	
$\Delta P \geq 0$	$\rho_a c_{p,a} Q_{l,i} T_{h,i}$	$\Delta P \geq 0$	$\rho_a c_{p,a} Q_{l,i} T_{h,i}$
$\Delta P < 0$	$\rho_a c_{p,a} Q_{l,i} T_{c,i}$	$\Delta P < 0$	$\rho_a c_{p,a} Q_{l,i} T_{c,i}$
ϕ_R			
$\rho_a c_{p,a} Q_{R,i} T_c$			

The dimensionless temperature and time are,

$$\theta = \frac{T - T_{ref}}{T_0 - T_{ref}}, \qquad (a) \qquad\qquad \tau = \frac{t}{t_0}. \qquad (b) \qquad (6.13)$$

where T_{ref} and t_0 denote constant values for temperature and time. Hence, dimensionless forms of the energy equations for the server are,

$$\frac{d\theta_{e,i}}{d\tau}+\frac{d\theta_{c,i}}{d\tau}=\frac{2\rho_a c_{p,a} Q_{s,i} t_0}{X}\left(\theta_{c,i}-\theta_{e,i}\right)+\frac{2t_0\dot{P}_s}{X(T_0-T_{ref})}, \tag{6.14}$$

and for the RMCU,

$$\frac{d\theta_c}{d\tau}+\frac{d\theta_h}{d\tau}=\frac{2Q_R t_0}{V_a}(\theta_h-\theta_c)-\frac{2t_0 UA}{\rho_a c_{p,a} V_a}\left(\theta_h+\theta_c-\theta_{i,w}-\theta_{o,w}\right), \tag{6.15}$$

$$\frac{d\theta_{i,w}}{d\tau}+\frac{d\theta_{o,w}}{d\tau}=\frac{2Q_w t_0}{V_w}\left(\theta_{i,w}-\theta_{o,w}\right)+\frac{2t_0 UA}{\rho_w c_{p,w} V_w}\left(\theta_h+\theta_c-\theta_{i,w}-\theta_{o,w}\right). \tag{6.16}$$

For each cold chamber zone, the dimensionless form is,

$$\frac{d\theta_{c,i}}{d\tau}=\frac{Q_{R,i}t_0}{V_c\gamma}\theta_c+\frac{Q_{in,i}t_0}{V_c\gamma}\theta_{c,i-1}-\frac{Q_{o,i}t_0}{V_c\gamma}\theta_{c,i}-\frac{Q_{s,i}t_0}{V_c\gamma}\theta_{c,i}+\frac{Q_{l,i}t_0}{V_c\gamma}\theta_{h,i}, \tag{6.17}$$

and for the hot chamber zones,

$$\frac{d\theta_{b,i}}{d\tau}=\frac{Q'_{in,i}t_0}{V_h\gamma}\theta_{h,i+1}-\frac{Q'_{o,i}t_0}{V_h\gamma}\theta_{h,i}+\frac{Q_{s,i}t_0}{V_h\gamma}\theta_{e,i}-\frac{Q_{l,i}t_0}{V_h\gamma}\theta_{h,i}. \tag{6.18}$$

The algorithm to determine the temperature of each zone at a particular time follows. (1) Include the initial temperatures as inputs, (2) include Q_R and Q_w as inputs as prescribed by a control system, (3) follow steps 1 and 2 to determine all flowrates, (4) solve Equations (6.14) to (6.18) for all zones to determine all temperatures at a successive time, and (5) repeat the process and advance it in time by $\Delta\tau$.

6.4 Results and discussion

6.4.1 Model validation

To validate the model, for the same initial values, the temperature profile for an arbitrary case is measured experimentally and compered with model predictions. Figure 6-8 demonstrates this comparison at four times, i.e., after (a) after 5, (b) 20, (c) 40 and (d) 60 minutes. The total IT load of the rack is 4 kW, the air and water flowrates of the RMCU are 0.18 m^3/s and 0.0005 m^3/s, respectively. The IT load configuration is also shown in the figure. The maximum difference between the temperature predictions and experimental results is smaller than 4% and at steady state is lower than 2%, which shows that the model represents transient and steady state effects reasonably. The model also mirrors recirculation through passive servers, accurately predicting the temperature gradient along the height of the rack.

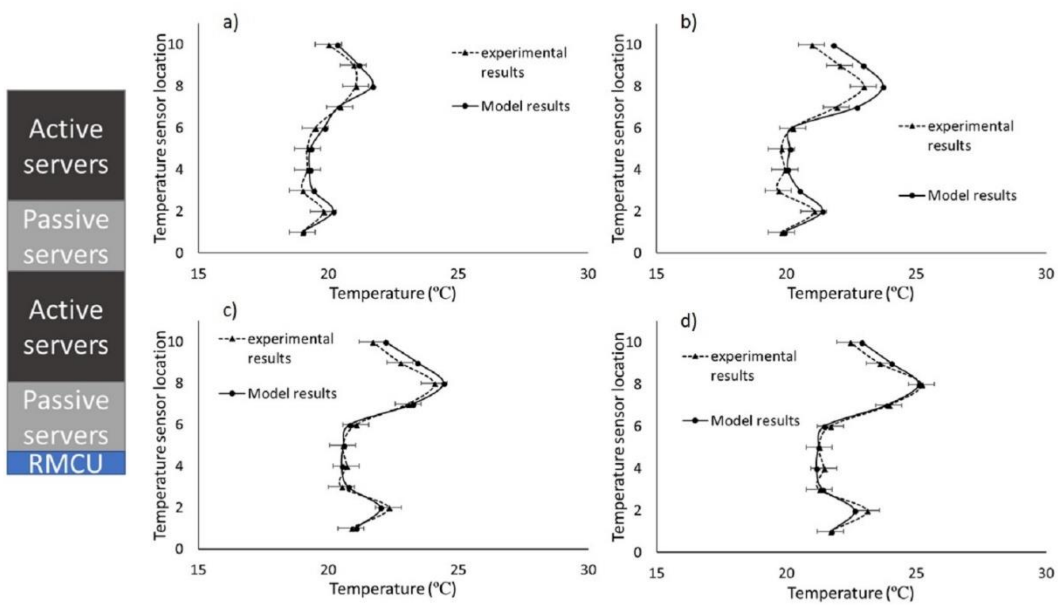

Figure 6-8: Comparison of model predictions of temperature profiles with experimental results for the demonstrated IT load configuration. a) t=5 min. b) t=20 min. c) t=40 min. d) t=60 min. The maximum difference between the temperature predictions and experimental results is smaller than 4%.

6.4.2 Influence of passive server location

Since passive servers can have a significant influence on the temperature distribution in the cold chamber, their locations in the rack should be carefully considered. Figure 6-9 shows the effect of a passive server on the temperature distribution in the rack. If the flowrate mismatch ($\sum_{\substack{Active \\ servers}} Q_{s,i} - Q_{CU}$) is negative, i.e., ΔP is positive, the location of a passive server is not as significant because the flow through the server occurs from the cold to the hot chamber, i.e., the server simply draws in cold air from the cold chamber (case 2 in Figure 6-3). However, a positive mismatch, i.e., a negative ΔP, drives leakage of hot air back through these servers to the cold chamber, thereby influencing the temperature (case 1 in Figure 6-3).

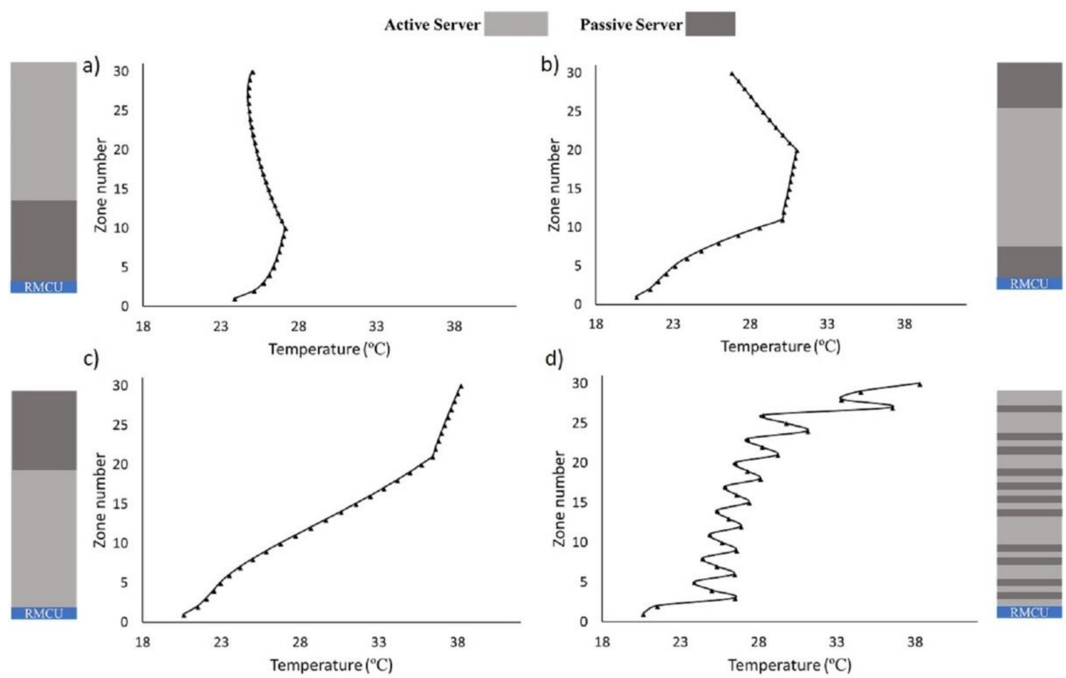

Figure 6-9: Effect of the placement of a passive server on the temperature distribution: a) At the bottom. b) Along the middle. c) At the top. d) Distributed along the rack. The maximum temperatures in the cold chamber are 27, 31, 38, and 38ºC, respectively, when the passive servers are located at the bottom, middle and top of the rack, and when they are distributed along the rack.

Figure 6-9 shows that the temperature increase in front of passive servers, whether they are placed in a cluster or single, is consistent with previous experiments. Moving upward from the RMCU to the top of the rack, the pressure in the cold chamber decreases (Figure 6-3) inducing higher leakage through passive servers, as reflected in Figure 6-9. With similar water and air flowrates into the RMCU (0.2 and 0.0005 m^3/s), the maximum temperatures in the cold chamber are 27, 31, 38, and 38ºC, respectively, when the passive servers are located at the bottom, middle and top of the rack, and when they are distributed along the rack. Thus, passive servers should be placed in proximity of the RMCU to minimize hot air recirculation.

6.4.3 Effect of water and air flowrates of the RMCU on temperature profile

Next, we consider the effect of water and air flowrates into the RMCU on the cold chamber temperature distribution for case “d” in Figure 6-9. Figure 6-10 demonstrates that a 10% change in water flowrate does not have a discernible effect on that temperature. The RMCU employs an air to water plate-fin heat exchanger which includes three thermal resistances, (1) through the metallic body of the heat exchanger (5%), (2) metal body to water (15%), and (3) metal body to air (80%) [38]. This is supported by Figure 6-10, where a 10% reduction in the airflow rate (Figure 6-10(a)) produces an appreciable increase in temperature compared to a similar proportional change in the water flow rate (Figure 6-10(b)). The reduced RMCU airflow also leads to higher flowrate mismatch, i.e., lower ΔP, which increases leakage through passive servers, further increasing the temperature.

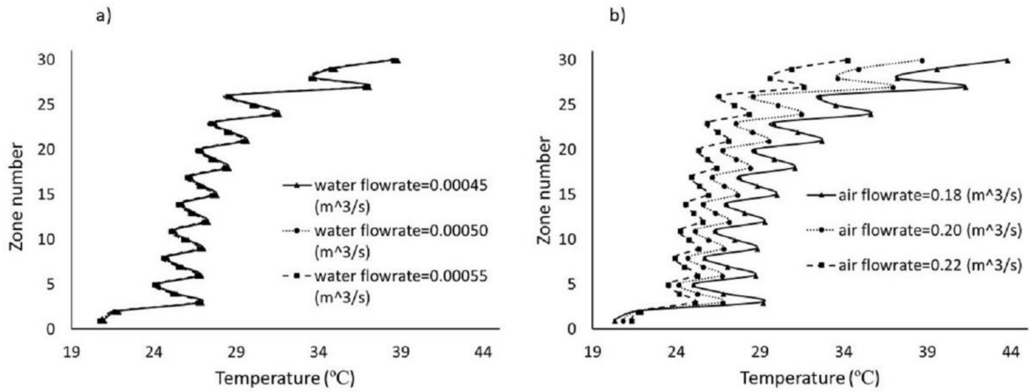

Figure 6-10: Influence of RCMU water and air flowrates on the temperature distribution. a) Temperature profile for three air flowrates. b) Temperature profile for three water flowrates. A 10% reduction in the airflow rate produces an appreciable increase in temperature compared to a similar percent change in the water flow rate.

6.4.4 Transient behavior

The proposed model can be utilized to analyze typical what-if failure scenarios, for example, how long it takes for the cold chamber temperature to increase after a chiller fails. We demonstrate this capability by characterizing the transient response of the system to step changes in various parameters, e.g., IT load, RCMU water inlet temperature and air flowrate, in Figure 6-11, where the temperature reported is for the middle of the cold chamber. A 1.1 kW increment in IT load results in a 3ºC temperature increase at the middle of the cold chamber.

There can be a sudden change in the water inlet temperature of the RMCU due to a failure in the building chilled water system or outdoor water chiller. A 4 ºC change in the water inlet temperature produces a greater than 4ºC increase in the air temperature, as shown in Figure 6-11(b). The total thermal mass of the system contains four contributions, i.e., from the servers, RMCU, cold chamber and hot chamber (Figure 6-11.d). The thermal mass and consequently the response time of the servers is considerably larger than for any of the other contributions. Therefore, changes in the IT load produce a more gradual increase in cold chamber temperature because an increase in IT load, i.e., higher heat dissipation from the CPU, is first perceived by the server body (Figure 6-11.d), then by the air flowing through it. A change in the RMCU water inlet temperature is associated with a faster response because first, the change is perceived by the RMCU and then by other parts of the system, resulting in a significant air temperature change. There is a similar response to changes in the RMCU air flowrate. A 20% decrease in RMCU air flowrate increases the temperature at the middle of the cold chamber by 9ºC. To further investigate transient effects, the servers that constitute the bulk of the thermal mass of the system are considered separately. By assuming constant temperature at server inlets, Equation 6.14 reduces to,

$$\frac{d\theta_{e,i}}{d\tau} = \frac{2\rho_a c_{p,a} Q_{s,i} t_0}{X}\left(\theta_{c,i} - \theta_{e,i}\right) + \frac{2t_0 \dot{P}_S}{X(T_0 - T_{ref})}. \tag{6.19}$$

The solution for this first order differential equation is,

$$\theta = \left(1 - \frac{\dot{P}}{\rho_a c_{p,a} Q_{s,i}(T_0 - T_{ref})}\right) e^{-\frac{2\rho_a c_{p,a} Q_{s,i} t_0}{X}\tau} + \frac{\dot{P}}{\rho_a c_{p,a} Q_{s,i}(T_0 - T_{ref})}. \tag{6.20}$$

The thermal time constant at a server exhaust is $(2\rho_a c_{p,a} Q_{s,i} t_0)/X$, which is a function of the server thermal mass and air flowrate through the server. The thermal mass depends upon server material and weight, arrangement of components inside the server, and the heat sink attached to the processor. By changing any of these parameters, server manufacturers can change the response time of servers to rapid changes in the DC environment. Since the air flowrate through the server is a function of fan speed, using more powerful fans results in shorter response times.

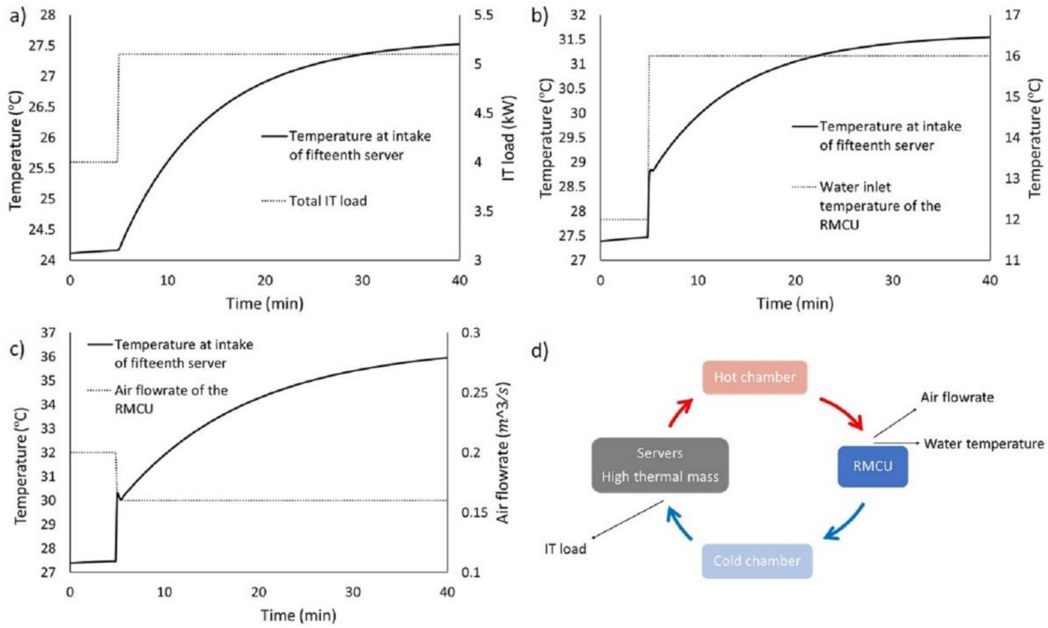

Figure 6-11: Transient response of temperature at the middle of the cold chamber to changes in input parameters. a) Step change in ITE load. b) Step change in RMCU water inlet temperature. c) Step change in RMCU air flowrate. d) Thermal mass representation. Changes in the IT load produce a more gradual increase in cold chamber temperature, but changes in RMCU water inlet temperature and RMCU air flowrate results in a sudden change in the cold chamber temperature.

6.4.5 Comparing the performance of a single RMCU with two RMCUs

The above cases consider a single RMCU within the enclosure that is located at the bottom of the rack. We now instead consider two RMCUs, with one unit placed at the bottom of the rack and the other at the top. An RMCU would rarely be installed in the middle of the rack since that would remove valuable eye-level space for IT equipment in the enclosure. Figure 6-12 compares the performance of a rack with two RMCUs and a single RMCU. While the IT load and configuration, geometry and other parameters for both cases are similar, the air and water flowrates into the two RMCUs are half the corresponding flowrates for a single RMCU. Implementing two RMCUs provides a lower cold chamber temperature since, (1) even though two units together have the same intake airflow the cold airflow is better distributed, resulting in more uniform pressure and temperature profiles, and (2) decreasing the air flowrate into an RMCU lowers its outlet air temperature. Depending on the IT load configuration, the use of two RMCUs can reduce the maximum temperature of the cold chamber by 1- 12ºC.

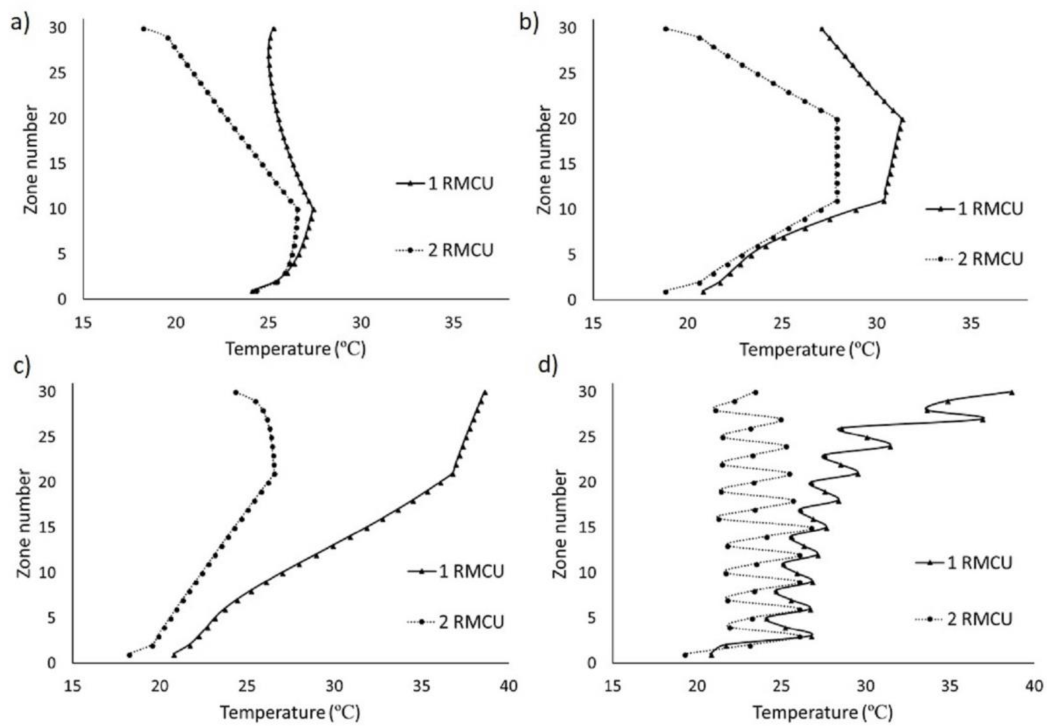

Figure 6-12: Comparison of performance while using one RMCU versus two RMCUs with different passive server placements. a) Accumulated at the bottom. b) Accumulated at the middle. c) Accumulated at the top. d) Distributed along the rack. Depending on the IT load configuration, use of two RMCUs can reduce the maximum temperature of the cold chamber by 1- 12ºC.

6.4.6 Computational time

Temperature predictions are intended for failure prognosis and to inform control decisions. Hence, the time required to calculate the predicted temperature profile accurately is a major consideration. Our model determines the temperature distribution much more rapidly than a CFD simulation. A 3D CFD test case for a similar system provides results after about an hour [18], [24], [39], while the model takes less than 30 s depending on the projected duration for the prediction. To design a DC room, several test cases must be considered to optimize the system. If a hundred such cases are required, it would take 4 days to complete the CFD simulations but only about 8 minutes for the model. This makes our method more suitable for real-time control. Two previous investigations report that their models require experimental data over about 15 hours to train their predictions to lie within reasonable error [40], [22]. Another model must evolve a random initial population for 30,000 generations to obtain accurate results that take 28 hours in a computer equipped with a Quadcore Intel i7 CPU @ 3.4 GHz and 8 GB of RAM [23]. A fourth model requires 30 different CFD simulations for training to predict the temperature in front of 30 servers [24].

Figure 6-13 illustrates the influence on the computational time of the duration over which predictions must be made and the number of zones that are considered. All these computations are performed with an Intel (R) Core (TM) i7 6700 HQ CPU @ 2.6 GHz and 16 GB of RAM. Since the model solves the energy balance for each zone at each time step, the computational time increases linearly when the number of zones and the prediction time increase. The time interval for all cases is 0.001 s. Increasing this time interval to 0.01 s decreases the computational time by a tenth. The computational or experimental effort required to generate training data for machine learning is significantly higher using previously formulated methods than it is with our approach. Prediction models based on machine learning fail if an operating condition is far removed from the circumstances embedded in a training data set. For instance, temperature predictions for server configurations different from those relevant to the training data set can be entirely inaccurate. This limitation is inherent to machine learning, where only a few parameters can be varied over a restricted range. Our model overcomes the limitation since all major parameters, such as the air and water flowrates through the cooling unit, IT load, and passive server locations, can be changed.

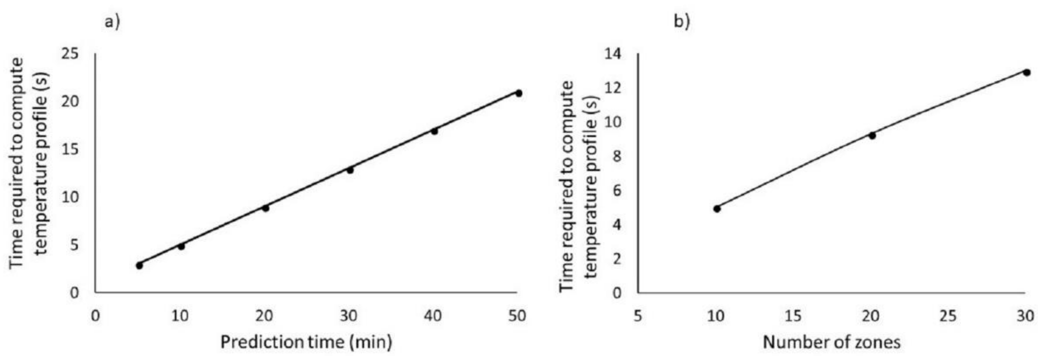

Figure 6-13: Dependence of the computational time required to determine the temperature profile by the model. a) Dependence on prediction time. b) Dependence on number of zones.

6.5 Conclusion

A model is presented to predict the temperature distribution within an IT server enclosure that is integrated with an RMCU. The flow field for this architecture can be predicted using fluid mechanics principles. Consequently, in contrast to other control schemes, no *a priori* training process is required. The model is validated by comparison with experiments, where the maximum difference between predictions and measurements is 4%.

The influence of parameters such as the IT load configuration, RMCU flowrates, step changes in system inputs, and utilization of two RMCUs rather than just one are investigated through the model. Our findings follow. (1) The optimal location for passive servers is adjacent to the RMCU. (2) A ten percent change in the RMCU water flowrate has a minor influence, less than 1%, on the cold chamber temperature but a ten percent reduction in the air flowrate results in a 14% increase in the cold chamber temperature. (3) Using two RMCUs with 50% of the cooling capacity of a single RMCU results in a lower cold chamber temperature compared to use of a single RMCU running at 100% capacity. (4) The response of the system to common DC changes such as an increase in the IT load occurs over about 30 minutes due to the high thermal mass of the system. The model will facilitate real-time control algorithms developed for IT enclosures with RMCU architectures.

6.6 Acknowledgment

This research was supported by the Natural Sciences and Engineering Research Council (NSERC) of Canada under a collaborative research and development (CRD) project titled: Adaptive Thermal Management of Data Centers. We also thank our colleagues from CINNOS Mission Critical Incorporated who provided insight and expertise that greatly assisted the research.

6.7 References

[1] J. Dai, M. M. Ohadi, D. Das, and M. G. Pecht, "Optimum Cooling of Data Centers, Application of Risk Assessment and Mitigation Techniques", Springer Science Business Media, New York, 2014, DOI: 10.1007/978-1-4614-5602-5.

[2] K. Ebrahimi, G. F. Jones, and A. S. Fleischer, "A review of data center cooling technology, operating conditions and the corresponding low-grade waste heat recovery opportunities," *Renew. Sustain. Energy Rev.*, vol. 31, pp. 622–638, 2014.

[3] H. M. Daraghmeh and C.-C. Wang, "A review of current status of free cooling in datacenters," *Appl. Therm. Eng.*, vol. 114, no. Supplement C, pp. 1224–1239, Mar. 2017.

[4] N. El-Sayed, I. A. Stefanovici, G. Amvrosiadis, A. A. Hwang, and B. Schroeder, "Temperature management in data centers: Why some (might) like it hot," *Sigmetrics '12*, no. TECHNICAL REPORT CSRG-615, pp. 163–174, 2012.

[5] M. K. Patterson, "The effect of data center temperature on energy efficiency," in *2008 11th Intersociety Conference on Thermal and Thermomechanical Phenomena in Electronic Systems*, 2008, pp. 1167–1174.

[6] J. Cho, J. Yang, and W. Park, "Evaluation of air distribution system's airflow performance for cooling energy savings in high-density data centers," *Energy Build.*, vol. 68, no. PARTA, pp. 270–279, 2014.

[7] A. Capozzoli and G. Primiceri, "Cooling systems in data centers: State of art and emerging technologies," *Energy Procedia*, vol. 83, pp. 484–493, 2015.

[8] A. Capozzoli, G. Serale, L. Liuzzo, and M. Chinnici, "Thermal metrics for data centers: A critical review," *Energy Procedia*, vol. 62, pp. 391–400, 2014.

[9] S. V. Patankar, "Airflow and Cooling in a Data Center," *J. Heat Transfer*, vol. 132, no. 7, p. 073001, 2010.

[10] T. Evans, "The different types of air conditioning equipment for IT environments," *APC White Pap.*, p. 24, 2004.

[11] K. Dunlap and N. Rasmussen, "Choosing Between Room, Row, and Rack-based Cooling for Data Centers," *Schneider Electr. White Pap. 130*, p. 18, 2012.

[12] J. V. Smith, V. P. Hester, and W. A. Wylie, "Rack mountable computer component fan cooling arrangement and method," US6801428 B2, 05-Oct-2004.

[13] R. J. Johnson, R. C. Pfleging, T. J. Anderson, and D. C. Kroupa, "Rack-mounted equipment cooling," US6668565 B1, 30-Dec-2003.

[14] J. Smith, V. Hester, and W. Wylie, "Rack mountable computer component cooling method and device," US20030221817 A1, 04-Dec-2003.

[15] V. A. Tsachouridis, P. Sobonski, H. Wiese, D. Mehta, K. Kouramas, and M. Cychowski, "Optimal Thermal Regulation of a Real Data Centre," IFAC-Pap., vol. 50, no. 1, pp. 4893–4898, Jul. 2017.

[16] K. Cho, H. Chang, Y. Jung, and Y. Yoon, "Economic analysis of data center cooling strategies," Sustain. Cities Soc., vol. 31, pp. 234–243, May 2017.

[17] H. Cheung, S. Wang, C. Zhuang, and J. Gu, "A simplified power consumption model of information technology (IT) equipment in data centers for energy system real-time dynamic simulation," Appl. Energy, vol. 222, pp. 329–342, Jul. 2018.

[18] E. Samadiani, Y. Joshi, H. Hamann, M. K. Iyengar, S. Kamalsy, and J. Lacey, "Reduced Order Thermal Modeling of Data Centers via Distributed Sensor Data," J. Heat Transf., vol. 134, no. 4, pp. 041401-041401–8, Feb. 2012.

[19] E. Samadiani and Y. Joshi, "Proper Orthogonal Decomposition for Reduced Order Thermal Modeling of Air Cooled Data Centers," *J. Heat Transfer*, vol. 132, no. 7, p. 071402, 2010.

[20] K. Fouladi, A. P. Wemhoff, L. Silva-Llanca, K. Abbasi, and A. Ortega, "Optimization of data center cooling efficiency using reduced order flow modeling within a flow network modeling approach," Appl. Therm. Eng., vol. 124, pp. 929–939, Sep. 2017.

[21] R. Ghosh and Y. Joshi, "Error estimation in POD-based dynamic reduced-order thermal modeling of data centers," Int. J. Heat Mass Transf., vol. 57, no. 2, pp. 698–707, Feb. 2013.

[22] Y. Fulpagare, Y. Joshi, and A. Bhargav, "Rack level forecasting model of data center," in 2017 16th IEEE Intersociety Conference on Thermal and Thermomechanical Phenomena in Electronic Systems (ITherm), 2017, pp. 824–829.

[23] M. Zapater, J. L. Risco-Martín, P. Arroba, J. L. Ayala, J. M. Moya, and R. Hermida, "Runtime data center temperature prediction using Grammatical Evolution techniques," Appl. Soft Comput., vol. 49, pp. 94–107, Dec. 2016.

[24] G. Varsamopoulos and M. Jonas, "Using transient thermal models to predict cyberphysical phenomena in data centers," ... *Informatics Syst.*, vol. 3, pp. 132–147, 2013.

[25] L. Wang, G. von Laszewski, F. Huang, J. Dayal, T. Frulani, and G. Fox, "Task scheduling with ANN-based temperature prediction in a data center: a simulation-based study," Eng. Comput., vol. 27, no. 4, pp. 381–391, Oct. 2011.

[26] J. Chen *et al.*, "A high-fidelity temperature distribution forecasting system for data centers," *Proc. - Real-Time Syst. Symp.*, pp. 215–224, 2012.

[27] E. Samadiani and Y. Joshi, "Reduced order thermal modeling of data centers via proper orthogonal decomposition: a review," *Int. J. Numer. Methods Heat Fluid Flow*, vol. 20, no. 5, pp. 529–550, 2010.

[28] Z. Song, B. T. Murray, and B. Sammakia, "A compact thermal model for data center analysis using the zonal method," *Numer. Heat Transf. Part A Appl.*, vol. 64, no. 5, pp. 361–377, 2013.

[29] H. S. Erden, H. E. Khalifa, and R. R. Schmidt, "A hybrid lumped capacitance-CFD model for the simulation of data center transients," *HVAC R Res.*, vol. 20, no. 6, pp. 688–702, 2014.

[30] Q. Tang, T. Mukherjee, S. K. S. Gupta, and P. Cayton, "Sensor-Based Fast Thermal Evaluation Model for Energy Efficient High-Performance Datacenters," in 2006 Fourth International Conference on Intelligent Sensing and Information Processing, 2006, pp. 203–208.

[31] R. Sharma, C. Bash, C. Patel, R. J. Friedrich, and J. S. Chase, "Balance of Power: Dynamic Thermal Management for Internet Data Centers," IEEE Internet Comput., vol. 9, pp. 42–49, Jan. 2005.

[32] J. W. Axley, "Surface-drag flow relations for zonal modeling," Build. Environ., vol. 36, no. 7, pp. 843–850, Aug. 2001.

[33] J. Gao, J. Zhao, X. Li, and F. Gao, "Evaluation of a Zonal Model for Large Enclosures Using Computational Fluid Dynamics," J. Asian Archit. Build. Eng., vol. 6, no. 2, pp. 379–385, Nov. 2007.

[34] J. Gao, J. Zhao, X. Li, and F. Gao, "A Zonal Model for Large Enclosures With Combined Stratification Cooling and Natural Ventilation: Part 1—Model Generation and its Procedure," J. Sol. Energy Eng., vol. 128, no. 3, pp. 367–375, Aug. 2006.

[35] F. Haghighat, Y. Li, and A. C. Megri, “Development and validation of a zonal model — POMA,” Build. Environ., vol. 36, no. 9, pp. 1039–1047, Nov. 2001.

[36] E. Wurtz, J. M. Nataf, and F. Winkelmann, “Two- and three-dimensional natural and mixed convection simulation using modular zonal models in buildings,” *Int. J. Heat Mass Transf.*, vol. 42, no. 5, pp. 923–940, 1999.

[37] Z. M. Pardey, D. W. Demetriou, J. W. Vangilder, H. E. Khalifa, and R. R. Schmidt, “Proposal for Standard Compact Server Model for Transient Data Center Simulations,” *Ashrae*, vol. 121, no. January, pp. 413–422, 2015.

[38] R. K. Shah and D. P. Sekulic, Fundamentals of Heat Exchanger Design. John Wiley & Sons, 2003.

[39] L. Phan and C.-X. Lin, “Reduced order modeling of a data center model with multi-Parameters,” *Energy Build.*, vol. 136, pp. 86–99, 2017.

[40] C. M. Liang, L. Li, J. Liu, S. Nath, A. Terzis, and C. Faloutsos, “ThermoCast: A Cyber-Physical Forecasting Model for Data Centers Categories and Subject Descriptors,” *7th ACM SIGKDD Int. Conf. Knowl. Discov. Data Min.*, pp. 1370–1378, 2011.

7 Modeling Temperature Distribution and Power Consumption in IT Server Enclosures with Row-Based Cooling Architectures

This chapter is reproduced from *"Temperature and Power Consumption in IT Server Enclosures with Row-Based Cooling Architectures"*, ***Hosein Moazamigoodarzi***, *Rohit Gupta, Souvik Pal, Peiying Jennifer Tsai, Suvojit Ghosh and Ishwar K. Puri, Under review in Applied Energy.* The author of this thesis is the first author and the main contributor of this publication.

7.1 Abstract

Traditional data center (DC) cooling methods cannot yet control cooling airflows and temperatures on demand, creating an intrinsic inefficiency. A recent solution places row-based cooling unit adjacent to servers and places the entire assembly within an enclosure, which improves airflow distribution and provides rapid real-time control. This is in particular attractive for micro-DCs where traditional room-based cooling is less energy and cost efficient. Currently, spatiotemporal predictions of temperatures are required to predict and control DC performance as the system configuration and other parameters are varied. Current methods, such as proper orthogonal decomposition (POD), machine learning (ML) and heuristic models are inapplicable in practice because they require a prohibitively large number of *a priori* simulations or experiments to generate training datasets. We provide an alternative a computationally inexpensive training-free model for enclosed micro-DCs that

are integrated with in-row cooling units that requires no *a priori* training. The model determines the air flowrate within each zone based on a mechanical resistance circuit analysis. These flowrates are then introduced into a zonal energy balance to predict the temperature of each zone. The model is validated with experimental measurements and coupled with a power consumption calculation. Its applicability is demonstrated by evaluating the influence of various system factors, such as IT server configurations, cooling unit air and water flowrates and the numbers of cooling units, on the temperature distributions and total cooling power consumption. Used as a tool, the method can improve micro-DC control and help optimize the design of any DC row-based cooling system.

Key words: In-row cooling unit - Temperature prediction - Zonal method – Mechanical resistance – Energy balance.

7.2 Nomenclature

A	Surface area of heat exchanger (m^2)	V	Volume (m^3)
C_p	Specific heat capacity (KJ kg^{-1} K^{-1})	X	Thermal mass of server (kJ K^{-1})
P	Pressure (Pa)	ΔP	Pressure difference (Pa)
$\dot{P}_{fans}$	Power consumption of fans (Watt)	α	Correction factor for thermal mass
$\dot{P}_s$	Power consumption of server (Watt)	θ	Non-dimensional temperature
Q_c	Air flowrate through the cooling units (m^3s^{-1})	τ	Non-dimensional time
Q_s	Air flowrate through each server (m^3s^{-1})	ρ	Density (kg m^{-3})
Q_w	Water flowrate through the cooling unit (m^3s^{-1})	s	Server
Q_{ch}	Chiller heat load (kW)	f	Front chamber
R	Mechanical Resistance (Pa m^{-3} s)	b	Back chamber

T_f	Temperature of the front chambers (K)	H	Horizontal
T_s	Temperature of server exhaust (K)	V	Vertical
T_c	Cooling unit exhaust air temperature (K)	i	Index of zone in *x*-direction
T_h	Cooling unit return air temperature (K)	j	Index of zone in *y*-direction
$T_{i,w}$	Inlet water temperature of cooling unit (K)	br	Brush (separator)
$T_{o,w}$	Outlet water temperature of cooling unit (K)	a	air
T_{ci}	Fluid temperature entering condenser (K)	w	water
T_{co}	Fluid temperature leaving evaporator (K)	ref	reference
U	Overall heat transfer coefficient	0	Initial

7.3 Introduction

Increasing electricity costs have necessitated strategies to reduce the power consumed by data centers (DCs), a third of which is used to cool its IT equipment (ITE) [1], [2]. Traditional DCs typically employ air cooling, rather than direct liquid cooling, because of reliability, and lower capital and maintenance costs [3], [4]. The cold air required for the ITE is provided by cooling units that are usually placed along the server room perimeter, an architecture that is inefficient because of two significant air distribution inefficiencies, hot air recirculation and cold air bypass [5]–[7], which increase the cold airflow to the ITE up to two times over the required amount [8].

To address this inefficiency, an enclosed row-based cooling architecture that supplies cold air in close proximity to ITE is an alternative [9], [10]. This architecture decreases the energy required for cooling as well as the initial cost, and improves agility, system availability, serviceability and manageability. Cooling energy is reduced since airflow paths are shortened, which in turn require less fan power and also facilitate better airflow distribution [11]. Cooling architectures with shorter airflow paths are able to more rapidly regulate cooling in response to dynamic changes in the ITE load or cooling unit perturbations and thus prevent the large temperature fluctuations that can produce equipment failure [12].

For purpose of real-time control, failure prediction, and design optimization, a rapid scheme to predict temperatures in an enclosed row-based DC is required. To reduce the magnitudes of harmful temperature fluctuations, control actions should occur over a smaller duration than the timescale of a characteristic DC thermal event, which for enclosed row-based DC cooling is of the order of seconds [13]–[15]. While different methods to predicts temperatures within DC environments have been developed, such as proper orthogonal decomposition (POD), machine learning (ML), and, more recently, heuristic models, their limitations preclude implementation in operational DCs.

Compared to a full field granular physics-based model, ML and POD based data-driven models are attractive due to their quicker runtimes when coupled with control algorithms [16]–[19]. These data-driven models are able to correlate the temperature field inside a DC with operational parameters, but completely neglect the physics of the flow [20]–[24]. There are other gray box models that capture some features of the flow, but these also have drawbacks. First, these models are auxiliary and can require an impractically large number ($\sim 10^2$-10^3) of datasets for training and accuracy. The sources for these datasets can be either real-time DC experiments, which are impractical or 3-dimensional full-field CFD simulations that are computationally expensive. Besides, to predict and control scenarios that lie outside the cluster of a training dataset, the models must extrapolate, which often leads to large errors in temperature predictions.

Other methods employ heuristic approaches that use empirical parameters to simplify the governing physical laws and then predict temperatures at the specific locations, such as server inlets [25]–[28]. For instance, a three-dimensional zonal model for room-based cooling with a raised floor employs a characteristic dimension of 1m to predict temperature distributions within zones in front of server racks [25]. It is intuitive the such a large zone should lead to a loss of granularity and therefore diminish the predictive accuracy. Besides, the model requires information about mass flowrates, which must be obtained from computationally expensive CFD simulations. A rapid CFD and lumped capacitance hybrid model can predict temperature fluctuations in front of servers as a function of transient events, such as server shutdown and cooling failure [26], but this method also requires CFD simulations for each case to determine parameters and index values. Thus, obtaining real-time temperature distributions and integrating them with the IT infrastructure control system is unfeasible with these heuristic methods.

Because it can predict temperatures with a higher resolution and accuracy than lumped models, zonal modeling is widely used for HVAC and building energy management [25], [29]–[33]. This method partitions a space into coarse zones assumed to have uniform physical characteristics, e.g., temperature, pressure and velocity, to which mass and energy conservation relations are applied. The method reduces the solution time considerably by replacing the partial differential equations for mass, momentum and energy conservation with a system of ordinary differential equations.

We provide a new parameter-free zonal transient model that is based on an analysis of mechanical resistances. The model predicts real-time temperature distributions within ITE enclosures. As a representative case study to demonstrate its applicability, an enclosed micro-DC containing separated cold and hot chambers, which is cooled by one or more in-row cooling units, is considered. The model conserves energy in each zone within the enclosure and determines its temperature. The air flowrates required to maintain energy conservation within the enclosed geometry for the pressure-driven flow are determined through an auxiliary mechanical resistance network and by applying mass conservation for each zone. This approach avoids the necessity of performing CFD simulations, experiments, or the training of empirical parameters through ML. The novelty of the work, therefore, is the development of a computationally inexpensive mechanical resistance network approach that resolves the flow field, unlike the conventional ML or CFD based approaches available in the literature. We integrate the mechanical resistance-based flow modeling with the energy balance equations to rapidly predict the temperature distribution inside enclosed DCs for different operating conditions. The model can be employed for, (a) thermal-aware workload management, (b) development of a model-predictive controller for the cooling units, (c) design optimization purposes, (d) investigating *what if scenarios* in DCs, and (e) fault prediction purposes.

Our objectives are to (1) demonstrate the applicability of mechanical resistance-based zonal modeling for enclosed micro-DCs that are integrated with in-row cooling units that have separated hot and front chambers, (2) validate the model using experiments, (3) investigate the effect of passive server placement on the evolution of local hot spots, (4) investigate the influence of in-row cooling unit operational parameters on the temperature distribution, (5) investigate the effect of IT load distribution across the racks and servers on chiller coefficient of performance (COP), and (6) compare thermal performance of the row-based cooling architecture when one or else two in-row cooling units are placed within the enclosure.

7.4 Methodology

7.4.1 System configuration

The geometry of an enclosed micro-DC cooled by in-row cooling units is shown in Figure 7-1, where the fans inside the cooling units are two prime airflow movers besides the fans in the servers. The cooling units draw warm air from a back chamber, extract heat from it and release cold air into a front chamber. The servers breathe in cold air from the front chamber and release warm air to the back chamber. The flowrate mismatch between the servers and the cooling units and the separation between the chambers creates a pressure difference $\Delta P = P_b - P_f$ between the chambers. This difference produces leakage between the chambers in the direction of the pressure differential, either from the front to the back chamber ($\Delta P < 0$) or vice versa ($\Delta P > 0$). By solving the energy balance for each zone considering the mass transfer between the two, the corresponding temperature can be determined. As mentioned, we use a mechanical resistance network to determine the flowrates within the enclosure instead of performing CFD simulations.

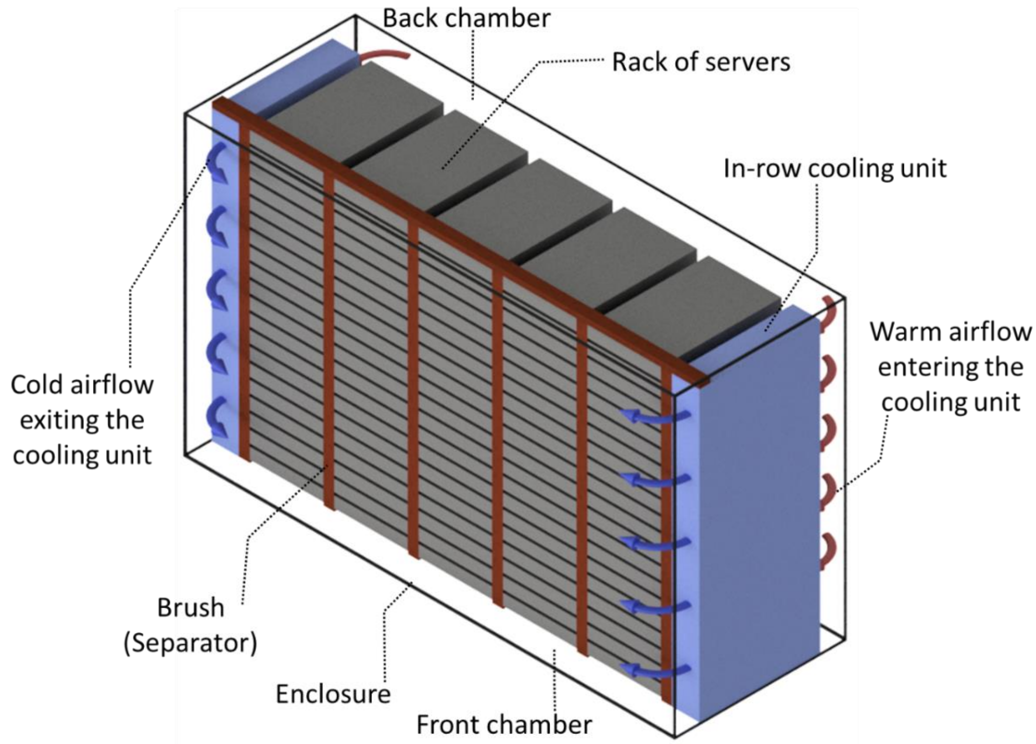

Figure 7-1: Schematic of the IT enclosure integrated with five IT racks and two in-row cooling units (CUs) with separated cold and back chambers. In the front chamber, cold air exits the CUs and is drawn into the servers. In the back chamber, hot air exits the servers and is drawn into the CUs. There is leakage airflow through the brushes that separate the two chambers, either from the hot to the front chamber or vice versa depending upon the pressure differences.

The zones inside the enclosure are presented in Figure 7-2. Neglecting heat and mass transfer between the enclosure and its ambient, six control volumes are considered, i.e., (1) the zones in front of each server, (2) the zones at the back of each server, (3) the zones in front of the cooling units, (4) the zones at the back of the cooling units, (5) each server itself, and (6) the cooling unit. The cooling unit contains a heat exchanger that transfers heat from the warmed air to a chilled water loop that is supplied by an external system consisting of a chiller and circulation pump.

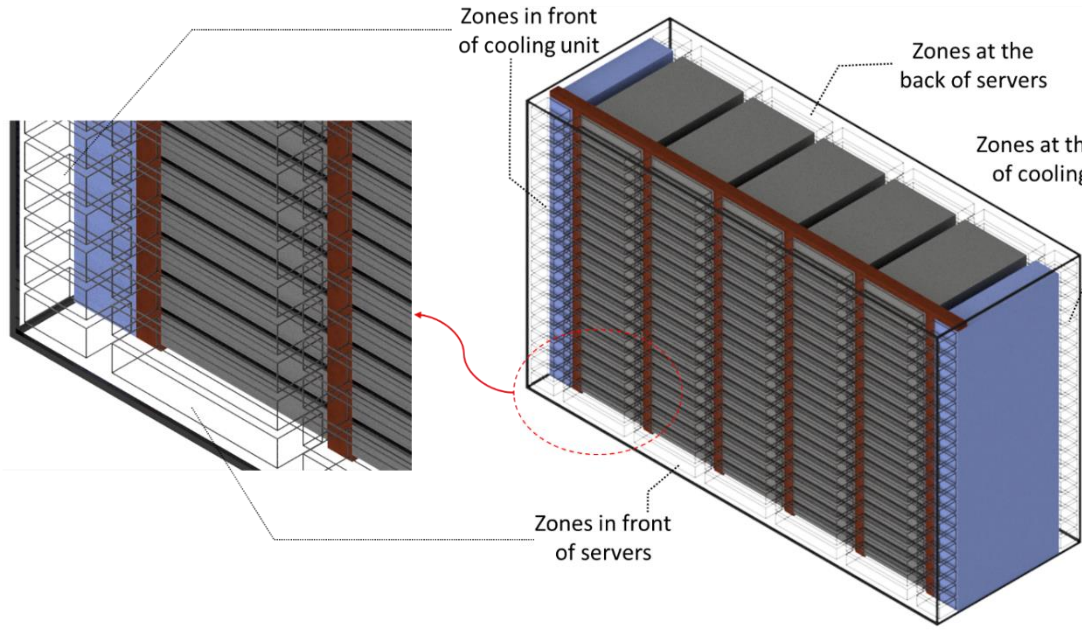

Figure 7-2: Zones considered inside the enclosure.

7.4.2 Flow-resistance network representation and flowrate calculation

Enclosed DCs contain a pressure driven airflow for which mechanical resistances can be described to determine the flowrates. The mechanical resistance network for the system is depicted in Figure 7-3, where voltage is analogous to pressure and current to airflow. The in-row cooling units are thus represented as a source of current, or the air flowrates Q_c. Each active server is a single current source because it draws in specific air flowrate Q_s. A passive server, i.e., one that is not powered, is a resistance R_s that is a porous separator that allows air to travel between the back and front chambers. Essentially, a passive server behaves as a porous duct through which the flowrate responds to the pressure difference between the front and back chambers [34]. Separators (or brushes) create resistances, R_{br} that prevent air leakage between the front and back chambers. The resistances to airflows along the vertical heights of the front and back chambers are denoted as $R_{f,V}$ and $R_{b,V}$, respectively, and those along the horizontal widths of the front and back chambers are likewise $R_{f,H}$ and $R_{b,H}$.

The flow Q_c is an order of magnitude larger than Q_s. Although $R_{br} > R_s$, these two resistances are of the same order of magnitude, but $R_{f,H}, R_{f,V}, R_{b,H}$, and $R_{b,V}$ are all an order of magnitude smaller in comparison because the characteristic dimensions of the corresponding chambers are an order of magnitude larger than those of the holes in the brushes and server channels through which air flows.

If the flowrate from the cooling units is smaller than the total flowrate through the servers, the resulting pressure difference ΔP is positive, i.e., hot air leaks through the passive servers and brushes into the front chamber. On the other hand, if the flowrate from the cooling units is larger than the total flowrate through the servers, ΔP is negative, i.e., cold air now leaks from the front into the back chamber.

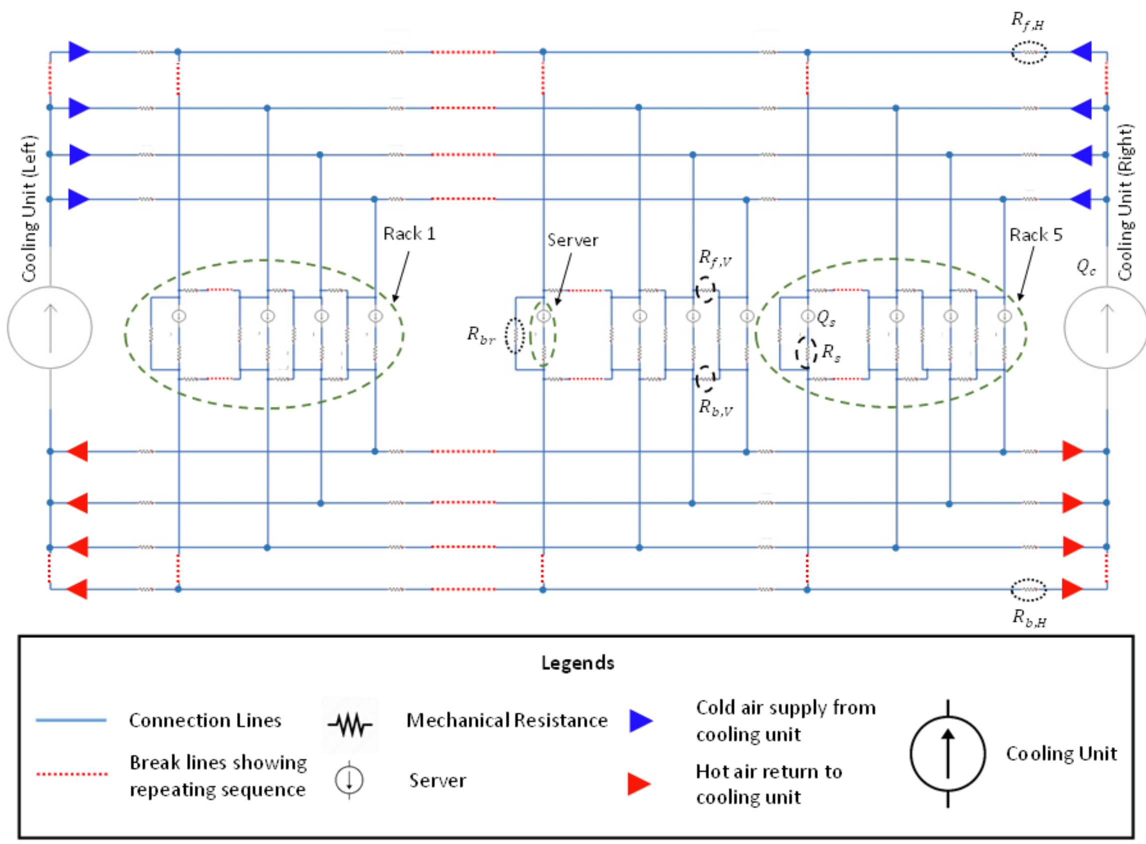

Figure 7-3: Generalized flow resistance network inside the IT server enclosure with five racks (each having 20 servers) and two in-row cooling units. The red and blue arrows show the warm air return and cold air supply path from the cooling unit. The repeating sequences of servers and mechanical resistances are shown with red dotted line.

The air flowrate through the cooling units is determined by the fan control system so that the flow through the in-row cooling unit is solely a function of its fan speed. However, the flowrate of the air drawn by each active server is a function of the server fan speed and the pressure difference between the front and the back of that server. The pressure difference between the chambers is typically of the order of 10 Pa [34], which is not significant enough to influence the flowrate. Consequently, airflow through a server is essentially a function of its fan speed alone. We can therefore assume that the airflow through each active server equals the measured airflow in open space. Since the inlet air temperature is the only factor influencing server fan speed, the air flowrate through an active server is a function of the temperature of the zone in front it. For sake of example, the airflow through an HP ProLiant DL360 G5 server is [34],

$$Q_{s,i,j}(m^3/s) = \begin{cases} 0.01415 & if \quad T_{i,j,f} < 25°C \\ 0.01415 + (T_{i,j,f} - 25) \times 0.00142 & if \quad 25°C < T_{i,j,f} < 35°C \end{cases} \tag{7.1}$$

In Figure 7-4, the zone in front of each server interacts with six airflows, i.e., the air exchange is between a zone of interest and the zones that (1) lie below it, i.e., $Q_{j\rightarrow j-1}$ and (2) lie above it, $Q_{j\rightarrow j+1}$, and on its (3) left, $Q_{i\rightarrow i-1}$ and (4) right, $Q_{i\rightarrow i+1}$, (5) within the corresponding server $Q_{i,j,s}$, and (6) the leakage airflow from the front to the back chamber $Q_{i,j,l}$. A mass balance conducted for the zones in front of active servers reveals,

$$\begin{aligned} &[(P_{i+1,j,f} - P_{i,j,f})/R_{f,H}]^{m} + [(P_{i-1,j,f} - P_{i,j,f})/R_{f,H}]^{m} + [(P_{i,j+1,f} - P_{i,j,f})/R_{f,V}]^{m} \\ &\quad + [(P_{i,j-1,f} - P_{i,j,f})/R_{f,V}]^{m} + [(P_{i,j,b} - P_{i,j,f})/R_{br}]^{m} - Q_{i,j,s} = 0 \end{aligned} \tag{7.2}$$

where m characterizes the relationship between the pressure drop and the flowrate, P denotes pressure, i and j are the horizontal and vertical indices of the zones, respectively, and f represents the zones in front of the servers.

With the mass balance for the zones in front of passive servers,

$$\begin{aligned} &[(P_{i+1,j,f} - P_{i,j,f})/R_{f,H}]^{m} + [(P_{i-1,j,f} - P_{i,j,f})/R_{f,H}]^{m} + \\ &[(P_{i,j+1,f} - P_{i,j,f})/R_{f,V}]^{m} + [(P_{i,j-1,f} - P_{i,j,f})/R_{f,V}]^{m} + [(P_{i,j,b} - P_{i,j,f})/R_{br}]^{m} + \\ &+ [(P_{i,j,b} - P_{i,j,f})/R_{s}]^{m} = 0, \end{aligned} \tag{7.3}$$

Considering the mass balance for the zones at the back of active servers,

$$[(P_{i+1,j,b} - P_{i,j,b})/R_{b,H}]^{\,m} + [(P_{i-1,j,b} - P_{i,j,b})/R_{b,H}]^{\,m} + [(P_{i,j+1,b} - P_{i,j,b})/R_{b,V}]^{\,m} + [(P_{i,j-1,b} - P_{i,j,b})/R_{b,V}]^{\,m} + [(P_{i,j,f} - P_{i,j,b})/R_{br}]^{\,m} + Q_{s,i,j} = 0, \tag{7.4}$$

Where b represents the zones at the back of the servers. The mass balance for the zones at the back of passive servers reveals,

$$[(P_{i+1,j,b} - P_{i,j,b})/R_{b,H}]^{\,m} + [(P_{i-1,j,b} - P_{i,j,b})/R_{b,H}]^{\,m} + [(P_{i,j+1,b} - P_{i,j,b})/R_{b,V}]^{\,m} + [(P_{i,j-1,b} - P_{i,j,b})/R_{b,V}]^{\,m} + [(P_{i,j,f} - P_{i,j,b})/R_{br}]^{\,m} + [(P_{i,j,f} - P_{i,j,b})/R_{s}]^{\,m} = 0, \tag{7.5}$$

The mass balance for the zones in front of the cooling unit leads to,

$$\textstyle\sum_j [(P_{i+1,j,f} - P_{i,j,f})/R_{f,H}]^{\,m} = Q_c, \tag{7.6}$$

where Q_c denotes the cooling unit volumetric air flowrate. Similarly, the mass balance for the zones at the back of the cooling unit is,

$$\textstyle\sum_j [(P_{i+1,j,b} - P_{i,j,b})/R_{b,H}]^{\,m} = Q_c, \tag{7.7}$$

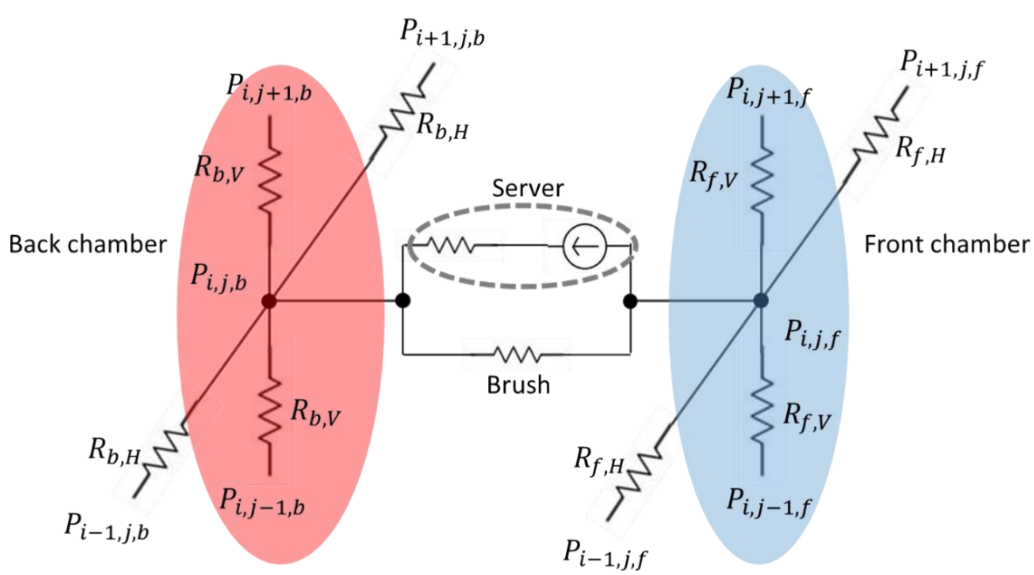

Figure 7-4: Airflows in the zones in front (right) and at the back (left) of servers.

To solve Eq. (7.1)-(7.7) and calculate the corresponding air flowrates for all zones we require the values of m and the resistances. The resistances of the front and back chambers are determined through experiments on an enclosed modular DC that contains two in-row cooling units with separated chambers, as shown in Figure 7-1. To measure the total pressure difference, a differential pressure sensor is used. The volumetric flowrate is calculated by measuring the average air velocity and the cross-section area. The average velocity is calculated by measuring the air velocity at five different points within each sectional area using a Testo-405 anemometer. The pressure drop with respect to the volumetric flowrate for the front and back chambers is reported in Figure 7-5.

The mechanical resistances of the passive servers and brushes are also determined experimentally by measuring the pressure drops and the air flowrates through them. The air flowrate is measured by a Kanomax TABmaster™ 6710 Flow Capture Hood with 0.00235 m^3s^{-1} accuracy and a differential pressure sensor is used to measure the pressure drop. The variation of pressure drop with respect to volumetric flowrate for the passive servers and brushes is presented in Figure 7-6. Based on Figures 7-5 and 6, $m \approx 1$ for all resistances so that these resistances can be reasonably extracted from both figures. We note that a different value, e.g., $m = 0.5$ denoting a parabolic relation between pressure drop and air flowrate can also be applied [35]. Applying equations (7.1)-(7.7) for all servers and their corresponding zones results in a system of linear equations that provide the pressure for each zone.

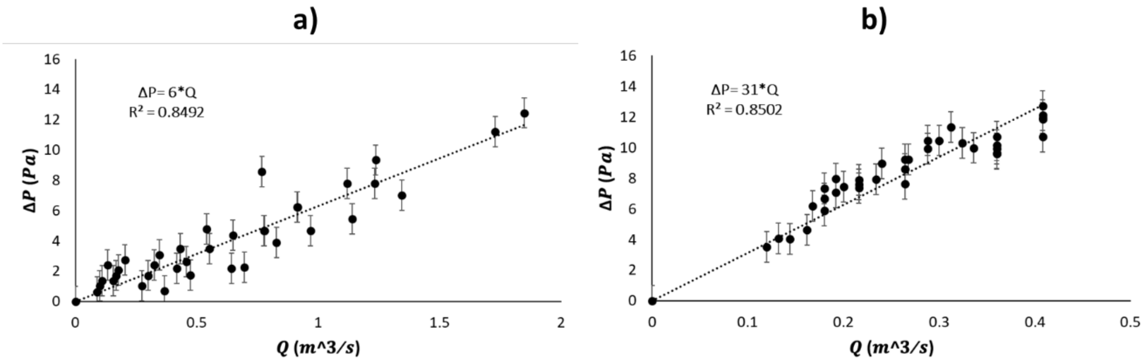

Figure 7-5: Pressure drop *vs*. volumetric air flowrate for the (a) cold front and (b) warm back chambers.

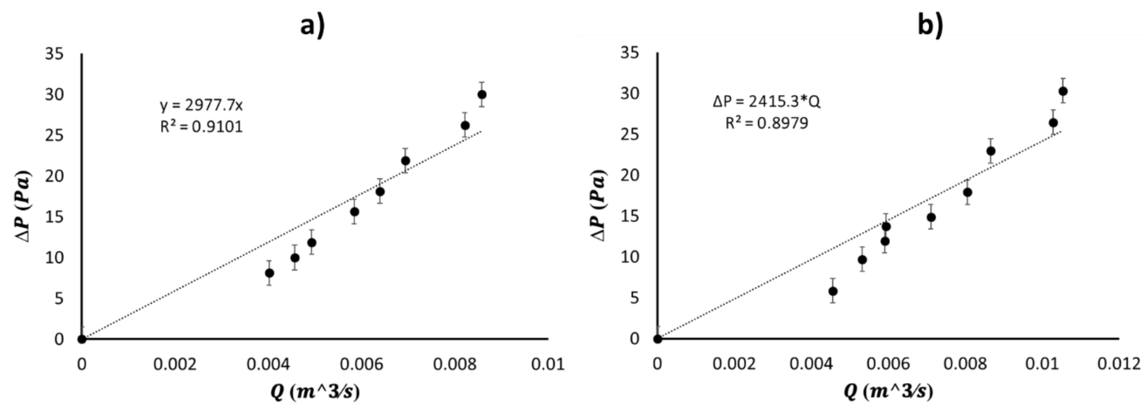

Figure 7-6: Pressure drop *vs*. volumetric air flowrate for (a) passive servers and (b) brushes.

7.4.3 Formulation of energy balance equations

Once the pressure of a zone and the mechanical resistances across it are known, the entering and exiting air flowrates through it can be calculated and the energy balances obtained thereupon. The energy balance for an active server is,

$$\frac{X}{2}\left(\frac{dT_{i,j,s}}{dt}+\frac{dT_{i,j,f}}{dt}\right)=\rho_a c_{p,a} Q_{i,j,s}\left(T_{i,j,f}-T_{i,j,s}\right)+\dot{P}_{i,j,s}, \tag{7.8}$$

where $T_{i,j,s}$ denotes the server exhaust temperature, $T_{i,j,f}$ the temperature of the zone in front of the server, ρ_a air density, $c_{p,a}$ the specific heat of air, X the thermal mass of the server that is available in the literature [36], and $\dot{P}_{i,j,s}$ the total power consumption of the corresponding server. For the airside of the in-row cooling unit,

$$\rho_a c_{p,a} V_a \left(\frac{dT_c}{dt} + \frac{dT_h}{dt}\right) = \rho_a c_{p,a} Q_c (T_h - T_c) - \frac{UA}{2}\left(T_h + T_c - T_{i,w} - T_{o,w}\right), \tag{7.9}$$

and for the waterside within that unit,

$$\rho_w c_{p,w} V_w \left(\frac{dT_{i,w}}{dt} + \frac{dT_{o,w}}{dt}\right) = \rho_w Q_w c_{p,w}\left(T_{i,w} - T_{o,w}\right) + \frac{UA}{2}\left(T_h + T_c - T_{i,w} - T_{o,w}\right), \tag{7.10}$$

where T_c denotes the air temperature at the exhaust of the in-row cooling unit, T_h the temperature of air entering the cooling unit, $T_{i,w}$ and $T_{o,w}$ the water inlet and outlet temperatures, Q_w the water flowrate, $c_{p,w}$ the specific heat of water, ρ_w the density of water, U the overall heat transfer coefficient inside the in-row cooling unit, which is a function of Q_c and Q_w, A the contact area on each fluid side, and V_a and V_w the air and water volumes inside the heat exchanger. Since the value of UA for air to water heat exchanger is a weak function of the water flowrate that depends primarily on the air flowrate, it is a function of Q_c.

For the zones in front and back of servers, the energy balance is,

$$\rho_a c_{p,a} V_z \alpha \left(\frac{dT_{i,j}}{dt}\right) = \phi_1 + \phi_2 + \phi_3 + \phi_4 + \phi_5 + \phi_6, \tag{7.11}$$

where α is a correction factor for the thermal masses of the zones which is experimentally determined, V_z the volume of the chamber, and ϕ the energy exchange for the zones. Table 7-1 contains expressions for each term in Equation (7.11).

Table 7-1: Expressions for the terms in Equation 7.11.

Zones in front of the servers		Zones at the back of the servers	
Φ_1		Φ_1	
$(P_{i+1,j,f} - P_{i,j,f}) \geq 0$	$\rho_a c_{p,a} [(P_{i+1,j,f} - P_{i,j,f})/R_{f,H}]\ T_{i+1,j,f}$	$(P_{i+1,j,b} - P_{i,j,b}) \geq 0$	$\rho_a c_{p,a} [(P_{i+1,j,b} - P_{i,j,b})/R_{b,H}]\ T_{i+1,j,b}$
$(P_{i+1,j,f} - P_{i,j,f}) < 0$	$\rho_a c_{p,a} [(P_{i+1,j,f} - P_{i,j,f})/R_{f,H}]\ T_{i,j,f}$	$(P_{i+1,j,b} - P_{i,j,b}) < 0$	$\rho_a c_{p,a} [(P_{i+1,j,b} - P_{i,j,b})/R_{b,H}]\ T_{i,j,b}$
Φ_2		Φ_2	
$(P_{i-1,j,f} - P_{i,j,f}) \geq 0$	$\rho_a c_{p,a} [(P_{i-1,j,f} - P_{i,j,f})/R_{f,H}]\ T_{i-1,j,f}$	$(P_{i-1,j,b} - P_{i,j,b}) \geq 0$	$\rho_a c_{p,a} [(P_{i-1,j,b} - P_{i,j,b})/R_{b,H}]\ T_{i-1,j,b}$
$(P_{i-1,j,f} - P_{i,j,f}) < 0$	$\rho_a c_{p,a} [(P_{i-1,j,f} - P_{i,j,f})/R_{f,H}]\ T_{i,j,f}$	$(P_{i-1,j,b} - P_{i,j,b}) < 0$	$\rho_a c_{p,a} [(P_{i-1,j,b} - P_{i,j,b})/R_{b,H}]\ T_{i,j,b}$
Φ_3		Φ_3	
$(P_{i,j+1,f} - P_{i,j,f}) \geq 0$	$\rho_a c_{p,a} [(P_{i,j+1,f} - P_{i,j,f})/R_{f,V}]\ T_{j+1,j,f}$	$(P_{i,j+1,b} - P_{i,j,b}) \geq 0$	$\rho_a c_{p,a} [(P_{i,j+1,b} - P_{i,j,b})/R_{b,V}]\ T_{i,j+1,b}$
$(P_{i,j+1,f} - P_{i,j,f}) < 0$	$\rho_a c_{p,a} [(P_{i,j+1,f} - P_{i,j,f})/R_{f,V}]\ T_{i,j,f}$	$(P_{i,j+1,b} - P_{i,j,b}) < 0$	$\rho_a c_{p,a} [(P_{i,j+1,b} - P_{i,j,b})/R_{b,V}]\ T_{i,j,b}$
Φ_4		Φ_4	
$(P_{i,j-1,f} - P_{i,j,f}) \geq 0$	$\rho_a c_{p,a} [(P_{i,j-1,f} - P_{i,j,f})/R_{f,V}]\ T_{j-1,j,f}$	$(P_{i,j-1,b} - P_{i,j,b}) \geq 0$	$\rho_a c_{p,a} [(P_{i,j-1,b} - P_{i,j,b})/R_{b,V}]\ T_{i,j-1,b}$
$(P_{i,j-1,f} - P_{i,j,f}) < 0$	$\rho_a c_{p,a} [(P_{i,j-1,f} - P_{i,j,f})/R_{f,V}]\ T_{i,j,f}$	$(P_{i,j-1,b} - P_{i,j,b}) < 0$	$\rho_a c_{p,a} [(P_{i,j-1,b} - P_{i,j,b})/R_{b,V}]\ T_{i,j,b}$
Φ_5		Φ_5	
$(P_{i,j,b} - P_{i,j,f}) \geq 0$	$\rho_a c_{p,a} [(P_{i,j,b} - P_{i,j,f})/R_{br}]\ T_{i,j,b}$	$(P_{i,j,f} - P_{i,j,b}) \geq 0$	$\rho_a c_{p,a} [(P_{i,j,f} - P_{i,j,b})/R_{br}]\ T_{i,j,f}$
$(P_{i,j,b} - P_{i,j,f}) < 0$	$\rho_a c_{p,a} [(P_{i,j,b} - P_{i,j,f})/R_{br}]\ T_{i,j,f}$	$(P_{i,j,f} - P_{i,j,b}) < 0$	$\rho_a c_{p,a} [(P_{i,j,f} - P_{i,j,b})/R_{br}]\ T_{i,j,b}$
Φ_6 (passive server)		Φ_6 (passive server)	
$(P_{i,j,b} - P_{i,j,f}) \geq 0$	$\rho_a c_{p,a} [(P_{i,j,b} - P_{i,j,f})/R_s]\ T_{i,j,b}$	$(P_{i,j,f} - P_{i,j,b}) \geq 0$	$\rho_a c_{p,a} [(P_{i,j,f} - P_{i,j,b})/R_s]\ T_{i,j,f}$
$(P_{i,j,b} - P_{i,j,f}) < 0$	$\rho_a c_{p,a} [(P_{i,j,b} - P_{i,j,f})/R_s]\ T_{i,j,f}$	$(P_{i,j,f} - P_{i,j,b}) < 0$	$\rho_a c_{p,a} [(P_{i,j,f} - P_{i,j,b})/R_s]\ T_{i,j,b}$
Φ_6 (Active server)		Φ_6 (Active server)	
$-\rho_a c_{p,a} Q_{i,j,s} T_{i,j,f}$		$\rho_a c_{p,a} Q_{i,j,s} T_{i,j,s}$	

The dimensionless forms of temperature and time are,

$$\theta = \frac{T - T_{ref}}{T_0 - T_{ref}}, \qquad (a) \qquad\qquad \tau = \frac{t}{t_0}, \qquad (b) \tag{7.12}$$

where T_{ref} and t_0 denote reference values for temperature and time and T_0 the initial temperature. Hence, the dimensionless forms of the energy equations for the server are

$$\frac{d\theta_{i,j,s}}{d\tau} + \frac{d\theta_{i,j,f}}{d\tau} = \frac{2\rho_a c_{p,a} Q_{i,j,s} t_0}{X} (\theta_{i,j,f} - \theta_{i,j,s}) + \frac{2 t_0 \dot{P}_{i,j,s}}{X(T_0 - T_{ref})}, \tag{7.13}$$

and for the in-row cooling units,

$$\frac{d\theta_c}{d\tau} + \frac{d\theta_h}{d\tau} = \frac{2Q_c t_0}{V_a}(\theta_h - \theta_c) - \frac{2t_0 UA}{\rho_a c_{p,a} V_a}(\theta_h + \theta_c - \theta_{i,w} - \theta_{o,w}), \tag{7.14}$$

$$\frac{d\theta_{i,w}}{d\tau} + \frac{d\theta_{o,w}}{d\tau} = \frac{2Q_w t_0}{V_w}(\theta_{i,w} - \theta_{o,w}) + \frac{2t_0 UA}{\rho_w c_{p,w} V_w}(\theta_h + \theta_c - \theta_{i,w} - \theta_{o,w}). \tag{7.15}$$

For zones in the front and back of the servers, the dimensionless form of the relation is,

$$\frac{d\theta_{i,j}}{d\tau} = \sum_{k=1}^{6} \frac{\Phi_k t_0}{\rho_a c_{p,a} V_z \alpha (T_0 - T_{ref})}, \tag{7.16}$$

The procedure to determine the temperature of each zone at a particular time follows. (1) Specify the initial temperatures, (2) prescribe Q_c and Q_w, (3) determine the flowrates by applying equations (7.1)-(7.7) for all zones and solve the system of linear equations, (4) solve equations (7.13)-(7.16) for all zones to determine the temperatures at a particular time, and (5) repeat the process by advancing it by $\Delta\tau$.

7.4.4 Power consumption calculation

The temperature distribution alone is insufficient to characterize the influence of different system parameters. Hence, the power consumption of the cooling components must also be determined. For the present configuration, the primary energy consuming components include (1) in-row cooling unit blowers, (2) chilled water pumps. and (3) the chiller. The chilled water pumps consume at most 3% of total cooling power [36], such that for a 30% increase in water pumping power, which is in any case unlikely to occur, the total cooling power change is a negligible 1%. Hence, only components (1) and (3) are considered. To determine the energy consumption of in-row cooling unit blowers and the chiller, the total heat rejection from ITEs, total cooling unit air flowrate, chilled water temperature entering the in-row cooling unit, and the ambient air temperature must be known.

The power consumed by the refrigeration system in the chiller is a function of the heat load of its evaporator, the temperature of the fluid entering condenser, the desired setpoint temperature of the water leaving the evaporator, and other operating and design parameters, including the loading of the chiller with respect to its rated capacity. While there are several analytical models available in the literature that characterize chiller operation, the Gordon–Ng model is selected for its simplicity and ease since readily available data can fit model coefficients. The model has the form [37],

$$y = a_1x_1 + a_2x_2 + a_3x_3, \text{ where} \tag{7.17}$$

$$x_1 = T_{co}/Q_{ch}, \tag{7.18}$$

$$x_2 = (T_{ci} - T_{co})/(T_{ci} \times Q_{ch}), \tag{7.19}$$

$$x_3 = ([(1/COP) + 1] \times Q_{ch})/T_{ci}, \text{ and} \tag{7.20}$$

$$y = [(1/COP) + 1] \times (T_{co}/T_{ci}) - 1, \tag{7.21}$$

where COP denotes the coefficient of performance defined as the ratio of the evaporator heat load to the electrical power consumed by the compressor, T_{ci}, and T_{co} the fluid temperatures entering the condenser and leaving the evaporator, respectively, and Q_{ch} the chiller heat load. Data for Q_{ch}, COP, T_{ci}, and T_{co} are obtained from the manufacturer of a 50 kW chiller [38] that, when fitted to Equation (7.17), provide the relation,

$$y = 0.023x_1 + 1.39x_2 + 0.32x_3. \tag{7.22}$$

Since the condenser temperature is assumed constant, we use 9 data points at a constant condenser temperature for regression for which the residual sum of squares is 1.4×10^{-6}. Equation (7.22) provides the chiller power consumption once the total cooling load, evaporator temperature, and condenser temperature are known.

The power consumption of the fans inside the in-row cooling unit is calculated for the Rittal TopTherm-LCP-Rack-CW [39]. Based on its data sheet and its fan [40], the relation between the air flowrate provided and the power consumption is,

$$\dot{P}_{fans} = 480 - 3073Q_c + 6031Q_c^2 \tag{7.23}$$

where $\dot{P}_{fans}$ denotes the total power consumption of the fans inside each cooling unit.

7.5 Results and discussion

7.5.1 Model validation

To validate the model, the temperature profiles for an arbitrary IT load distribution are experimentally measured for three different cooling unit air flowrates and compared with model predictions. The experiments are performed on an enclosed modular DC with separated chambers. The DC has five racks and two in-row cooling units located at the ends.

Figure 7-7 demonstrates this comparison for three cooling unit air flowrates, i.e., (a) high ($Q_c > \sum Q_s$), (b) medium ($Q_c \sim \sum Q_s$), and (c) low ($Q_c < \sum Q_s$). The total IT load of the racks is 20kW. Each rack contains 5 temperature sensors, i.e., 25 sensors are mounted at different locations in the front chamber . The difference between the predicted and measured temperatures at each location is reported in the figure.

Figure 7-7.a shows that the maximum difference between the model and the experiment is lower than 1ºC. The probability of hot spot formation is low due to cold air oversupply which results in more a uniform temperature distribution in the front chamber. In Figure 7-7.b, the difference between the model and experiment for 20 locations is lower than 1ºC, for 4 locations smaller than 1.6ºC, and for a single location is more than 2ºC. In Figure 7-7.c, for 20 locations the deviation of the predictions from measurements is again lower than 1ºC, for 3 locations it is smaller than 1.6ºC, and for two locations more than 2ºC. For the two last cases, more hot spots appear in the cooler front chamber because the cold air flowrate is lower. Overall though, Figure 7-7 shows that the model predicts the temperature distribution reasonably well.

$$\varepsilon = T_f^{exp} - T_f^{model}\ (°C)$$

a

0.1	0.2	-0.3	-0.1	-0.1
0.1	-0.1	-0.2	0.1	0.4
-0.4	-0.1	-0.2	-0.2	0.2
-0.2	-0.1	-0.3	-0.1	0.1
0.1	-0.2	-0.3	-0.3	-0.1

$Q_c > \sum Q_s$

b

-0.5	0.8	-0.6	-0.7	-0.2
-0.3	0.0	0.8	-0.2	-0.2
-0.5	0.4	0.9	0.1	-0.2
-0.7	0.0	-0.8	1.1	0.5
-1.3	-1.6	-2.4	0.2	1.4

$Q_c \sim \sum Q_s$

c

0.9	0.1	-0.2	-1.4	0.3
0.4	0.5	0.2	0.4	-0.1
0.8	-0.2	-0.9	-0.2	0.0
1.0	-0.9	0.2	-0.6	-0.9
1.4	1.4	-0.2	-2.8	-2.1

$Q_c < \sum Q_s$

Figure 7-7: Difference ε between the temperature predicted by the model and the measured temperature at 25 different locations in the front chamber. (a) High cooling unit air flowrate, i.e., $Q_c > \sum Q_s$. (b) Medium cooling unit air flowrate, i.e., $Q_c \sim \sum Q_s$. (c) Low cooling unit air flowrate, i.e., $Q_c < \sum Q_s$. The. total IT load of the racks is 20 kW. Green, yellow, and red colors specify that ε is lower than 1°C, 1.6 °C, and 3 °C respectively.

7.5.2 Influence of passive server location

Passive servers that are not utilized in DCs are usually switched off. In an enclosed DC with separated hot and front chambers, passive servers act as porous ducts connecting the two chambers. This behavior enables flow and energy transport across the chambers and significantly influences the temperature of the front chamber. We investigate when (a) a passive server plays an important role in altering the front chamber temperature, and (b) the influence of its location inside the enclosure. Figure 7-8 demonstrates the influence of cooling unit air flowrate on the temperature distribution in the front chamber when there are passive servers for the micro-DC configuration of Figure 7-1. Each rack is assumed to contain five passive servers. For all the scenarios, we consider the same water flowrate and water inlet temperature.

Based on Figure 7-8, when the cooling unit air flowrate is high, or $Q_c > \sum Q_s$, a passive server does not have any effect on the temperature distribution. When the cooling unit air flowrate $Q_c \leq \sum Q_s$, the hot air recirculation through the passive server increases. As shown in Figure 7-3, passive servers are mechanical resistances and the direction of the airflow through them is a function of pressure difference across the servers. If the air flowrate of the cooling units is greater than that drawn by the servers, or $Q_c > \sum Q_s$, the pressure of the front chamber is higher than that of the back chamber, resulting in air flow through the passive servers from the front to the back chamber, a phenomena known as cold air bypass. If the air flowrate of the cooling units is lower than that drawn by the servers, i.e., $Q_c \leq \sum Q_s$, the pressure in the front chamber is lower than in the back chamber, resulting in air flow through the passive server from the back to the front chamber, termed as hot air recirculation.

The location of a passive server, specifically its distance from the cooling unit, influences the airflow distribution and consequently the temperature distribution, since the mechanical resistance circuit depends on the location of the passive server. Figure 7-9 presents the influence of passive server location on the maximum and average temperatures in the front chamber. For all cases, the air and water flowrates, and water inlet temperature of the cooling unit are the same. Each case considers 20 passive servers within a rack of interest.

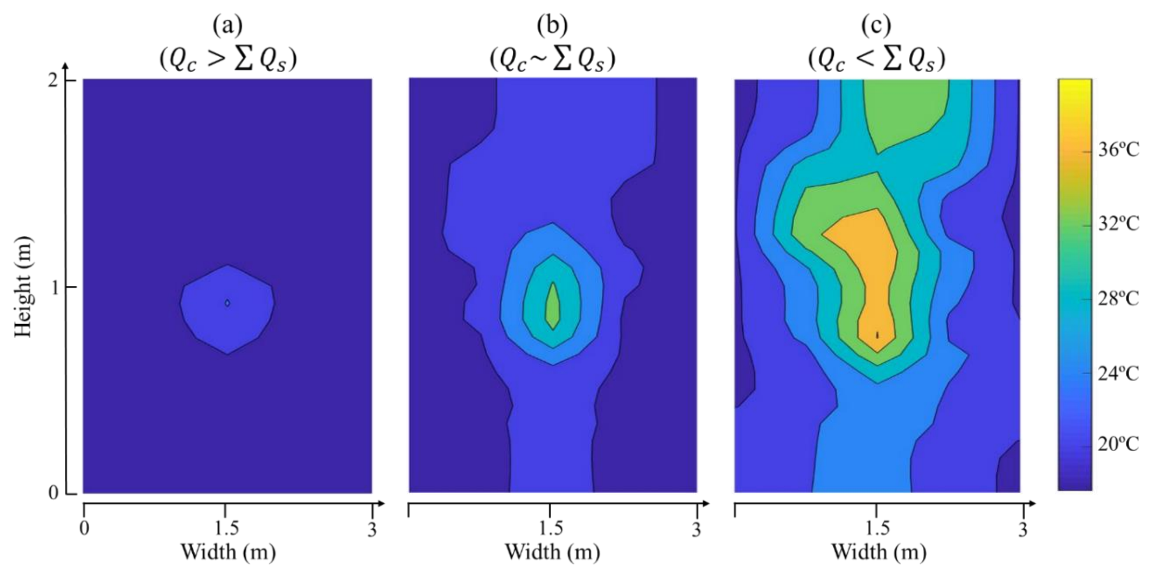

Figure 7-8: Influence of cooling unit air flowrate on the temperature distribution of the front chamber in the presence of passive servers.

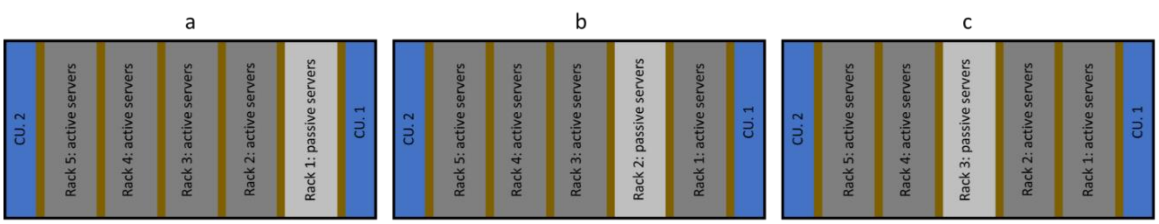

case	Average temperature of the front chamber (ºC)	Maximum temperature of the front chamber (ºC)
a	20.8	25.2
b	21.7	29.3
c	23.5	37.5

Figure 7-9: Influence of passive server location on the maximum and average temperature in the front chamber.

Figure 7-9 shows that placing passive servers near the cooling units reduces the magnitude of hot air recirculation through these servers. The recirculation through passive servers is a function of the pressure difference ($P_b - P_f$) across them. Moving from the cooling unit toward the middle of the rack, P_f decreases and P_b increases, increasing ($P_b - P_f$) which in turn increases the hot air recirculation through passive servers. Thus, passive servers should be placed in proximity to the in-row cooling unit to minimize hot air recirculation.

7.5.3 Effect of water inlet temperature, water flowrate, and air flowrates of the cooling unit

We now investigate the influence of the (1) water inlet temperature, (2) water flowrate, and (3) air flowrate of the cooling unit on the temperature distribution in the front chamber and the cooling power consumption for an arbitrary load distribution. Figure 7-10 depicts the influence of a 10% change in each of these three parameters. Figure 7-10.1 shows that a 1.25 °C reduction in water inlet temperature results in 1.3 °C rise in the average temperature of the front chamber, whereas the cooling power changes by only 170 W, an overall 2.5% increase. Figure 7-10.2 reveals that a 10% change in the water flowrate does not significantly influence the temperature distribution, but a 10% change in the air flowrate (Figure 7-10.3) alters the average front chamber temperature by 3.1 °C. Although changing the water flowrate does not alter the cooling power consumption since water flow is regulated by controlling the valves, increasing the air flowrate by 10% results in a 430 Watt increment, or a 7% change, in cooling power consumption.

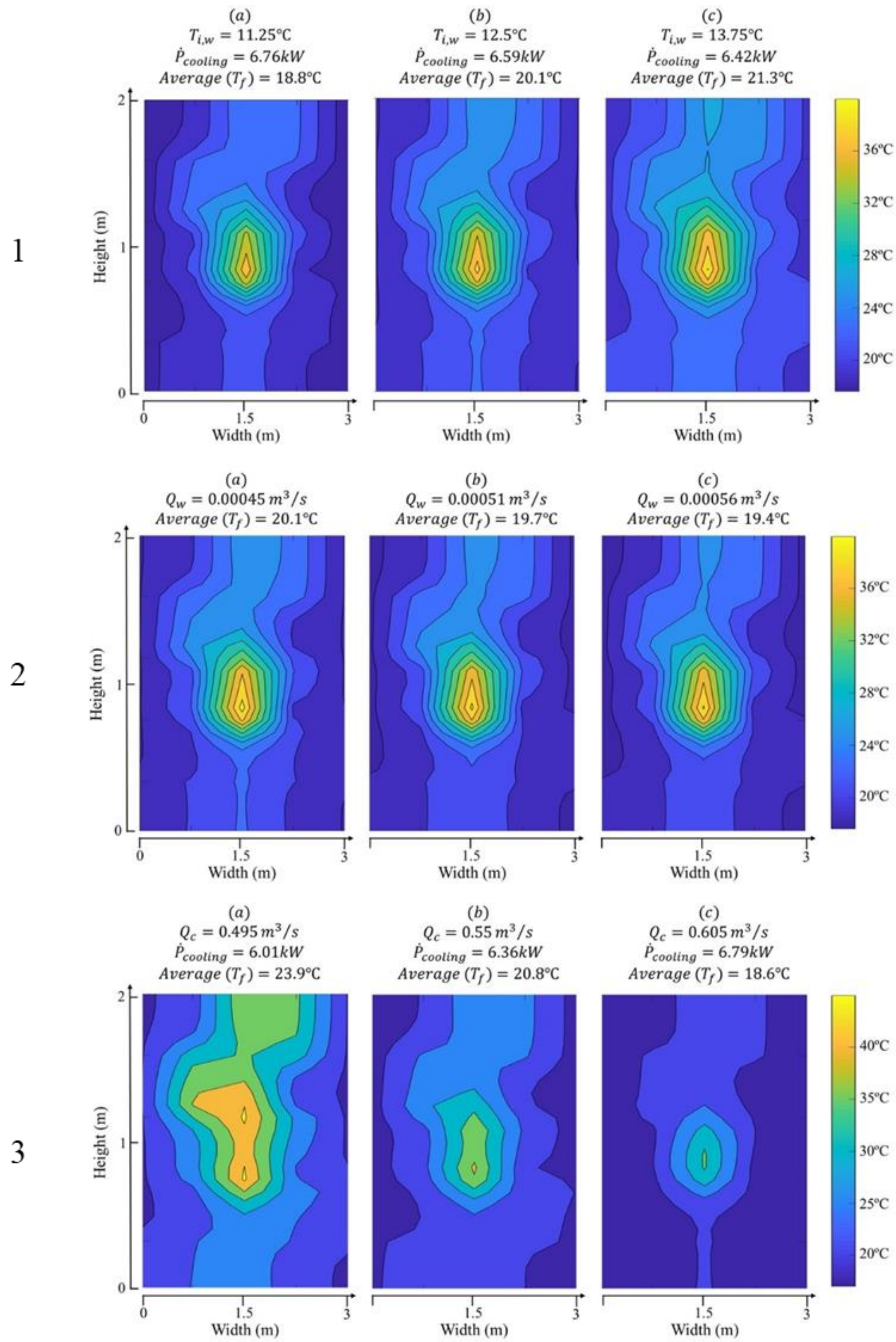

Figure 7-10: Influence of water inlet temperature (1), water flowrate (2), and air flowrate (3) of the in-row cooling unit on temperature distribution and power consumption.

The cooling unit employs an air to water finned tube heat exchanger for which,

$$T_{air} = (Q/R_{tot-HE}) + T_{water} \quad (7.25)$$

where R_{tot-HE} denotes the total thermal resistance of the heat exchanger, T_{air} and T_{water} the average temperatures of the air and water inside the heat exchanger respectively, and Q the heat transfer rate. Increasing water flowrate results in a minor reduction in R_{tot-HE}, while increasing air flowrate considerably reduces R_{tot-HE} because the total thermal resistance of the heat exchanger includes three thermal resistances, i.e., (1) through the metallic body of the heat exchanger (which is 5% of the total), (2) metal body to water (15%), and (3) metal body to air (80%) [41]. This is supported by Figure 7-10 where a 10% reduction in the air flowrate produces an appreciable increase in temperature compared to a proportional change in the water flowrate.

The water inlet temperature does not influence R_{tot}, implying a linear relation (see Equation 7.25) between T_{water} and T_{air}, which is supported by Figure 7-10.1. For all cases demonstrated in Figure 7-10, the heat load at steady state is constant.

7.5.4 Effect of IT load on coefficient of performance (COP)

The cooling system efficiency is measured by calculating the COP as the ratio of total heat load (the IT load in this case) to the cooling power consumption. We investigate the effect of IT load on the COP for our specific DC architecture. Figure 7-11 describes the relationship between the IT load and COP. Figure 7-11.a shows that increasing the IT load by changing the utilization improves the cooling efficiency because (1) the total air flowrate drawn by the servers remains constant, and (2) the temperature of heat source, i.e., CPU temperature, increases, resulting in a larger temperature difference between the hottest (CPU) and coldest (chilled water) points of the system, in turn improving the heat transfer efficiency. Figure 7-11.b shows that increasing the IT load by changing the number of servers reduces the cooling efficiency because the total air flowrate drawn by the servers increases, resulting in higher fan power consumption in the cooling unit. Therefore, to increase cooling energy efficiency, the IT load should be increased by increasing utilization but not the number of active servers.

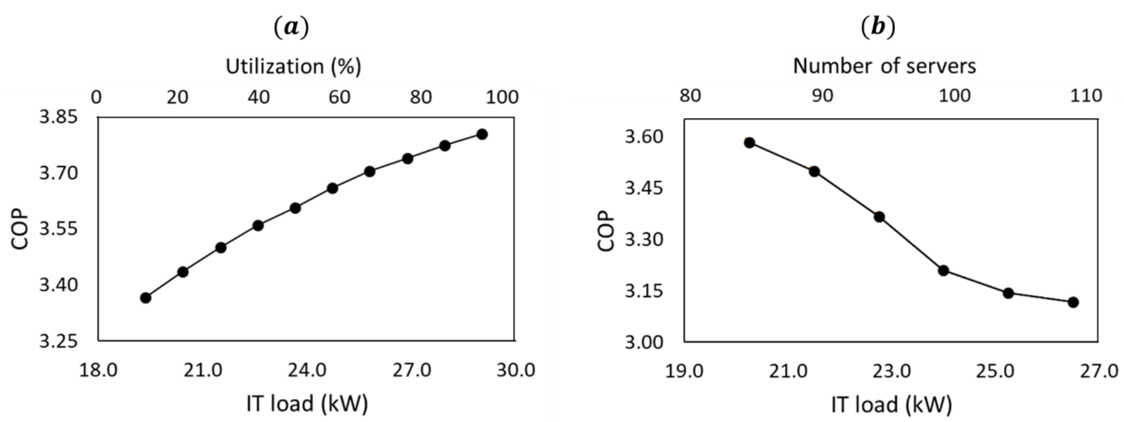

Figure 7-11: Effect of IT load on COP. (a) The number of servers is constant, and the IT load is increased by increasing the utilization of each server. (b) The utilization of each server remains constant, but the IT load is increased by increasing the number of active servers.

7.5.5 Comparing a single in-row cooling unit with two in-row cooling units

The above cases consider two in-row cooling units within the enclosure that are located at the left and right ends of the rows. Table 7-2 compares cooling of an enclosed row with two in-row cooling units and a single unit, keeping the IT load distribution, geometry and other parameters for both cases the same. The air flowrates into the cooling units are adjusted to maintain a maximum temperature no greater than 27ºC in the front chamber.

Installing two cooling units results in a lower average temperature in the front chamber as well as lower power consumption. Further away from the cooling unit, the pressure in the front chamber is reduced while the pressure in the back chamber increases (Figure 7-3), i.e., $(P_b - P_f)$ and the intensity of hot air recirculation through the passive server increase. For a single cooling unit, the rack farthest from the cooling unit is now the fifth. The temperature distribution is more uniform with two cooling units, leading to a lower required cold air flowrate and lower fan power consumption. The reason for lower power consumption for scenario (b) in Table 7-2 is that the relation between air flowrate and power consumption is parabolic. Distributing the total required air flowrate to a larger number of fans considerably reduces the total power consumption.

Table 7-2: Comparison of the cooling performance for an enclosed row with a single in-row cooling unit and one with two in-row cooling units.

	(a) One cooling unit	**(b) Two cooling units**
Maximum temperature of the front chamber (°C)	27	27
Ave temperature of the front chamber (°C)	21.4	18.2
Total air flowrate of the cooling units (m^3/s)	1.49 (1.49+0)	1.35 (0.675+0.675)
Fan power consumption (kW)	4.2	2.1
Chiller power consumption (kW)	5.3	5.3
Total cooling power consumption (kW)	9.5	7.4
IT load (kW)	24	24

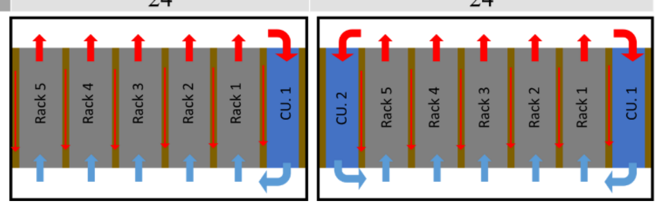

7.5.6 Comparison with other temperature prediction tools

Temperature prediction tools inform the controllers and facilitate failure prognosis. Hence, the computational time required to accurately predict the temperature distribution is an important consideration. Compared to CFD, the model described here is able to more quickly determine temperatures. The model provides results in less than 60s, while a CFD simulation for a similar geometry takes hours [17], [21], [34]. For instance, if a DC design requires that a hundred cases be investigated, the model can provide results in less than 100 minutes whereas it would take around 4 days to perform the corresponding CFD simulations. This time-saving advantage of the model makes it suitable for real-time control. ML-based temperature prediction tools, which use experimental data, usually require about 15 hours of training for a specific geometry and IT load distribution [42], [43]. Some ML-based tools which use CFD simulations as their source require even a longer duration. For example, a model reported in the literature that requires CFD simulations takes 28 hours to run on a computer equipped with a Quadcore Intel i7 CPU @ 3.4 GHz and 8 GB of RAM [20]. Another model requires 30 different CFD simulations for training to predict the temperature in front of 30 servers [21]. We use an Intel (R) Core (TM) i7 6700 HQ CPU @ 2.6 GHz with 16 GB of RAM. Since the model solves the energy balance for each zone at each time step, the computational time increases linearly when the numbers of zones and the prediction times increase. The time interval to advance the simulation for all cases is 0.001 seconds. Increasing this interval to 0.01 seconds decreases the computational time by a tenth. Table 7-3 compares the method with other temperature prediction methods reported in the literature.

Table 7-3: Comparison of the method with other available temperature prediction methods.

	CFD	**Machine Learning-based**	**Present work**
Required time to simulate one specific scenario	Hours	Minutes	Minutes
Required time to train, calibrate, or setup the model	Hours/days	Hours/days	Hour
Resolution	(~cm)	(~m)	(~m)
Training, calibrating or simulating should be redone because of changing the IT load configuration	Yes	Depends on the model	No
Training, calibrating or simulating should be redone because of changing the geometry	Yes	Yes	No
Capturing major physical aspects	Yes	No	Yes
Capturing minor physical aspects	Yes	No	No
Possibility of inaccuracy because of difference in training and testing data	NA	Yes	NA
Number of required cases for training or calibrating	NA	~100	NA

7.6 Conclusion

We provide an efficient model to characterize the real time temperature distribution within an IT server enclosure that contains an integrated in-row cooling unit. The flow field is predicted based on mechanical resistances and coupled with zonal energy balance equations, a process that is computationally less expensive than typical methods. In contrast to control schemes such as POD, ML, and other heuristic models, the model requires no *a priori* training. Upon experimental validation, model predictions of the temperatures deviate at most by 2.8 °C from experimental measurements. The model is also combined with calculations of cooling power consumption to determine the influence of different IT infrastructure parameters on energy consumption for cooling.

The influence of the (1) locations of passive servers, (2) cooling unit water inlet temperature, and water and air flowrates, (3) imposed IT load distribution, and (4) utilization of two cooling units rather than a single unit are investigated. Salient findings include:

1. Passive servers should be located in racks placed closer to the cooling unit to maintain a colder temperature in the front chamber.
2. A 10% change in water flowrate increases temperatures in the front chamber by lower than 2%. A 10% increase in the water temperature increases the average temperature in the front chamber by 7% and decreases the cooling power consumption by 2.5%.
3. Increasing the airflow rate by 10% increases the cooling power consumption by 7% and decreases the mean temperature in the front chamber by 13%.
4. In order to increase the cooling energy efficiency, the IT load should be increased by increasing the utilization of each server rather than increasing the number of servers.
5. Using two in-row cooling units to lower the portion of the total cooling capacity provided by each unit decreases the front chamber temperature on average by 15% and provides up to 22% reduction in cooling power consumption as compared to using a single in-row unit that carries the entire cooling capacity.

The model facilitates real-time spatiotemporal control for enclosed IT infrastructures equipped with in-row cooling units.

7.7 Acknowledgment

This research was supported by the Natural Sciences and Engineering Research Council (NSERC) of Canada under a collaborative research and development (CRD) project, “Adaptive Thermal Management of Data Centers”. We also thank our colleagues from CINNOS Mission Critical Inc. who provided insight and expertise that assisted the research.

7.8 References

[1] A. Shehabi, S. Smith, D. Sartor, R. Brown, M. Herrlin, "United States Data Center Energy Usage Report, LBNL-1005775", BERKELEY NATIONAL LABORATORY, 2016.

[2] J. Dai, M. M. Ohadi, D. Das, and M. G. Pecht, "Optimum Cooling of Data Centers, Application of Risk Assessment and Mitigation Techniques", Springer Science Business Media, New York, 2014, DOI: 10.1007/978-1-4614-5602-5.

[3] K. Ebrahimi, G. F. Jones, and A. S. Fleischer, "A review of data center cooling technology, operating conditions and the corresponding low-grade waste heat recovery opportunities," Renew. Sustain. Energy Rev., vol. 31, no. Supplement C, pp. 622–638, Mar. 2014.

[4] H. M. Daraghmeh and C.-C. Wang, "A review of current status of free cooling in datacenters," *Appl. Therm. Eng.*, vol. 114, no. Supplement C, pp. 1224–1239, Mar. 2017.

[5] M. K. Patterson, "The effect of data center temperature on energy efficiency," in *2008 11th Intersociety Conference on Thermal and Thermomechanical Phenomena in Electronic Systems*, 2008, pp. 1167–1174.

[6] J. Cho, J. Yang, and W. Park, "Evaluation of air distribution system's airflow performance for cooling energy savings in high-density data centers," *Energy Build.*, vol. 68, no. PARTA, pp. 270–279, 2014.

[7] A. Capozzoli and G. Primiceri, "Cooling systems in data centers: State of art and emerging technologies," *Energy Procedia*, vol. 83, pp. 484–493, 2015.

[8] S. V. Patankar, "Airflow and Cooling in a Data Center," *J. Heat Transfer*, vol. 132, no. 7, p. 073001, 2010.

[9] T. Evans, "The different types of air conditioning equipment for IT environments," *APC White Pap.*, p. 24, 2004.

[10] K. Dunlap and N. Rasmussen, "Choosing Between Room, Row, and Rack-based Cooling for Data Centers," *Schneider Electr. White Pap. 130*, p. 18, 2012.

[11] H. Moazamigoodarzi, P. Jennifer, S. Pal, S. Ghosh, and I. K. Puri, "Influence of cooling architecture on data center power consumption," *Energy*, vol. 183, pp. 525–535, 2019.

[12] N. El-Sayed, I. A. Stefanovici, G. Amvrosiadis, A. A. Hwang, and B. Schroeder, "Temperature management in data centers: Why some (might) like it hot," *Sigmetrics '12*, no. TECHNICAL REPORT CSRG-615, pp. 163–174, 2012.

[13] V. A. Tsachouridis, P. Sobonski, H. Wiese, D. Mehta, K. Kouramas, and M. Cychowski, "Optimal Thermal Regulation of a Real Data Centre," IFAC-Pap., vol. 50, no. 1, pp. 4893–4898, Jul. 2017.

[14] K. Cho, H. Chang, Y. Jung, and Y. Yoon, "Economic analysis of data center cooling strategies," Sustain. Cities Soc., vol. 31, pp. 234–243, May 2017.

[15] H. Cheung, S. Wang, C. Zhuang, and J. Gu, "A simplified power consumption model of information technology (IT) equipment in data centers for energy system real-time dynamic simulation," Appl. Energy, vol. 222, pp. 329–342, Jul. 2018.

[16] E. Samadiani and Y. Joshi, "Proper Orthogonal Decomposition for Reduced Order Thermal Modeling of Air Cooled Data Centers," *J. Heat Transfer*, vol. 132, no. 7, p. 071402, 2010.

[17] E. Samadiani and Y. Joshi, "Reduced order thermal modeling of data centers via proper orthogonal decomposition: a review," *Int. J. Numer. Methods Heat Fluid Flow*, vol. 20, no. 5, pp. 529–550, 2010.

[18] R. Ghosh and Y. Joshi, "Error estimation in POD-based dynamic reduced-order thermal modeling of data centers," Int. J. Heat Mass Transf., vol. 57, no. 2, pp. 698–707, Feb. 2013.

[19] L. Phan and C.-X. Lin, "Reduced order modeling of a data center model with multi-Parameters," *Energy Build.*, vol. 136, pp. 86–99, 2017.

[20] M. Zapater, J. L. Risco-Martín, P. Arroba, J. L. Ayala, J. M. Moya, and R. Hermida, "Runtime data center temperature prediction using Grammatical Evolution techniques," Appl. Soft Comput., vol. 49, pp. 94–107, Dec. 2016.

[21] G. Varsamopoulos and M. Jonas, "Using transient thermal models to predict cyberphysical phenomena in data centers," ... *Informatics Syst.*, vol. 3, pp. 132–147, 2013.

[22] L. Wang, G. von Laszewski, F. Huang, J. Dayal, T. Frulani, and G. Fox, "Task scheduling with ANN-based temperature prediction in a data center: a simulation-based study," Eng. Comput., vol. 27, no. 4, pp. 381–391, Oct. 2011.

[23] U. Dvhg, R. I. Dqg, O. R. Z. Lq, J. Athavale, Y. Joshi, and M. Yoda, "Artificial Neural Network Based Prediction of Temperature and Flow Profile in Data Centers," 2018 17th IEEE Intersoc. Conf. Therm. Thermomechanical Phenom. Electron. Syst., pp. 871–880, 2020.

[24] V. A. Tsachouridis and T. Scherer, "Data centre adaptive numerical temperature models," vol. 40, no. 6, pp. 1911–1926, 2018.

[25] Z. Song, B. T. Murray, and B. Sammakia, “A compact thermal model for data center analysis using the zonal method,” *Numer. Heat Transf. Part A Appl.*, vol. 64, no. 5, pp. 361–377, 2013.

[26] H. S. Erden, H. E. Khalifa, and R. R. Schmidt, “A hybrid lumped capacitance-CFD model for the simulation of data center transients,” *HVAC R Res.*, vol. 20, no. 6, pp. 688–702, 2014.

[27] Q. Tang, T. Mukherjee, S. K. S. Gupta, and P. Cayton, “Sensor-Based Fast Thermal Evaluation Model for Energy Efficient High-Performance Datacenters,” in 2006 Fourth International Conference on Intelligent Sensing and Information Processing, 2006, pp. 203–208.

[28] R. Sharma, C. Bash, C. Patel, R. J. Friedrich, and J. S. Chase, “Balance of Power: Dynamic Thermal Management for Internet Data Centers,” IEEE Internet Comput., vol. 9, pp. 42–49, Jan. 2005.

[29] J. W. Axley, “Surface-drag flow relations for zonal modeling,” Build. Environ., vol. 36, no. 7, pp. 843–850, Aug. 2001.

[30] F. Haghighat, Y. Li, and A. C. Megri, “Development and validation of a zonal model — POMA,” Build. Environ., vol. 36, no. 9, pp. 1039–1047, Nov. 2001.

[31] J. Gao, J. Zhao, X. Li, and F. Gao, “A Zonal Model for Large Enclosures With Combined Stratification Cooling and Natural Ventilation: Part 1—Model Generation and its Procedure,” J. Sol. Energy Eng., vol. 128, no. 3, pp. 367–375, Aug. 2006.

[32] E. Wurtz, J. M. Nataf, and F. Winkelmann, “Two- and three-dimensional natural and mixed convection simulation using modular zonal models in buildings,” *Int. J. Heat Mass Transf.*, vol. 42, no. 5, pp. 923–940, 1999.

[33] J. Gao, J. Zhao, X. Li, and F. Gao, “Evaluation of a Zonal Model for Large Enclosures Using Computational Fluid Dynamics,” J. Asian Archit. Build. Eng., vol. 6, no. 2, pp. 379–385, Nov. 2007.

[34] H. Moazamigoodarzi, S. Pal, S. Ghosh, and I. K. Puri, “Real-time temperature predictions in IT server enclosures,” *Int. J. Heat Mass Transf.*, vol. 127, pp. 890–900, 2018.

[35] F. M. White, *Fluid Mechanics,* 7th ed. New York: McGraw-Hill, 2009.

[36] Z. M. Pardey, D. W. Demetriou, J. W. Vangilder, H. E. Khalifa, and R. R. Schmidt, “Proposal for Standard Compact Server Model for Transient Data Center Simulations,” *Ashrae*, vol. 121, no. January, pp. 413–422, 2015.

[37] M. Iyengar and R. Schmidt, "Analytical Modeling for Thermodynamic Characterization of Data Center Cooling Systems," *J. Electron. Packag.*, vol. 131, no. 2, p. 021009, 2009.

[38] Product Data Sheet, *Trane*, Air-Cooled Liquid Chillers 10 to 60 Tons, CG-PRC007-EN, April 2004.

[39] Product Data Sheet, *RITTAL*, TopTherm LCP Rack/Inline CW, Model Number: 3311.130/3311.530, 2015.

[40] Product Data Sheet, *ebm-papst* , EC centrifugal fan, Model Number: R3G250-RO40-A9, 2012.

[41] R. K. Shah and D. P. Sekulic, Fundamentals of Heat Exchanger Design. John Wiley & Sons, 2003.

[42] Y. Fulpagare, Y. Joshi, and A. Bhargav, "Rack level forecasting model of data center," in 2017 16th IEEE Intersociety Conference on Thermal and Thermomechanical Phenomena in Electronic Systems (ITherm), 2017, pp. 824–829.

[43] C. M. Liang, L. Li, J. Liu, S. Nath, A. Terzis, and C. Faloutsos, "ThermoCast: A Cyber-Physical Forecasting Model for Data Centers Categories and Subject Descriptors," *7th ACM SIGKDD Int. Conf. Knowl. Discov. Data Min.*, pp. 1370–1378, 2011.

8 Conclusions and future directions

8.1 Conclusions

We compared the power consumption of three DC cooling architectures. Distributed cooling architectures, i.e., row- and rack-based are more energy efficient as compared to the conventional room-based architecture. Adding enclosures within distributed cooling architectures reduces their cooling cost further. These energy savings occur due to significant reductions in recirculation and bypass. Beside improving energy efficiency, distributed cooling architectures, both row- and rack-based, have lower initial cost and are more easily maintained, with greater agility and manageability. Considering all of the above aspects, employing enclosed distributed cooling architectures is the best choice for DC cooling.

We also investigated the temperature and airflow distribution inside an enclosed rack that is internally integrated with an RMCU. Experiments reveal effects due to passive servers, IT load density, IT load distribution and cold chamber depth that guide server configurations and rack geometry. A new metric, *ASTD*, is developed to assess RMCU performance. This investigation proves the potential of placing an RMCU in an enclosed rack as a highly efficient cooling architecture, which requires almost 50% lower airflow as compared to traditional methods.

Based on the knowledge obtained in the previous section, a model is presented to predict the temperature distribution within an IT server enclosure that is integrated with an RMCU. The flow field for this architecture can be predicted using fluid mechanics principles. Consequently, in contrast to other control schemes, no *a priori* training process is required. The model is validated by comparison with experiments, where the maximum difference between predictions and measurements is 4%. The influence of parameters such as the IT load configuration, RMCU flowrates, step changes in system inputs, and utilization of two RMCUs rather than just one are investigated through the model. The model will facilitate real-time control algorithms developed for IT enclosures with RMCU architectures.

Row-based cooling architecture with enclosure is well stablished in the DC industry. Therefore, we provided an efficient model to characterize the real time temperature distribution within an IT server enclosure that contains an integrated in-row cooling unit. The flow field is predicted based on mechanical resistances and coupled with zonal energy balance equations, a process that is computationally less expensive than typical methods. In contrast to control schemes such as POD, ML, and other heuristic models, the model requires no *a priori* training. Upon experimental validation, model predictions of the temperatures deviate at most by 2.8 °C from experimental measurements. The model is also combined with calculations of cooling power consumption to determine the influence of different IT infrastructure parameters on energy consumption for cooling.

In summary, after proving the benefit of distributed cooling for DCs, the knowledge about temperature and airflow distribution inside the enclosed DCs with rack- and row-based cooling architectures were developed. Employing this knowledge, real-time temperature prediction tools for these two architectures were developed.

8.2 Future directions

The results and findings in this work indicate that distributed cooling system for DCs possesses considerable potential for future development. Therefore, the following avenues for future research are recommended based on the results of this research:

- Comparing three cooling architectures for DCs in terms of exergy destruction and potential of waste heat recovery.
- Investigating the possible waste heat recovery technologies which are compatible with DCs with rack- and row-based cooling architectures.
- Employing the proposed models in chapters 6 and 7 for thermal aware workload management in modular DCs.
- Developing model predative controllers (MPC) for DCs with rack- and row-based cooling architectures using the models presented in chapters 6 and 7.

9 Appendix I

9.1 The relation between CPU utilization, server power consumption and cooling power consumption

The total power consumption of a computing server is reported as a linear function of the CPU utilization in the literature [1]–[4]:

$$P_{server} = a + bU \tag{9.1}$$

Where, a and b are constants, and U and P_{server} denote the CPU utilization and server power consumption respectively. Based on this model, the effect of inlet air temperature on the server power consumption is neglected while the power consumption of the fans inside the server is a function of the inlet air temperature. Ham et al. [5] showed that 15ºC increment in inlet air temperature increases the total power consumption of a server up to 3%. Therefore, it is reasonable to ignore the effect of inlet air temperature.

To validate Equation 9.1, we measured the total power consumption of a server (Dell PowerEdge R710) as a function of utilization and inlet air temperature which is presented in Figure 9-1. Based on this figure, 12ºC increment in inlet air temperature causes less than 5% change in the total power consumption. A more accurate model for the power consumption of a server is:

$$P_{server} = a + bU + cT_{in} \tag{9.2}$$

Where, c is a constant, and T_{in} denotes the inlet air temperature. c is an order of magnitude smaller than a and b.

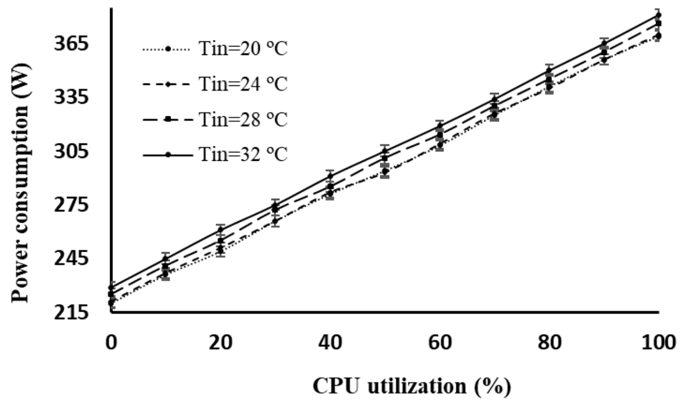

Figure 9-1: Measured power consumption of a computing server (Dell PowerEdge R710) as a function of utilization and inlet air temperature.

Increasing CPU utilization (consequently servers power consumption) results in an increment of heat load. Therefore, the cooling power consumption will be affected directly because (1) the heat load on the chiller is raised, and (2) the air temperature inside the DC room raises, resulting in higher required air flowrate and fans power consumption to keep temperatures in front of the server less than a threshold. Figure 9-2 shows the effect of utilization on the (a) chiller and air handler power consumption (left), and (b) average temperature of the front chamber, and the ratio of the cooling power consumption to the IT load (right). The demonstrated data are for an enclosed DC integrated with two in-row cooling units which are obtained from the model presented in chapter 7. The criterion is to keep the temperature in front of the servers less than 27ºC. The utilization of the servers is increased uniformly.

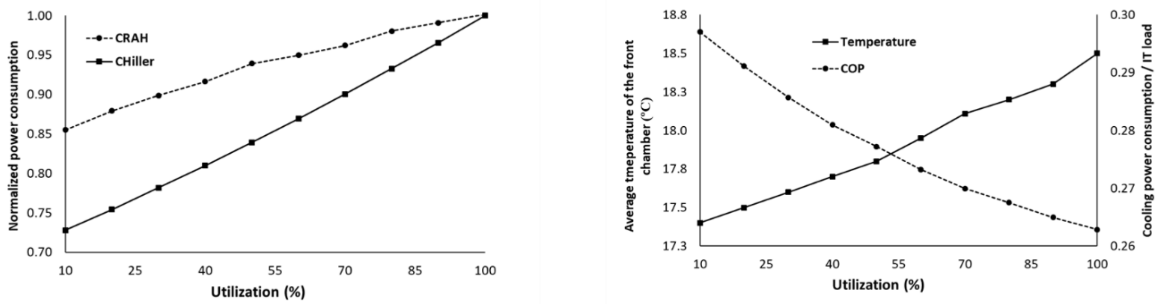

Figure 9-2: The effect of utilization on the (a) chiller and air handler power consumption (left), and (b) front chamber temperature, and ratio of the cooling power consumption to the IT load (right). Normalized power consumption is the ratio of the power consumption to its maximum value.

9.2 Relation between the network analysis and the physics of the dimensionless analysis

The proposed dimensionless numbers in chapter 4 capture the physical parameters that influence air distribution deficiency. Here, we expound these dimensionless numbers using mechanical resistance network analysis. The two dimensionless numbers are:

$$B = \sqrt{\frac{\mu}{\rho \bar{V} L}} \times \frac{\dot{m}_{CU}}{\dot{m}_{IT}} \times \frac{L^2}{A_{IT}} \times \frac{(\pi + 2k\pi)}{(\alpha + 2k\pi)} \tag{9.3}$$

$$R = \sqrt{\frac{\mu}{\rho \bar{V}' L'}} \times \frac{\dot{m}_{IT}}{\dot{m}_{CU}} \times \frac{L'^2}{A_{CU}} \times \frac{(\pi + 2k\pi)}{(\alpha' + 2k\pi)} \tag{9.4}$$

Where, B and R characterize bypass and recirculation respectively. ρ and μ are the density and dynamic viscosity of air respectively. $\bar{V}$ denotes the air velocity exiting the cooling unit, $\bar{V}'$ the air velocity exiting the servers, L the distance from the cooling unit exhaust to the servers inlet, L' the distance between the cooling unit inlet and servers exhaust, $\dot{m}_{CU}$ the air flowrate of the cooling unit, $\dot{m}_{IT}$ the air flowrate of the servers, A_{IT} cross section area of the servers inlet, and A_{CU} cross section area of the cooling unit inlet.

α is the angle between the normal vectors orthogonal to the cooling unit exhaust and the server inlet, α' the angle between the normal vectors orthogonal to the cooling unit entrance and the servers exhaust, and k a positive integer.

Figure 9-3 demonstrates a simplified mechanical resistance network for an enclosed DC including one single rack and a RMCU.

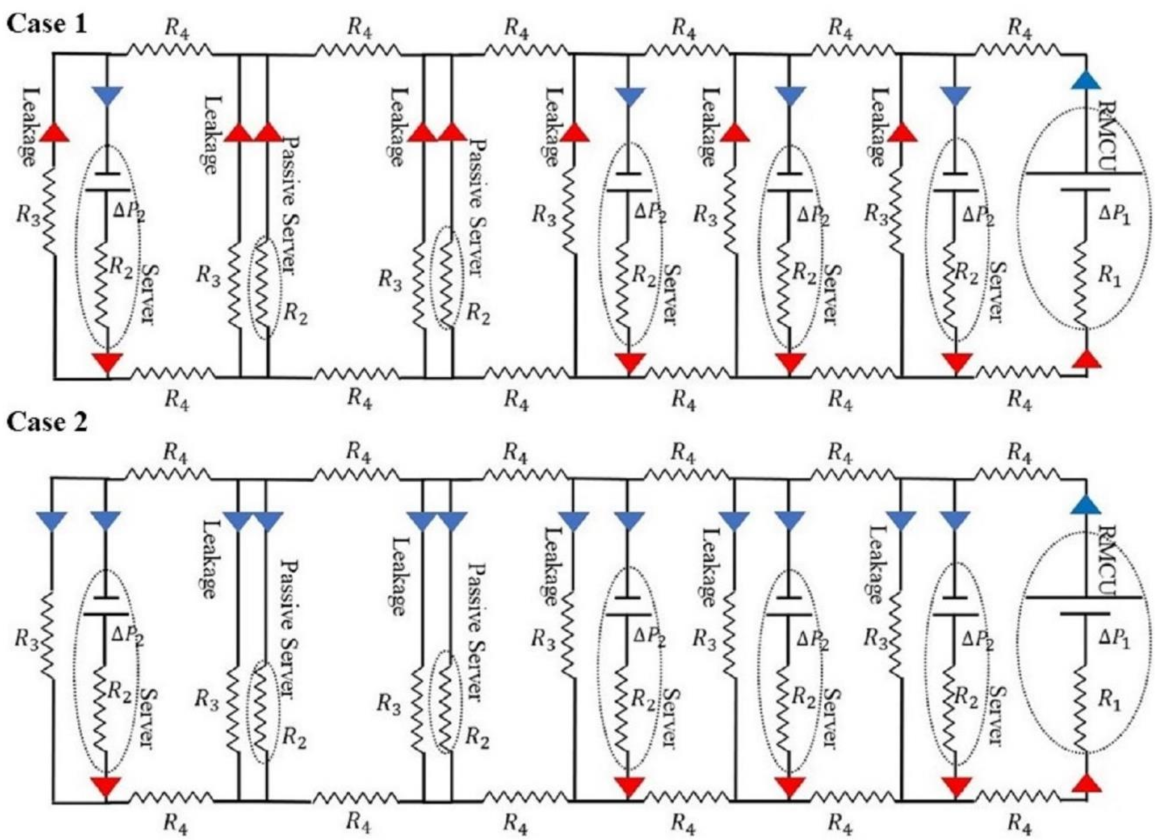

Figure 9-3: Simplified flow-resistance network inside the enclosure. Case 1: Recirculation. Case 2: Bypass. The RMCU is considered as a power supply (ΔP_1) and the airflow resistance across the heat exchanger is assumed to be in series (R_1). Similarly, active servers are represented as a single power supply (ΔP_2) with an airflow resistance (R_2), but their power supplies (essentially, their fans) increase the pressure in the reverse direction. Passive servers are simply considered to be a resistance (R_2). The resistance against the airflow between the hot and cold chambers is (R_3). The third airflow resistance in the enclosure lies along the height in the cold and hot chambers (R_4).

In Figure 9-3, higher $\Delta P_1/\Delta P_2$ results in higher possibility of bypass, while higher $\Delta P_2/\Delta P_1$ leads to higher possibility of recirculation. $\Delta P_1/\Delta P_2$ can be translated to $\dot{m}_{CU}/\dot{m}_{IT}$ and based on Equation 9.1, higher $\dot{m}_{CU}/\dot{m}_{IT}$ leads to a higher chance of bypass. Similar explanation applies to $\Delta P_2/\Delta P_1$ and $\dot{m}_{IT}/\dot{m}_{CU}$ in Equation 9.2. L^2/A_{IT} in Equation 9.1, influences R_4 for the front chamber directly. Longer the distance between the cooling unit exhaust and the servers inlet, higher the value of R_4, while larger the section area of the target (servers inlet), lower the value of R_4. Therefore, the higher value of L^2/A_{IT} results in higher R_4 for the front chamber leading to higher amount of bypass. Employing a similar reasoning, the higher value of L'^2/A_{CU} results in higher R_4 for the back chamber and higher possibility of recirculation. The value of α is ranging from 0 to π. Lower value of α means more misalignment between the cooling unit exhaust and the servers inlet resulting in higher R_4 for the front chamber and higher possibility of bypass. Similarly, Lower value of α' results in higher R_4 for the back chamber and higher possibility of recirculation.

So, three of the four dimensionless ratios presented in R and B are expounded by employing mechanical resistance network analysis. The network presented here is for rack-based architecture, but this methodology can be applied for other cooling architectures.

9.3 Effect of IT load on COP

The cooling system efficiency is measured by calculating the COP as the ratio of total heat load (the IT load in this case) to the cooling power consumption. Here, we investigate the effect of IT load on the COP for the DC architecture presented in chapter 7. To increase the IT load there are two options: (1) increasing the workload (CPU utilization) of each server while the number of active servers remains the same, and (2) increasing the number of active servers while the workload (CPU utilization) of the servers remains constant.

Figure 9-4 shows the effect of IT load on the power consumption, COP, and temperature when the IT load is adjusted by controlling servers workload (CPU utilization). The criterion is to keep the temperature in front of each server below 27ºC. The cooling energy efficiency is improved by increasing the CPU utilization, because (1) the total air flowrate drawn by the servers remains constant, and (2) the temperature of heat source, i.e., CPU temperature, increases, resulting in a larger temperature difference between the hottest (CPU) and coldest (chilled water) points of the system, in turn improving the heat transfer efficiency.

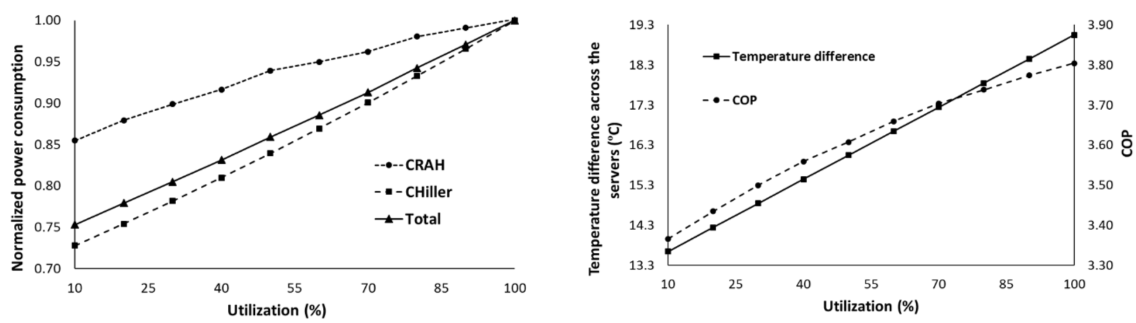

Figure 9-4: Effect of CPU utilization on the cooling power consumption (left), temperature difference across the servers and COP (right). The temperature in front of the servers is kept lees than 27ºC. Normalized power consumption is the ratio of the power consumption to its maximum value.

Figure 9-5 shows the effect of IT load on the power consumption, COP, and temperature when the IT load is adjusted by controlling the number of servers. The criterion is to keep the temperature in front of each server less than 27ºC. Increasing the IT load by introducing further active servers to the system reduces the cooling energy efficiency because the total air flowrate drawn by the servers increases, resulting in higher fan power consumption in the cooling unit. Therefore, to improve the cooling energy efficiency, the IT load should be increased by increasing the CPU utilization rather than increasing the number of active servers.

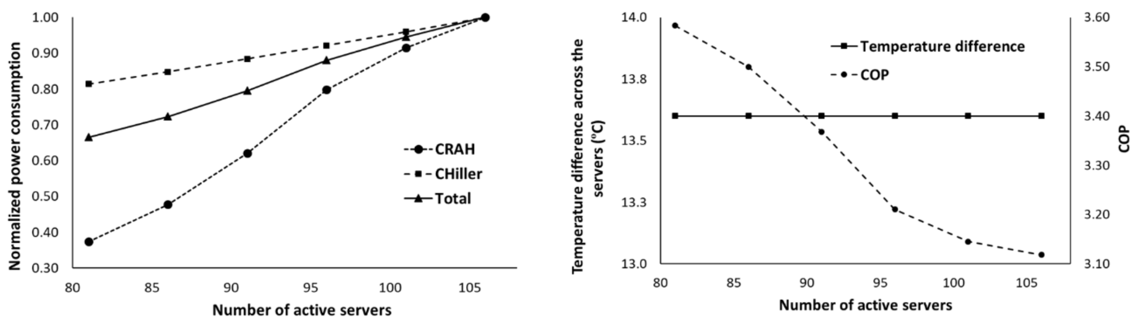

Figure 9-5: Effect of number of active servers on the cooling power consumption (left), temperature difference across the servers and COP (right). The temperature in front of the servers is kept lees than 27ºC. Normalized power consumption is the ratio of the power consumption to its maximum value.

9.4 Implications

The first part of this study, which compares traditional room-based cooling architectures with row- and rack-based, can be used as a guideline to push DC designers toward modular DCs with distributed cooling. The industrial funder of this research (CINNOS Mission Critical Inc.) and other companies who design, fabricate, and install modular DCs with row- and rack-based cooling architectures, refer to the paper published based on the results of chapter 4 to prove the benefits of the distributed cooling for DCs.

The temperature prediction models in chapters 6 and 7 are being used as a tool for (1) thermal aware workload management, (2) model-based control algorithms, (3) cooling fault prediction, and (4) cooling system design in modular DCs with rack- and row-based cooling architectures. Here are some implications of the results of chapter 5, 6 and 7:

- *"Joint Data Center Cooling and Workload Management: A Thermal-Aware Approach",* SeyedMorteza MirhoseiniNejad, **Hosein Moazamigoodarzi**, Ghada Badawy, and Douglas G. Down, Published in *Journal of Future Generation Computer Systems.*
- *"Energy-efficient data-based zonal control of temperature for data centers",* Masoud Kheradmandi, **Hosein Moazamigoodarzi**, and Douglas G. Down, Accepted in *The Tenth international green and sustainable computing conference.*
- CINNOS Mission Critical Inc. is developing a design tool to determine the required number of in-row cooling units and their optimum locations using the temperature prediction tool developed in chapter 7.
- *"Data driven fault tolerant thermal management of data centers"* Masoud Kheradmandi and Douglas G. Down, Submitted in *International Conference on Computing, Networking and Communications (ICNC 2020)*.
- *"Temperature distribution estimation via data-driven model and adaptive Kalman filter in modular data centers"*, Kai Jiang, Shizhu Shi, **Hosein Moazamigoodarzi**, Chuan Hu, Souvik Pal and Fengjun Yan, under review in *Proceedings of the Institution of Mechanical Engineers, Part I: Journal of Systems and Control Engineering.*
- *"Rack-based Data Center Temperature Regulation Using Data-driven Model and Predictive Controller"* Shizhu Shi, Kai Jiang, Masoud Kheradmandi, **Hosein**

Moazamigoodarzi, Souvik Pal and Fengjun Yan, Under review in *Journal of Process Control*.

9.5 General applicability and limitations of the presented modeling method and indices

9.5.1 Temperature prediction tools

The temperature prediction tools developed in chapters 6 and 7 are applicable to all enclosed DCs with either rack mountable or in-row cooling units, but the following information about the system is required:

- The air and water flowrate of the cooling unit
- Overall heat transfer coefficient of the heat exchanger inside the cooling unit
- IT load and air flowrate of the servers
- Mechanical resistance (lost coefficient) of the separator (e.g., brushes), servers, front and back chambers

Therefore, after obtaining the abovementioned information, the proposed temperature predictors are applicable as a design or evaluation tool for any enclosed DC with rack mountable or in-row cooling unit.

9.5.2 Indices

In chapter 4, recirculation (*R*) and bypass (*B*) numbers are proposed to capture the physical parameters affecting the air distribution deficiency. There are many dimensionless indices in the literature, e.g., return heat index (RHI), rack cooling index (RCI), and recirculation index (RI), but all of these capture the temperature distribution which is the result of recirculation and bypass, while *R* and *B* represent the causes of these phenomena. Like other DC thermal performance indices, *R* and *B* are applicable to all DCs with any configuration and cooling architecture. Although all existing indices, including *R* and *B*, are applicable for DC thermal performance evaluation, they cannot be used as a design tool.

9.6 The role of the standard deviation in active server temperature distribution (ASTD)

To quantitatively evaluate the influence of different parameters on the temperature distribution, ASTD metric was introduced in chapter 5. The primary cooling requirement in a DC is to provide air to servers that is colder than a specific temperature. The average of temperature in front of servers can be considered as the simplest representative of temperature distribution. Additionally, a smaller temperature gradient along the height of the rack is desirable, because the high temperature gradient indicates hot air recirculation. Therefore, the proposed metric should capture the uniformity of the temperature distribution. The simplest metric to demonstrate the level of nonuniformity is standard deviation. Our proposed metric is based on the average temperature at the inlets of active servers $\bar{T}_{fa}$ and the standard deviation of active server inlet temperatures $\sigma_{T_{fa}}$,

$$ASTD = \bar{T}_{fa} + \sigma_{T_{fa}} \tag{9.5}$$

Defining the metric depends on the purpose of evaluation, for example, if the target is to keep the servers safe and functional, the maximum temperature is a proper metric. Here, ASTD is defined to minimize the temperature gradient along the height of the rack, which is an indication of hot air recirculation. Performing further statistical analysis on the probability density distribution of temperatures is not applicable here, since the data points are not independent, as the temperatures of different points are correlated to each other.

9.7 Clarifications for Chapters 4 and 5

9.7.1 Schematic of physical parameters in Equation 4.7

$$B = \sqrt{\frac{\mu}{\rho \bar{V} L}} \times \frac{\dot{m}_{CU}}{\dot{m}_{IT}} \times \frac{L^2}{A_{IT}} \times \frac{(\pi + 2k\pi)}{(\alpha + 2k\pi)} \tag{4.7}$$

where ρ and μ are the density and dynamic viscosity of air respectively, $\bar{V}$ the jet velocity exiting the cooling unit, and L the distance from the jet source (from the cooling unit to the ITEs). $\dot{m}_{IT}$ and $\dot{m}_{CU}$ are the mass flowrate through the servers and cooling units. A_{IT} is the cross-section area of the server inlets and α is the angle between the normal vectors orthogonal to the cooling unit exhaust and the server inlet.

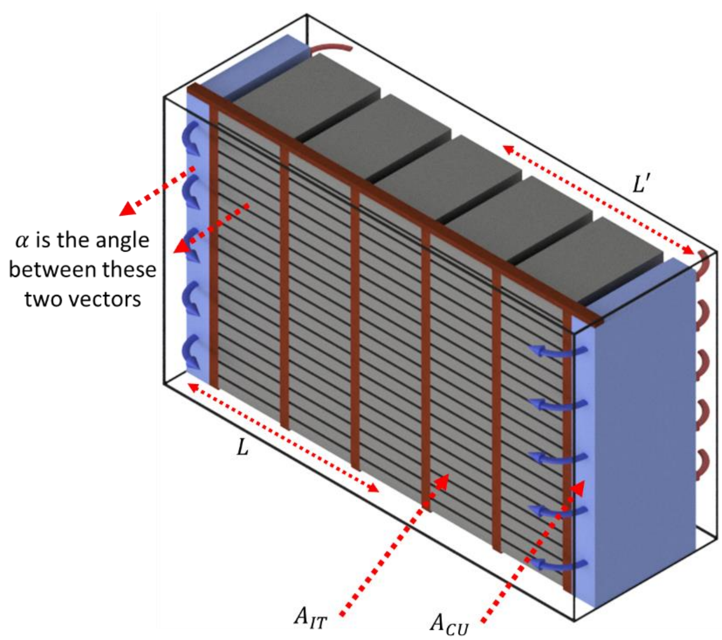

Figure 9-6: Schematic of physical parameters in Equation 4.7.

9.7.2 Schematic of the plate used to capture the temperature contour (Figure 5.7)

Here, the position of the aluminum plate that is used to capture the temperature contour by FLIR ONE Pro thermal camera in chapter 5 is demonstrated (Figure 5.7).

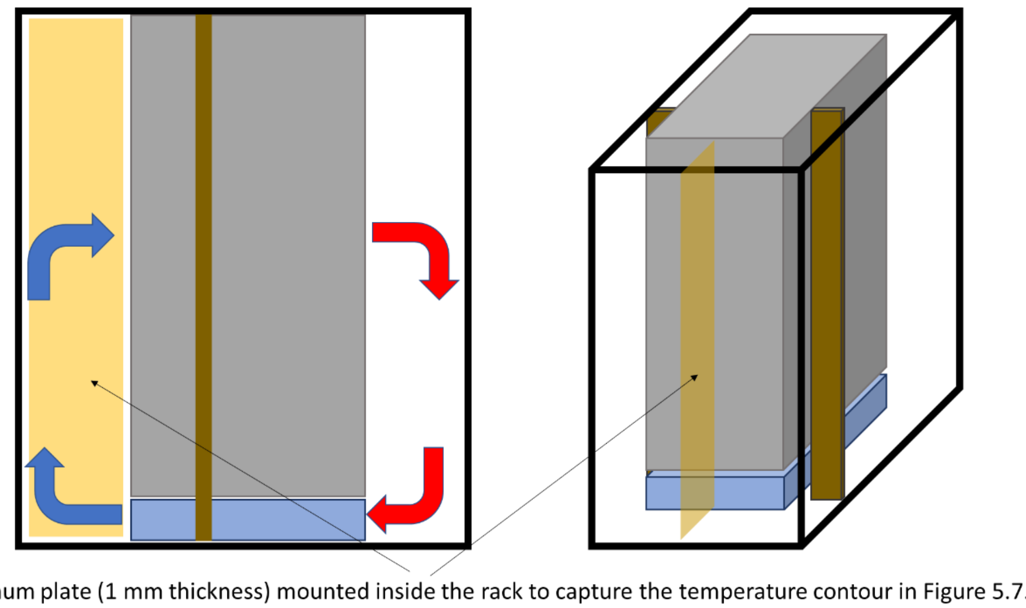

Figure 9-7: Schematic of the plate used to capture the temperature contour.

9.8 More information about the CFD simulations in Chapter 4

9.8.1 Temperature contour and velocity vector

In this section, the temperature contour and velocity vector for two specific cases of enclosed rack- and row-based cooling architectures are presented.

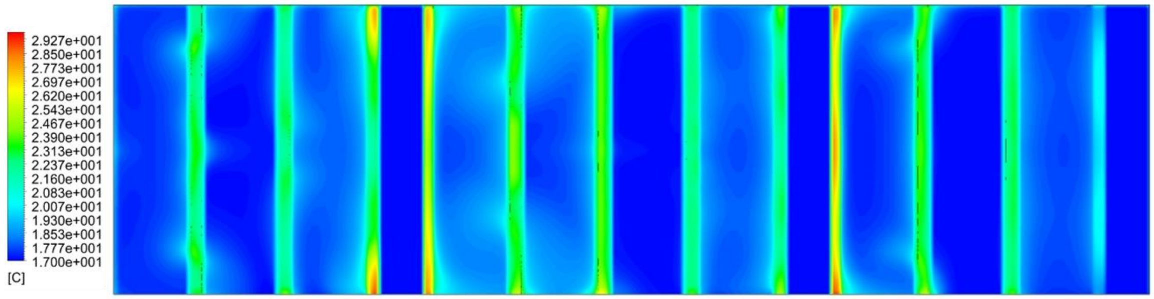

Figure 9-8: Temperature contour of the front chamber, for row-based cooling architecture. The cooling unit setpoint: 18ºC. Cooling units air flowrate: 1.375 m^3/s. Each rack IT load: 5kW.

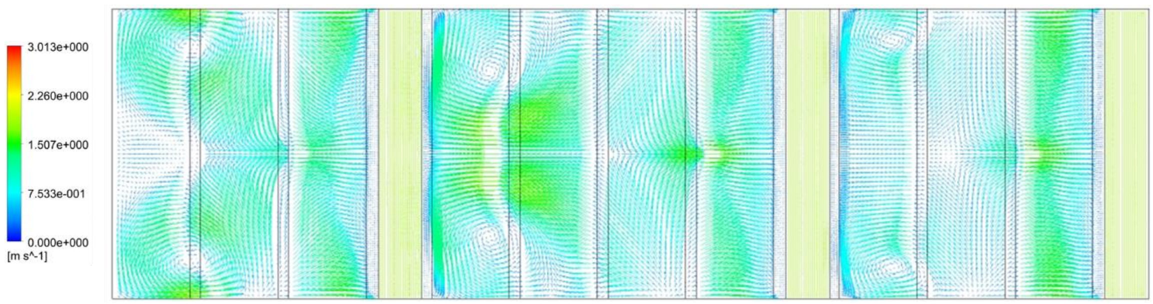

Figure 9-9: Velocity vector of the front chamber, for row-based cooling architecture. The cooling unit setpoint: 18ºC. Cooling units air flowrate: 1.375 m^3/s. Each rack IT load: 5kW.

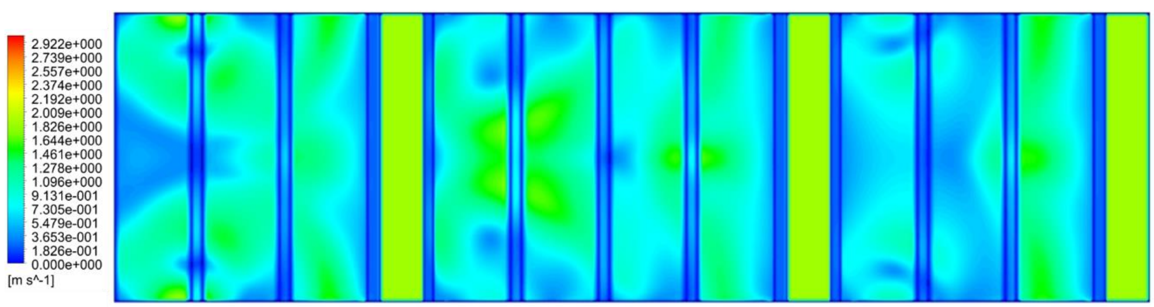

Figure 9-10:Velocity contour of the front chamber, for row-based cooling architecture. The cooling unit setpoint: 18ºC. Cooling units air flowrate: 1.375 m^3/s. Each rack IT load: 5kW.

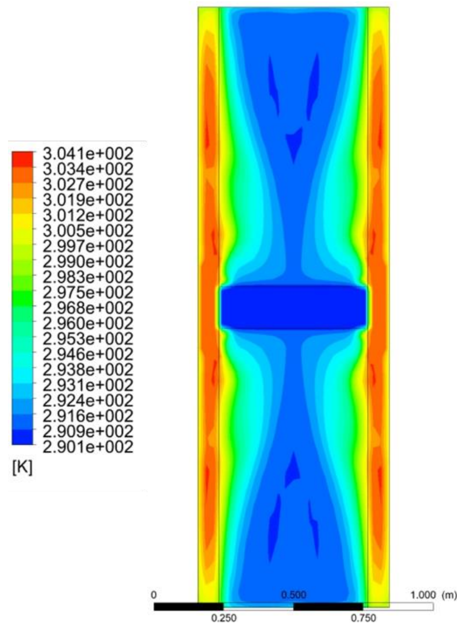

Figure 9-11:Temperature contour of the front chamber, for rack-based cooling architecture. The cooling unit setpoint: 17ºC. Cooling unit air flowrate: 0.36 m^3⁄s. Total IT load: 5kW.

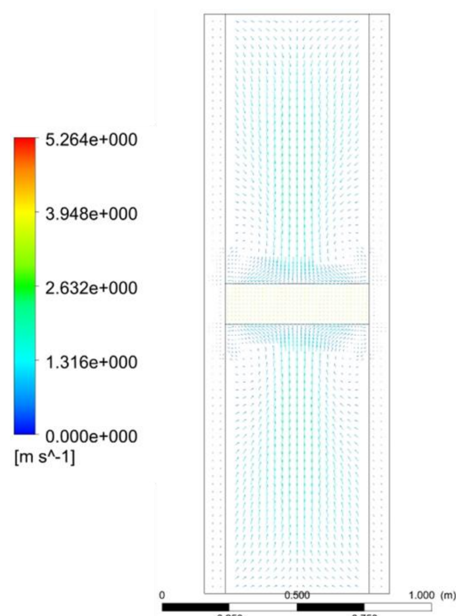

Figure 9-12:Velocity vector of the front chamber, for rack-based cooling architecture. The cooling unit setpoint: 17ºC. Cooling unit air flowrate: 0.36 m^3⁄s. Total IT load: 5kW.

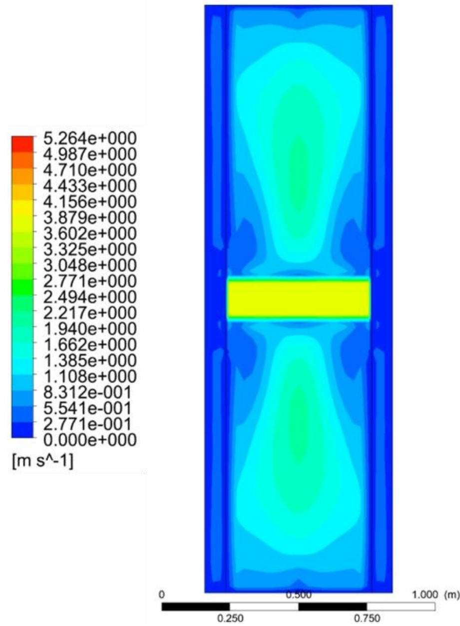

Figure 9-13:Velocity contour of the front chamber, for rack-based cooling architecture. The cooling unit setpoint: 17ºC. Cooling unit air flowrate: 0.36 m^3⁄s. Total IT load: 5kW.

9.8.2 Details of the simulations

The mesh is Cartesian cut-cell mesh, which is dominated by hexahedral volume elements. The meshes are refined by cutting the cells into smaller size that fits the local geometry, and therefore the interfaces between the different refinement levels are non-conformal. The Pressure-Based solver with segregated algorithm that employs Semi-Implicit Method for Pressure Linked Equations (SIMPLE) scheme for pressure-velocity coupling is used. The special discretization scheme for gradient is least squares cell based, for pressure is 2nd order, for momentum, turbulent kinetic energy, turbulent dissipation rate, and energy are 2nd order upwind.

9.9 References

[1] Z. Abbasi, G. Varsamopoulos, and S. K. S. Gupta, "Thermal Aware Server Provisioning And Workload Distribution For Internet Data Centers " School of Computing, Informatics and Decision Systems Engineering Arizona State University.

[2] A. C. Approach, Q. Tang, S. K. S. Gupta, and S. Member, "Energy-Efficient Thermal-Aware Task Scheduling for Homogeneous High-Performance Computing Data Centers :," IEEE TRANSACTIONS ON PARALLEL AND DISTRIBUTED SYSTEMS, vol. 19, no. 11, pp. 1458–1472, 2008.

[3] N. Vasi, T. Scherer, and W. Schott, "Thermal-Aware Workload Scheduling for Energy Efficient Data Centers," *ICAC'10,* June 7–11, 2010, Washington, DC, USA.

[4] Q. Tang, S. K. S. Gupta, and G. Varsamopoulos, "Thermal-Aware Task Scheduling for Data centers through Minimizing Heat Recirculation." The IMPACT Laboratory, School of Computing and Informatics, Arizona State University, Tempe, AZ 85287.

[5] S. Ham, M. Kim, B. Choi, and J. Jeong, "Simplified server model to simulate data center cooling energy consumption," *Energy Build.*, vol. 86, pp. 328–339, 2015.